國 立 交 通 大 學

材料科學與工程學系

博 士 論 文

氮化鋁與鈦介面相的生成機構與微觀結構的演變

Phase Formation Mechanisms and Microstructural Evolution of the AlN/Ti Interface between 1000° and 1500°C

研究生：邱家祥

指導教授：林健正　教授

中華民國九十七年六月

氮化鋁與鈦介面相的生成機構與微觀結構的演變

Phase Formation Mechanisms and Microstructural Evolution of the AlN/Ti Interface between 1000° and 1500°C

研 究 生 ： 邱家祥　　　　student : Chia-Hsiang Chiu

指導教授 ： 林健正　　　　Advisor : Chien-Chang Lin

國立交通大學

材料科學與工程學系

博士論文

A Thesis

Submitted to Department of Materials Science and Engineering

National Chiao Tung University

in partial Fulfillment of the Requirements

for the Degree of

Doctor of Philosophy

in

Materials Science and Engineering

June 2008

Hsinchu, Taiwan, Republic of China

中華民國九十七年六月

氮化鋁與鈦介面相的生成機構與微觀結構的演變

研究生：邱家祥　　　　　　　　　　指導教授：林健正

國 立 交 通 大 學

材 料 科 學 與 工 程 學 系

摘　要

本研究係利用解析式掃描式電子顯微鏡(SEM/EDS)與穿透式電子顯微鏡(TEM/EDS)，深入分析不同熱處理溫度的介面微觀結構，並利用Ti-Al-N平衡相圖以及擴散路徑圖，探討AlN與Ti介面微觀結構的演化及生成機構。

AlN與Ti介面處反應主要是由於AlN中的Al與N原子經擴散進入Ti側，而造成在Ti側產生一系列的氮化物與鋁化物。AlN與Ti經1000^{o}C之擴散反應，δ-TiN首先生成在介面處，而α_2-Ti_3Al會在δ-TiN/Ti介面處產生。隨熱處理時間增加，τ_1-Ti_3AlN會在δ-TiN反應層中生成，其方位關係為$[111]_{\tau_1-Ti_3AlN}//[111]_{\delta-TiN}$與$(1\bar{1}0)_{\tau_1-Ti_3AlN}//(1\bar{1}0)_{\delta-TiN}$。隨著N原子擴散進入$\alpha_2$-$Ti_3Al$，δ-TiN與雙晶結構$\alpha_2$-$Ti_3Al(N)$會在$\alpha_2$-$Ti_3Al$反應層中生成。當N原子進入$\alpha_2$-$Ti_3Al$的八面體間隙位置，會造成$\tau_1$-$Ti_3AlN$的生成而形成兩相區($\tau_1$-$Ti_3AlN$+$\alpha_2$-$Ti_3Al$)，其方位關係為$[111]_{\tau_1-Ti_3AlN}//[0001]_{\alpha_2-Ti_3Al(N)}$與$(0\bar{1}1)_{\tau_1-Ti_3AlN}//(\bar{1}\bar{1}20)_{\alpha_2-Ti_3Al(N)}$。

AlN與Ti金屬經1300℃擴散反應，其反應生成物從AlN側至Ti側依序為δ-TiN、τ_2-Ti_2AlN、τ_1-Ti_3AlN、α_2-Ti_3Al，與兩相區(α_2-Ti_3Al+α-Ti)。在兩相區中α_2-Ti_3Al與α-Ti的方位關係為$[0001]_{\alpha-Ti}//[0001]_{\alpha_2-Ti_3Al}$與

$(1\bar{1}00)_{\alpha\text{-Ti}}//(1\bar{1}00)_{\alpha_2\text{-Ti}_3\text{Al}}$。在1400℃反應下，反應生成物$\tau_1$-$Ti_3AlN$逐漸消失，而γ-TiAl與層狀結構(γ-TiAl+α_2-Ti_3Al)生成，其中層狀結構(γ-TiAl+α_2-Ti_3Al)的方位關係為$[011]_{\gamma-TiAl}//[2\bar{1}\bar{1}0]_{\alpha_2-Ti_3Al}$與$(1\bar{1}\bar{1})_{\gamma-TiAl}//(01\bar{1}0)_{\alpha_2-Ti_3Al}$。比較1500℃與1400℃反應後反應區的差異，並未發現γ-TiAl的存在。

為了進一步研究N原子對於AlN/Ti介面所造成的影響，進行氮化鋁與鈦金屬(箔)在1400℃的擴散反應，可發現γ-TiAl逐漸受到N的影響而產生fiber-like τ_2-Ti_2AlN。γ-TiAl與τ_2-Ti_2AlN的方位關係為$[011]_{\gamma-TiAl}//[11\bar{2}0]_{\tau_2-Ti_2AlN}$與$(\bar{1}\bar{1}1)_{\gamma-TiAl}//(1\bar{1}0\bar{3})_{\tau_2-Ti_2AlN}$。隨著$\tau_2$-$Ti_2AlN$的生成而釋放出Al原子，使γ-TiAl變成富鋁相的Ti_3Al_5。此外在α-Ti(Al, N)受到氮化而形成兩相區(α-Ti+δ-TiN)，α-Ti與δ-TiN的方位關係為$[110]_{\delta-TiN}//[11\bar{2}0]_{\alpha-Ti}$與$(111)_{\delta-TiN}//(0001)_{\alpha-Ti}$。

Phase Formation Mechanisms and Microstructural Evolution of the AlN/Ti Interface between 1000° and 1500°C

Student : Chia-Hsiang Chiu Advisors: Prof. Chien-Cheng Lin

Department of materials science and Engineering National Chiao Tung University, Hsinchu, Taiwan

Abstract

The diffusional reaction between aluminum nitride (AlN) and titanium (Ti) was carried out isothermally in argon at temperatures ranging from 1000° to 1500°C. The microstructural characterization and phase development were investigated using analytical scanning electron microscopy (SEM) and analytical transmission electron microscopy (TEM), both attached with an energy-dispersive spectrometer (EDS).

It is well known that the decomposition of AlN and the diffusion of Al and N atoms into Ti gave rise to various reaction layers at the interface. After annealing at 1000°C, a δ-TiN layer was initially formed in the reaction zone between AlN and Ti, and the α_2-Ti_3Al layer subsequently developed between δ-TiN and Ti. Then an intergranular τ_1-Ti_3AlN phase was formed in the δ-TiN layer with the orientation relationships $[111]_{\tau_1-Ti_3AlN}//[111]_{\delta-TiN}$ and $(1\bar{1}0)_{\tau_1-Ti_3AlN}//(1\bar{1}0)_{\delta-TiN}$. The further diffusion of N atoms into the α_2-Ti_3Al layer led to the growth of δ-TiN and a twinned α_2-$Ti_3Al(N)$ solid solution, wherein N atoms went to one of the octahedral interstitial sites in an orderly manner upon cooling, resulting in the formation of τ_1-Ti_3AlN. The orientation relationships between τ_1-Ti_3AlN and α_2-$Ti_3Al(N)$ were $[111]_{\tau_1-Ti_3AlN}//[0001]_{\alpha_2-Ti_3Al(N)}$ and

$(0\bar{1}1)_{\tau_1-Ti_3AlN} // (\bar{1}\bar{1}20)_{\alpha_2-Ti_3Al(N)}$.

After annealing at 1300°C, an interfacial reaction zone, consisting of TiN, τ_2-Ti_2AlN, τ_1-Ti_3AlN, α_2-Ti_3Al, and a two-phase (α_2-Ti_3Al + α-Ti) region in sequence, was observed in between AlN and Ti. The α_2-Ti_3Al region revealed equiaxed and elongated morphologies with $[0001]_{equiaxed} // [\bar{1}100]_{elongated}$ and $(\bar{1}010)_{equiaxed} // (\bar{1}\bar{1}22)_{elongated}$. In the two-phase ($\alpha_2$-$Ti_3Al$ + α-Ti) region, α_2-Ti_3Al and α-Ti were found to satisfy the following orientation relationship: $[0001]_{\alpha-Ti} // [0001]_{\alpha_2-Ti_3Al}$ and $(1\bar{1}00)_{\alpha\text{-Ti}} // (1\bar{1}00)_{\alpha_2\text{-Ti}_3\text{Al}}$. The γ-TiAl and a lamellar two-phase (γ-TiAl+α_2-Ti_3Al) structure, instead of τ_1-Ti_3AlN, were found in between τ_2-Ti_2AlN and α_2-Ti_3Al after annealing at 1400°C. The orientation relationship of γ-TiAl and α_2-Ti_3Al in the lamellar structure was identified to be as follows: $[011]_{\gamma-TiAl} // [2\bar{1}\bar{1}0]_{\alpha_2-Ti_3Al}$ and $(1\bar{1}\bar{1})_{\gamma-TiAl} // (01\bar{1}0)_{\alpha_2-Ti_3Al}$. Compared with the reaction zone after annealing at 1400°C, the γ-TiAl was not found at the interface after annealing at 1500°C.

In the other respective, AlN was bonded with a titanium foil at 1400ºC for up to 1 h in Ar. It was noted that the diffusion of N atoms into the reaction zone played an important role to the microstructural development at the AlN/Ti/AlN interface. The diffusion of N atoms into the reaction zone led to the precipitation of a chopped fiber-like τ_2-Ti_2AlN in the matrix of γ-TiAl, with $[110]_{\gamma-TiAl} // [11\bar{2}0]_{\tau_2-Ti_2AlN}$ and $(1\bar{1}\bar{1})_{\gamma-TiAl} // (1\bar{1}0\bar{3})_{\tau_2-Ti_2AlN}$, by substituting N atoms for one-half Al atoms after annealing at 1400°C for 1 h. The released Al atoms, due to the precipitation of τ_2-Ti_2AlN, resulted in an ordered Al-rich γ-TiAl or Ti_3Al_5. Furthermore, the α-Ti (Al, N) was nitridized into a lamellar layer (δ-TiN + α-Ti) with $[110]_{\delta-TiN} // [11\bar{2}0]_{\alpha-Ti}$ and $(111)_{\delta-TiN} // (0001)_{\alpha-Ti}$.

The microstructural development at the AlN/Ti interface is elucidated with the aid of the Ti-Al-N ternary phase diagram and a modified Ti-Al binary phase diagram. Finally, diffusion paths are proposed for the interfacial reactions at various stages.

誌謝

在博士班研究生涯中，首先最感謝我的指導教授林健正博士的指導與鼓勵，在研究方向、實驗方法、同時在待人處世的態度方面，亦使我受益良多，使我能順利完成博士學位，更衷心感謝諸位口試委員對本論文的指正與建議。

同時感謝實驗室一起奮鬥的夥伴，對我的砥礪與協助。另外更感謝所有幫助與關心我的朋友們。

更感謝阿瑤的陪伴與鼓勵，讓我的研究所的生活多采多姿，沒有你我的研究所的回憶將不會這麼甜美。

最後我要特別感謝我的父母，多年來辛苦的教導與栽培，並且長久在我背後默默支持與關懷，不時地給予我鼓勵，使我能順利完成學業。

謹以此篇論文，獻給所有曾協助過我的師長與朋友們。

CONTENTS

page

Chapter 1 Introduction 1

1.1 Introduction 1

1.2 Literature Data 2

1.3 Thesis Outline 3

Chapter 2 Microstructural Development of the AlN/Ti Diffusion Couple Annealed at 1000°C 8

2.1 Introduction 8

2.2 Experimental Procedures 11

2.3 Results and discussion 12

2.4 Conclusions 21

Chapter 3 Microstructural Characterization and Phase Development at the Interface between Aluminum Nitride and Titanium after Annealing at 1300°–1500°C 30

3.1 Introduction 30

3.2 Experimental Procedure 33

3.3 Results and Discussion 34

3.4 Conclusions 45

Chapter 4 Formation Mechanisms and Atomic Configurations of Nitride Phases at the Interface of Aluminum Nitride and Titanium 56

4.1 Introduction 56

4.2 Experimental Procedures 58

4.3 Results and Discussion 60

4.4 Conclusions 66

Chapter 5 Summary 74

References 76

List of Publications 83

List of Tables

page

Table 1. 1. Ti-Al crystal structure and lattice parameter data 5

Table 1. 2. Ti-N crystal structure and lattice parameter data............................. 6

Table 1. 3. Ti-Al-N crystal structure and lattice parameter data 7

Table 2. 1. Summary of some previous studies on the AlN/Ti interfacial reactions.. 22

Table 3. 1. New phases formed in the interfacial reaction zone of AlN/Ti diffusion couples 47

List of Figures

page

Fig. 2. 1. SEM micrographs showing the AlN/Ti interfaces after annealing at 1000 °C for (a) 0.1 h; (b) 0.5 h; (c) 3 h; (d) 36 h, respectively...... 23

Fig. 2. 2. (a) A bright field image of the residual δ-TiN phase in τ_1-Ti_3AlN after annealing at 1000°C/10 h; (b) an SADP of δ-TiN, z=[111]; (c) an SADP of τ_1-Ti_3AlN, z=[111]; (d) the SADPs of τ_1-Ti_3AlN and δ-TiN, showing the orientation relationships of $[111]_{\tau_1-Ti_3AlN}//[111]_{\delta-TiN}$ and $(1\bar{1}0)_{\tau_1-Ti_3AlN}//(1\bar{1}0)_{\delta-TiN}$; (e) the EDS spectrum of δ-TiN; (f) the EDS spectrum of τ_1-Ti_3AlN................ 24

Fig. 2. 3. After annealing at 1000°C/10 h: (a) the bright field image of the (τ_1-Ti_3AlN + α_2-Ti_3Al) twinned structure; (b) the SADPs of τ_1-Ti_3AlN (z=$[1\bar{1}01]$) and α_2-Ti_3Al (z=$[011]$) with the orientation relationships $[011]_{\tau_1-Ti_3AlN}//[1\bar{1}01]_{\alpha_2-Ti_3Al}$ and $(100)_{\tau_1-Ti_3AlN}//(1\bar{1}0\bar{2})_{\alpha_2-Ti_3Al}$; (c) the schematic illustration of the SADPs in (b) (●: α_2-Ti_3Al matrix, ○: α_2-Ti_3Al twin, Δ: τ_1-Ti_3AlN); (d) the SADPs of τ_1-Ti_3AlN (z=$[111]$) and α_2-Ti_3Al (z=$[0001]$) with the orientation relationships $[111]_{\tau_1-Ti_3AlN}//[0001]_{\alpha_2-Ti_3Al}$ and $(0\bar{1}1)_{\tau_1-Ti_3AlN}//(\bar{1}\bar{1}20)_{\alpha_2-Ti_3Al}$. 25

Fig. 2. 4. After annealing at 1000°C/10 h: (a) the bright field image of the (τ_1-Ti_3AlN+α_2-Ti_3Al) twinned structure; (b) the central dark field (CDF) image of the (τ_1-Ti_3AlN+α_2-Ti_3Al) twinned structure formed by the diffraction spot $(0\bar{1}10)$ of α_2-Ti_3Al. 26

Fig. 2. 5. **(a)** Crystal structures of α_2-Ti_3Al and τ_1-Ti_3AlN projected along the $[0001]_{\alpha-Ti_3Al}$ or $[111]_{\tau_1-Ti_3AlN}$ direction; (b) the stacking sequence of closely packed planes viewed along $[01\bar{1}0]_{\alpha_2-Ti_3Al}$ or $[1\bar{2}1]_{\tau_1-Ti_3AlN}$; (c) the lattice relationship of the cubic τ_1-Ti_3AlN (red line) and the

hexagonal α_2-Ti_3Al (black line). 27

Fig. 2. 6. Microstructural development in the AlN/Ti diffusion couple after annealing at 1000°C for 0.1-36 h; (a) formation of the δ-TiN layer; (b) formation of the α_2-Ti_3Al layer and various titanium aluminides; (c) formation of τ_1-Ti_3AlN in the δ-TiN layer; (d) formation of δ-TiN and twinned α_2-Ti_3Al due to the nitridization of the α_2-Ti_3Al layer; (e) formation of (τ_1-Ti_3AlN+α_2-Ti_3Al) twinned structure during cooling. 28

Fig. 2. 7. (a) An isothermal section of the Ti-Al-N system at 1000°C, and the diffusion paths (path 1: A-B-C-H for 0.1h; path 2: A-B-C-G-H for 0.5h; path 3: A-B-C-D-E-F-G-H for 36h); (b) Schematic microstructure at the AlN/Ti interface on annealing at 1000°C/36h; (c) Schematic microstructure of the AlN/Ti interface after cooling. 29

Fig. 3. 1. SEM micrographs of the interface between AlN and Ti after annealing at: (a) 1300°C/36 h; (b) 1400°C/36 h; (c) 1500°C/36 h. 48

Fig. 3. 2. (a) BF image of the AlN/Ti interface after annealing at 1300°C for 3 h; (b) SADP of TiN, Z=[001]; (c) SADP of τ_2-Ti_2AlN, Z=[$11\bar{2}0$]; and (d) SADP of τ_1-Ti_3AlN, Z=[001]. 49

Fig. 3. 3. After annealing at 1300°C for 3 h: (a) BF image of the equiaxed α_2-Ti_3Al (abutting the τ_1-Ti_3AlN layer in Fig. 3.1(a)); (b) BF image of the elongated α_2-Ti_3Al (abutting the two-phase (α_2-Ti_3Al + α-Ti) layer in Fig. 3.1(a)); (c) Variation in the grain size of the equiaxed α_2-Ti_3Al along the direction from the AlN side (bottom) to the Ti side (top); (d) SADP of both elongated and equiaxed α_2-Ti_3Al, showing the orientation relationship of $[0001]_{equiaxed}//[\bar{1}100]_{elongated}$ and $(\bar{1}010)_{equiaxed}//(\bar{1}\bar{1}22)_{elongated}$. 50

Fig. 3. 4. After annealing at 1300°C for 3 h: (a) BF image of the two-phase

(α_2-Ti_3Al + α-Ti) region in Fig. 3.1(a); (b) DF image of α_2-Ti_3Al from the $(11\bar{2}0)_{Ti_3Al}$ diffraction spot; (c) Superimposed SADPs obtained from the two-phase (α_2-Ti_3Al + α-Ti) region, showing the orientation relationship of $[0001]_{\alpha-Ti} // [0001]_{Ti_3Al}$ and $(1\bar{1}00)_{\alpha\text{-Ti}} // (1\bar{1}00)_{Ti_3Al}$; (d) Schematic illustration of α-Ti and α_2-Ti_3Al crystals structure. 51

Fig. 3. 5. (a) BF image of γ-TiAl between the τ_2-Ti_2AlN and the lamellar structure after annealing at 1500°C/0.5 h; (b) BF image of the lamellar two-phase (γ-TiAl + α_2-Ti_3Al) structure; (c) Superimposed SADP's of γ-TiAl (Z = $[011]$) and α_2-Ti_3Al (Z = $[2\bar{1}\bar{1}0]$) from the lamellar structure region, and the orientation relationship of γ-TiAl and α_2-Ti_3Al was identified to be as follows: $[011]_{TiAl} // [2\bar{1}\bar{1}0]_{Ti_3Al}$ and $(1\bar{1}\bar{1})_{TiAl} // (01\bar{1}0)_{Ti_3Al}$; (d) Schematic illustration corresponding to the SADP's in (c). 52

Fig. 3. 6. (a) Isothermal section of the Ti-Al-N phase diagram at 1300°C.[30] The diffuse path was drawn as arrows; (b) the microstructure of an AlN/Ti diffusion couple at 1300°C; (c) the microstructure of an AlN/Ti diffusion couple after cooling. 53

Fig. 3. 7. A modified Ti-Al phase diagram because of the stabilization of α-Ti by dissolving N (see the dashed line), showing the cooling processes of the various aluminides after annealing at 1300°C (lines 1-3) and at 1400°C (lines 4 and 5). The increase in the α → β transformation temperature has been exaggerated for clarification. 54

Fig. 3. 8. Proposed reaction mechanisms of the AlN and Ti diffusion couple annealed at 1300°C: (a) first stage: formation of TiN; (b) Second stage: formation of τ_1-Ti_3AlN, α-Ti(Al, N)+β-Ti(Al, N), and α-Ti(Al, N); (c) third stage: formation of τ_2-Ti_2AlN; (d) fourth stage:

formation of α_2-Ti_3Al and/or the two-phase layer (α_2-Ti_3Al + α-Ti) during cooling. (τ_1: Ti_3AlN; τ_2: Ti_2AlN; α_2:Ti_3Al; α: hexagonal Ti(Al, N); β: cubic Ti(Al, N)). 55

Fig. 4. 1. Secondary electron images showing the interfacial microstructures of the AlN/Ti/AlN specimens: (a) after annealing at 1400°C/0.1 h; (b) after annealing at 1400°C/1 h [A: δ-TiN, B: τ_2-Ti_2AlN, C: τ_2-Ti_2AlN+γ-TiAl+Ti_3Al_5, D: a lamellar structure (δ-TiN+α-Ti), E: α-Ti]. (c) A magnified secondary electron image of reaction layer C in Fig. 1(b) showing a chopped fiber like τ_2-Ti_2AlN in the (Ti_3Al_5+γ-TiAl) matrix; (d) a magnified secondary electron image of reaction layer D showing a lamellar structure of (δ-TiN+α-Ti). All specimens were etched by the Kroll reagent. 68

Fig. 4. 2. (a) The isothermal section of the Ti-Al-N phase diagram at 1400°C and (b) the Ti-Al binary phase diagram. 69

Fig. 4. 3. (a) A bright field image showing a residual γ-TiAl grain embedded in τ_2-Ti_2AlN after annealing at 1400°C/1 h; (b) the alternating (001) layers of Ti and Al viewed along the direction [110] in γ-TiAl; (c) the stacking sequence AB'ABAB'AB… of the (0001) layers viewed along the direction $[11\bar{2}0]$ in τ_2-Ti_2AlN. 70

Fig. 4. 4. (a) A bright field image showing the precipitation of τ_2-Ti_2AlN in the matrix of Ti_3Al_5+γ-TiAl, taking place in reaction layer C in Fig. 4.1(b) after annealing at 1400°C/1 h; (b) the superimposed selected area diffraction patterns (SADPs) of τ_2-Ti_2AlN and a two-phase (Ti_3Al_5+γ-TiAl), showing the orientation relationships $[110]_{\gamma-TiAl}//[11\bar{2}0]_{\tau_2-Ti_2AlN}$ and $(1\bar{1}\bar{1})_{\gamma-TiAl}//(\bar{1}10\bar{3})_{\tau_2-Ti_2AlN}$ 71

Fig. 4. 5. After annealing at 1400°C/1 h: (a) a bright field image of the modulated structure of Ti_3Al_5+γ-TiAl; (b) the superimposed SADPs of Ti_3Al_5 and γ-TiAl, with the superlattice deflections resulting from the ordering of substitutional Al atoms on the Ti sublattice; (c)

a central dark field image of Ti_3Al_5+γ-TiAl formed by the 1/4(100) superlattice diffraction of Ti_3Al_5, as marked by a circle in Fig. 4.5 (b).. 72

Fig. 4. 6. (a) A bright field image of the lamellar structure (δ-TiN+α-Ti) after annealing at 1400°C/1 h; (b) the SADPs of δ-TiN (Z=$[110]_{\delta-TiN}$) and α-Ti (Z=$[11\bar{2}0]_{\alpha-Ti}$); (c) the schematic illustration of the SADPs in (b); (d) the atomic configuration at the δ-TiN/α-Ti interface viewed along the $[110]_{\delta-TiN}$ or $[11\bar{2}0]_{\alpha-Ti}$ direction. The TEM specimen was acquired from a cross-sectional SEM specimen along the direction perpendicular to the precipitate using FIB. 73

Chapter 1 Introduction

1.1 Introduction

Aluminum nitride (AlN) shows a wide range of engineering applications, including piezoelectric, optical, semiconducting, structural, and/or mechanical purposes. It belongs to a group of the hexagonal wurtzite structure with the 6mm symmetry. Among these group III nitrides, AlN has a wide band gap and has a variety of potential applications. It is a hard material with bulk hardness similar to quartz about 20 GPa. Pure AlN is chemically stable to attack by atmospheric gases at temperatures less than 700°C. The combination of these mechanical and chemical properties has stirred a considerable interest in practical applications of AlN in both bulk and thin film forms. These applications include use in integrated circuit packaging, ignition modules, r.f./microwave packages, heat sinks, cutting tools, and laser diode heat spreaders.[1, 2]

1896

AlN exhibits a very good resistance with respect to a wide variety of materials. It is wetted by molten Al but does not react with it. Most metals, including Cu, Li, U, ferrous alloys and some superalloys, do not attack AlN. In spite of the obvious scientific and technological importance, interdiffusional reactions at AlN ceramic/metal interfaces have not been subjected to an extensive study. Among all the metals, reactions between Ti and AlN arouse the greatest interest due to the high affinity of Ti to both aluminum and nitrogen, and the stability of the resultant titanium aluminides and nitrides. This work focuses on the phase formation mechanisms and phase development of the AlN-Ti interfaces.[1, 2]

The AlN/Ti system is a ceramic/metal system that has increasing important

applications, for example, in package, in composites, in coating or joining technology. The reliability of these systems depends on the interfacial properties between the ceramic and metal, e.g. adhesion properties and thermal stability. Therefore a better understanding of the reaction at these interfaces is of essence. In order to optimize the joining technique, the knowledge of the interfacial reactions occurring between AlN and Ti during joining is of great importance.

1.2 Literature Data

The solubility of nitrogen in Al(s) and Al(l) is very small. Only one compound AlN exists in the Al-N binary system.

The equilibrium phases in the Ti-Al system are: the disordered solution phases, liquid, α-Ti, β-Ti, and Al, and the ordered intermetallic compounds, α_2-Ti_3Al, which has an ordered hexagonal close-packed superlattice structure, γ-TiAl and $TiAl_3$, both of which have an ordered face-centered cubic (fcc)-based superlattice structure. Crystal structure data on the Ti-Al binary phases are summarized in Table 1.1.

The solubility of nitrogen both in (α-Ti) and (β-Ti) is significant. The congruently melting δ-TiN_{1-x} compound with wide homogeneity range and incongruently melting Ti_2N compound exist in this binary system. Crystal structure data on the Ti-N binary phases are summarized in Table 1.2.

Three compounds (τ_1-Ti_3AlN, τ_2-Ti_2AlN and τ_3-$Ti_3Al_2N_2$) are formed in this system. τ_1-Ti_3AlN which exhibits a negligible range of homogeneity has a cubic structure. τ_2-Ti_2AlN is the most stable and belongs to the group of H phases. It has been

observed to exist over the temperature range from 700-1600^oC. τ_3-$Ti_3Al_2N_2$ is stable only in a narrow temperature range between 1250° and 1400^oC with hexagonal structure. Crystal structure data on the Ti-Al-N ternary phases are summarized in Table 1.3.[3-6]

1.3 Thesis Outline

The present work focuses on the phase evolution and formation mechanism between AlN and Ti at 1000°-1500^oC using analytical scanning electron microscopy (SEM) and analytical transmission electron microscopy (TEM), both attached with an energy-dispersive spectrometer (EDS). All these results, obtained at elevated temperatures, can be explained on the basis of the ternary Ti-Al-N phase diagram and the diffusion paths that connect the phases formed by the reaction between AlN and Ti.

Chapter 2 studies the morphologies, crystal structures, chemical compositions, and formation mechanisms of various formed phases in the AlN/Ti interface after annealed at 1000^oC for various periods. The twinned α_2-$Ti_3Al(N)$ solid solution and τ_1-Ti_3AlN are first found to exist in the α_2-Ti_3Al layer after annealing, and studies their relationships.

Chapter 3 describes the phase formation mechanisms at the AlN/Ti interface after annealed at temperatures ranging from 1300° to 1500^oC. The distinct microstructures were found at the AlN/Ti interface after annealing. The microstructural evolution at the AlN/Ti interface can be explained with the aid of Ti-Al-N phase diagram and a modified Ti-Al binary phase diagram.

Chapter 4 will further discuss the effect of nitridization at the AlN/Ti interface after annealing. It was found that the microstructure in the AlN/Ti interface strongly

depended on the inward diffusion of N. The phase transformation mechanisms at the AlN/Ti interface are explained from the viewpoint of N atom inward diffusion into the Ti-Al reaction layers.

Chapter 5 will summarize the results obtained from the previous Chapters.

Table 1. 1. Ti-Al crystal structure and lattice parameter data.[4, 5]

Phase	System	Homogeneity Range,at.%Al	Pearson symbol	Space group	StrukturBericht designation	prototype	Lattice parameter(nm)		
							a	b	c
α-Ti	Hexagonal	0 to 45	hP2	$P6_3$/mmc	A3	Mg	0.295		0.468
β-Ti	Cubic	0 to 47.5	cI2	*I*m3m	B2	W	0.328		
α_2-Ti_3Al	Hexagonal	22 to 39	hP8	$P6_3$/mmc	$D0_{19}$	Ni_3Sn	0.578		0.466
γ-TiAl	Tetragonal	48 to 69.5	tP4	*P*4/mmm	$L1_o$	AuCu	0.396		0.41
Ti_3Al_5	Tetragonal	58 to 63(a)	tP32	*I*4/mbm		Ti_3Al_5	1.129		0.404
$TiAl_2$	Tetragonal	65 to 68	tI24	$I4_1$/amd		Ga_2Hf	0.398		2.436
$TiAl_2$	Orthorhombic	(b)	oC12	*C*mmm		Ga_2Zr	0.389		3.392
δ		70 to 72.5	(c)						
$TiAl_3$(h)	Tetragonal	74.5-75	tI8	*I*4/mmm	$D0_{22}$	Al_3Ti	0.3875		3.384
$TiAl_3$(l)	Tetragonal	75	(b,d)	I4/mmm			0.388		3.383
(Al)	Cubic	99.3 to 100	cF4	Fm3m	A1	Cu	0.405		

(a) Not an equilibrium phase.(b)Not shown on the assessed diagram.(c)long-period superlattice
(d)Tetragonal. A superstructure of the $D0_{22}$ lattice.

Table 1. 2. Ti-N crystal structure and lattice parameter data.[4]

Phase	System	Homogeneity Range,at.%N	Pearson symbol	Space group	StrukturBericht designation	prototype	Lattice parameter(nm) a	b	c
α-Ti	Hexagonal	0 to 22	hP2	$P6_3/mmc$	A3	Mg	0.29511(a)		0.46843(a)
β-Ti	Cubic	0 to 6	cI2	Im3m	B2	W	0.3306(a)		
Ti_2N	Tetragonal	33	tP6	$P4_2/mnm$	C4	Anti-O_2Ti (rutile)	0.4943		0.3036
TiN	Cubic	30 to 55	cF8	Fm3m	$B1_o$	NaCl	0.4241 ± 0.0002(b)		
δ'	Tetragonal	38	tI12	$I4_1/amd$	C_c	Si_2Th	0.4198		0.8591

(a)Pure Ti(0 at.%N).(b)50.0 at.%N.

Table 1. 3. Ti-Al-N crystal structure and lattice parameter data.[3]

Phase	System	Structure type	Pearson symbol	Space group	Lattice parameter(nm) a	b	c
$AlNTi_2$	Hexagonal	$AlCCr_2$	hP8	$P6_3/mmc$	0.2994		1.361
$AlNTi_3$	Cubic	CaO_3Ti	cP5	$Pm\bar{3}m$	0.4112		
$Al_2N_2Ti_3$	Hexagonal	$Al_2N_2Ti_3$	hP22	P31c	0.29875		2.335

Chapter 2　Microstructural Development of the AlN/Ti Diffusion Couple Annealed at 1000°C

2.1 Introduction

A low dielectric constant and good thermal dissipation are the two most important requirements for electronic packaging materials, since small modern VLSIs are operated at high power and high speed. AlN has been used as a replacement for alumina in electron packaging applications because it can fulfill these requirements.[7-9] Highly reactive Ti has been used as an interlayer because of good wetting and adhesion between Cu and AlN, while retaining a ductile layer to minimize residual stresses that are caused by the difference in thermal expansion coefficients.[10-12]

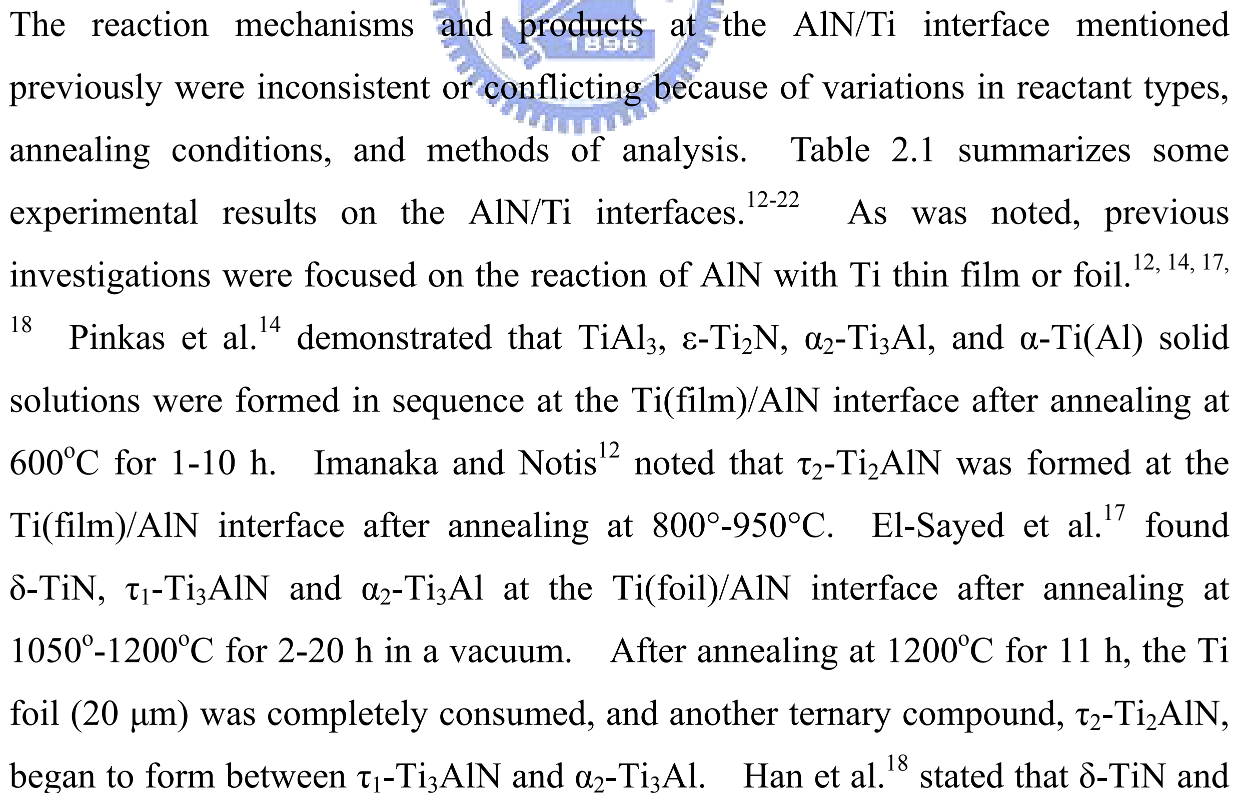

The reaction mechanisms and products at the AlN/Ti interface mentioned previously were inconsistent or conflicting because of variations in reactant types, annealing conditions, and methods of analysis. Table 2.1 summarizes some experimental results on the AlN/Ti interfaces.[12-22] As was noted, previous investigations were focused on the reaction of AlN with Ti thin film or foil.[12, 14, 17, 18] Pinkas et al.[14] demonstrated that $TiAl_3$, ε-Ti_2N, α_2-Ti_3Al, and α-Ti(Al) solid solutions were formed in sequence at the Ti(film)/AlN interface after annealing at 600°C for 1-10 h. Imanaka and Notis[12] noted that τ_2-Ti_2AlN was formed at the Ti(film)/AlN interface after annealing at 800°-950°C. El-Sayed et al.[17] found δ-TiN, τ_1-Ti_3AlN and α_2-Ti_3Al at the Ti(foil)/AlN interface after annealing at 1050°-1200°C for 2-20 h in a vacuum. After annealing at 1200°C for 11 h, the Ti foil (20 μm) was completely consumed, and another ternary compound, τ_2-Ti_2AlN, began to form between τ_1-Ti_3AlN and α_2-Ti_3Al. Han et al.[18] stated that δ-TiN and

τ_1-Ti_3AlN were present in the reaction zone after AlN/Ti(150 μm)/AlN sandwiched specimens were annealed at 1000°C for 200 h in a vacuum.

Several researchers have investigated the AlN/Ti interfacial reactions in bulk or powder.[18, 20, 21, 23] Paransky et al.[20, 21, 23] found that δ-TiN, τ_1-Ti_3AlN and α_2-Ti_3Al were formed between AlN (powder) and Ti (powder) after annealing at 900°-1100°C for 1-40 h. A lamellar (α_2-Ti_3Al + τ_1-Ti_3AlN) layer was observed between τ_1-Ti_3AlN and α_2-Ti_3Al after annealing at 1000° or 1100°C. Han et al.[18] observed δ-TiN, τ_1-Ti_3AlN and α_2-Ti_3Al after the mixtures of AlN and Ti powders (AlN:Ti = molar ration of 1:2) were annealed at 1000°C for 200 h under vacuum. However, the crystallographic relationships and mechanisms of phase transformation among these phases have not yet been fully explored.

As Table 2.1 indicates, x-ray diffraction (XRD) and scanning electron microscopy/energy dispersive spectrometry (SEM/EDS) are most frequently used to investigate the AlN/Ti interface. However, chemical SEM/EDS analyses and crystallographic XRD analyses are based on microscopic and macroscopic scales, respectively.[20] In addition, SEM/EDS analysis is complicated by the coexistence of several binary and ternary phases with similar compositions (Ti_3AlN, Ti_3AlN_{1-x}, Ti_2AlN, Ti_2N, and TiN_{1-x}) and by the overlap of titanium L and nitrogen K spectral series.[20] As a result, the combination of XRD and SEM/EDS does not allow for full characterization of the AlN/Ti interface.

Recently, Paransky et al.[8-10] investigated the AlN-Ti interface using the electron backscatter diffraction (EBSD) attached to the SEM. One major advantage of the EBSD technique is its ability to provide crystallographic information which is supplementary to traditional SEM/EDS analyses. However, the EBSD can only

be operated over a very limited range of incident angles, and cannot provide resolution on a submicron scale, such as a fine precipitate and/or a fine lamellar structure at the AlN-Ti interface.

Selected electron diffraction patterns can be conducted over a wide range of incident angles and on a submicron scale using a transmission electron microscope (TEM). Since TEM/EDS can provide simultaneous microstructural observation, crystallographic and compositional analyses with good resolution, it is a much more effective tool for microstructural characterization than methods such as SEM/EDS, XRD, and EBSD. However, TEM/EDS has only been applied to the investigation of the AlN/Ti interface in very few studies[12, 14] since it is very challenging to prepare the cross-sectional TEM specimens.

Recently, Chiu and Lin proposed the phase formation mechanisms in the AlN/Ti diffusion couple at 1300º-1500°C based on microstructural characterization using TEM/EDS and SEM/EDS.[22] An interfacial reaction zone, consisting of δ-TiN, τ_2-Ti_2AlN, τ_1-Ti_3AlN, α_2-Ti_3Al and a two-phase (α_2-Ti_3Al + α-Ti) region in sequence, was observed in the AlN/Ti diffusion couple after annealing at 1300ºC. The γ-TiAl and a lamellar two-phase (γ-TiAl + α_2-Ti_3Al) structure were present between τ_2-Ti_2AlN and α_2-Ti_3Al after annealing at 1400°C, while no γ-TiAl was present at the interface after annealing at 1500°C.

In this work, TEM/EDS was utilized to examine the phase evolution of the interfacial reaction zone between AlN and Ti after annealing at 1000ºC for 0.1-36 h in an Ar atmosphere. The interfacial reactions for various periods are described in terms of diffusion paths, which are depicted in an isothermal Al-N-Ti ternary phase diagram. The crystallographic relationships and phase transformation

mechanisms of δ-TiN, τ_1-Ti_3AlN and α_2-Ti_3Al are also elucidated.

2.2 Experimental Procedures

AlN plates (SH-15, with a nominal composition of 62.8 % Al, 32.1 % N, 3.4 % Y, 1.7 % O, Tokuyama Soda Corp., Tokyo, Japan) and commercially pure Ti billets (99.7% purity, Alfa Aesar, Ward Hill, MA) were cut into pieces with dimensions of approximately 15 × 10 × 4 mm. Using a precision polishing machine (Model Minimet 1000, Buehler Ltd., Lake Bluff, IL), all of the pieces were ground with a 15 μm diamond matted disc and then polished with 3 μm diamond paste and a 1 μm alumina suspension. After they were rinsed ultrasonically in an acetone bath and distilled water, the sandwiched samples, with the Ti metal placed between two pieces of AlN, were annealed under a low pressure of 2 MPa at 1000°C for various periods in an atmosphere of argon (with $O_2 < 1$ ppm, $H_2O < -76$ ppm/°C and $N_2 < 3$ ppm).

A slice with a thickness of approximately 300 μm was cut from each annealed sample perpendicular to the interface of AlN and Ti. The slice was then ground and polished down to a thickness of 80~100 μm following the standard metallographic procedures described above. Each metallographic sample was etched using the Kroll reagent (10 ml HF + 30 ml HNO_3 + 60 ml H_2O) for SEM/EDS analyses. The cross-sectional slab was further thinned to a thickness of 20~30 μm by dimpling, and was finally argon-ion-milled at 5 kV and 20 μA for TEM/EDS analyses.

The AlN/Ti interfacial microstructures were characterized using a transmission electron microscope (Model 2000FX, JEOL, Tokyo, Japan) and a scanning electron microscope (Model JSM-6500, JEOL, Tokyo, Japan), both equipped with an

ultra-thin window EDS detector (Model 9900, EDAX International, Prairie View, IL). The Cliff–Lorimer standardless technique was applied to analyze the compositions of various phases at the thin edge of the TEM samples.

2.3 Results and discussion

(1) Microstructures of the AlN/Ti interface

Figure 2.1 illustrated the variation in the interfacial microstructures of AlN and Ti after annealing at 1000°C for various periods. Figure 2.1(a) presented the secondary electron image (SEI) of the cross section of the AlN/Ti interface after annealing at 1000°C/0.1 h, revealing that the reaction zone consisted of one well-defined reaction layer, which was identified as δ-TiN with less than 2 at.% Al in solid solution. A similar result was also demonstrated in previous works.[24, 25] Figure 2.1 (b) displayed the interfacial reaction zone of AlN/Ti after annealing at 1000°C/0.5 h, indicating the presence of δ-TiN and α_2-Ti_3Al at the AlN/Ti interface. Some investigations[13, 14, 26] have reported that δ-TiN and $TiAl_3$ are initially formed at the AlN/Ti interface after annealing between 600° and 800°C. Pinkas et al.[14] investigated the early stage of interface reactions between AlN and Ti thin films at 600°C for 1-10 h, indicating that the phase sequence was AlN/$TiAl_3$/Ti_2N/Ti_3Al/α-(Ti, Al)ss. However, $TiAl_3$ was not observed in the reaction zone between AlN and Ti after annealing at 1000°C/0.5 h, as shown in Fig. 2.1(b). Figure 2.1(c) revealed that the insular τ_1-Ti_3AlN began to precipitate in the δ-TiN layer after annealing at 1000°C/3 h. The τ_1-Ti_3AlN in the δ-TiN layer became interconnected during annealing at 1000°C/36 h, as displayed in Fig. 2.1(d). Moreover, the twinned structure (τ_1-Ti_3AlN + α_2-Ti_3Al) and insular δ-TiN were present at the interface between δ-TiN and α_2-Ti_3Al after annealing at 1000°C/36 h. The insular δ-TiN grains, mentioned above, appeared as the brightest phase in Fig. 2.1(d). It was believed that the formation of the twinned structure (τ_1-Ti_3AlN +

α_2-Ti_3Al) and insular δ-TiN was caused by the nitridization of the α_2-Ti_3Al layer, as discussed below in detail. The comparison between Figs. 2.1(c) and (d) revealed that the δ-TiN layer hardly grew at the AlN/Ti interface at 1000°C, although the thickness of the α_2-Ti_3Al layer increased with annealing time.

According to the Ti-Al-N ternary phase diagram at 1000°C, ternary compounds such as τ_1-Ti_3AlN and τ_2-Ti_2AlN exist in the equilibrium system. Han et al.[18] reported that the formation energies of τ_1-Ti_3AlN and τ_2-Ti_2AlN at 1000°C were -360 and -323 kJ/mol, respectively, revealing that their formation was thermodynamically favorable. Magnan et al.[27] indicated that α_2-Ti_3Al could be nitridized to τ_1-Ti_3AlN upon annealing at 1000°C, and τ_1-Ti_3AlN was gradually replaced by τ_2-Ti_2AlN with time. However, no τ_2-Ti_2AlN was found in this study. Only limited Al and N atoms diffused through δ-TiN to react with α_2-Ti_3Al in the AlN/Ti diffusion couple. This prohibited the further formation of any Al and N rich phase, e.g., τ_2-Ti_2AlN, in the AlN/Ti diffusion couple.

As mentioned above, τ_1-Ti_3AlN was formed at the grain boundaries of the δ-TiN layer during annealing at 1000°C/3 h [Fig. 2.1(c)], and became interconnected during annealing at 1000°C/36 h [Fig. 2.1(d)]. Figure 2.2(a) revealed that the residual δ-TiN was embedded in the growing τ_1-Ti_3AlN during annealing at 1000°C/10 h, suggesting that the τ_1-Ti_3AlN grew as the δ-TiN layer was consumed. The lattice parameter of τ_1-Ti_3AlN deviated from that of δ-TiN by less than 3% (a = 4.24 nm for δ-TiN and a = 4.11 nm for τ_1-Ti_3AlN). The selected area diffraction patterns (SADPs) of τ_1-Ti_3AlN and δ-TiN were distinguished by whether the superlattice diffractions were present in the SADPs, as shown in Figs. 2.2(b) and (c). No superlattice diffractions such as (110) and (101) were present in the SADPs of the δ-TiN with the NaCl-like structure, while the SADPs of the

τ_1-Ti_3AlN were typical (001)* patterns for the pervoskite-like structure, revealed by the superlattice diffractions (100), (010), (110) and others. The SADPs in Fig. 2.2(d) revealed that the orientation relationships of δ-TiN and τ_1-Ti_3AlN were $[111]_{\tau_1-Ti_3AlN} // [111]_{\delta-TiN}$ and $(1\bar{1}0)_{\tau_1-Ti_3AlN} // (1\bar{1}0)_{\delta-TiN}$. Both δ-TiN and τ_1-Ti_3AlN could be discernible based upon elemental quantitative analyses using TEM/EDS because δ-TiN dissolved a very limited amount of Al (≈ 0.3 at.%) and τ_1-Ti_3AlN contained approximately 20 at.% Al, as shown in Fig. 2.2(e) and (f), respectively. From the crystallographic viewpoint, the phase transformation from δ-TiN to τ_1-Ti_3AlN can be understood as follows: one Ti atom (at a corner) in a unit cell of δ-TiN was replaced by Al and three N atoms (at the octahedral interstitial sites) were evolved, based upon the following chemical reaction.

$$4\delta\text{-}TiN + Al \rightarrow \tau_1\text{-}Ti_3AlN + 3N + Ti \quad (1)$$

Paransky et al.[20, 21, 23] alleged that a lamellar structure was present at the interface between AlN and Ti powders after annealing at 900°-1100°C for 1-40 h, revealing that the τ_1-Ti_3AlN phase precipitated from supersaturated α_2-Ti_3Al with N in solid solution during cooling. However, Fig. 2.3(a) revealed that the system existed as a twinned rather than lamellar structure after annealing at 1000°C/10 h. Figure 2.3(b) displayed the superimposed SADPs of α_2-Ti_3Al (Z=$[1\bar{1}01]$) and τ_1-Ti_3AlN (Z=$[011]$), with the electron beam in the edge-on direction of the twin plane $(0\bar{1}11)_{\alpha_2-Ti_3Al}$. The twinned structure was implied by the streaking of the diffraction spots along the direction perpendicular to the twin plane and the presence of extra spots symmetrical with respect to the twin plane in the SADPs, as shown in Fig. 2.3(b). For clarity, the superimposed SADPs in Fig. 2.3(b) were redrawn and indexed in Fig. 2.3(c). The superimposed SADPs, shown in Figs. 2.3(b) and (d),

clearly illustrated that the twinned structure contained two phases, identified as hcp ordered α_2-Ti_3Al and cubic τ_1-Ti_3AlN, respectively, and that they were orientated with the relationships $[111]_{\tau_1-Ti_3AlN}//[0001]_{\alpha_2-Ti_3Al}$ and $(0\bar{1}1)_{\tau_1-Ti_3AlN}//(\bar{1}\bar{1}20)_{\alpha_2-Ti_3Al}$.

Figures 2.4(a) and (b) presented the bright field image (BFI) and central dark field image (CDFI), respectively, of the twinned structure as shown in Fig. 2.3(a). The bands of the twin and the matrix were somewhat discernible while comparing Figs. 2.4(a) and (b) with Fig. 2.3(a). The central dark field image was formed by the diffraction spot $(0\bar{1}10)$ of α_2-Ti_3Al such that the α_2-Ti_3Al phase appeared bright in Fig. 2.4(b). Two phases appeared to be present and the chopped fiber-like α_2-Ti_3Al was aligned with τ_1-Ti_3AlN in the direction perpendicular to the twin plane.

The mechanism of phase transformation from α_2-Ti_3Al to τ_1-Ti_3AlN could be seen with the help of Fig. 2.5. The ordering of N atoms was responsible for the formation of τ_1-Ti_3AlN. At high temperatures, α_2-Ti_3Al could dissolve a significant amount of N atoms, which occupied one of the octahedral interstitial sites of α_2-Ti_3Al in an orderly manner during cooling. The crystal structures of α_2-Ti_3Al and τ_1-Ti_3AlN were hexagonal and pervoskite, respectively. The most closely packed {0001} planes of α_2-Ti_3Al and the most closely packed {111} planes of τ_1-Ti_3AlN were parallel based on the SADPs in Fig. 2.3(d). The {0001} interlayer distance of hexagonal α_2-Ti_3Al was calculated as c/2 or 0.233 nm, while the {111} interlayer distance of cubic τ_1-Ti_3AlN was calculated as the diagonal length $\sqrt{3}a$ divided by 3 or 0.237 nm. The equality of their closely packed interlayer distances was consistent with the crystallographic relationships mentioned above. The closely packed planes of α_2-Ti_3Al and τ_1-Ti_3AlN, lying in

the plane of the paper, could be seen in Fig. 2.5(a) along the $[0001]_{\alpha_2-Ti_3Al}$ or $[111]_{\tau_1-Ti_3AlN}$, while the stacking sequences of closely packed planes in Fig. 2.5(b) were viewed along $[01\bar{1}0]_{\alpha 2-Ti3Al}$ or $[1\bar{2}1]_{\tau 1-Ti3AlN}$. Although Ti and Al atoms were not redistributed during the phase transformation, N atoms were inserted between two neighboring closely packed planes. Figure 2.5(c) presented the crystallographic relationships between pervoskite τ_1-Ti_3AlN (red line, with Al atoms at corners, Ti at face-center positions and N at body-center positions) and hexagonal α_2-Ti_3Al (black line), indicating that N atoms occupied one of the octahedral interstitial sites of α_2-Ti_3Al in an orderly manner during cooling.

(2) Microstructural development of the AlN/Ti interface

The microstructural development at the AlN/Ti interface at temperatures from 1300° to 1500°C has been described elsewhere.[22] Very different microstructures were obtained after annealing at 1000°C, and the reactions and phase formations at the interface between AlN and Ti at 1000°C are described in the following sections.

(a) Stage 1: formation of the δ-TiN layer

The formation mechanism of the δ-TiN layer has been described in a previous study,[22] and is again schematically illustrated in Fig. 2.6(a). According to the Ti-N binary phase diagram,[4] α-Ti is stable with up to 23 at.% N in solid solution at 1000°C, beyond which there exists a two-phase (α-Ti + δ-TiN) region in the range of 23 – 30 at.% N. This implies that the δ-TiN is not formed until more than 23 at.% N is dissolved in α-Ti at 1000°C. The δ-TiN phase, with an NaCl-like structure, has a non-stoichiometric composition (designated as δ-TiN_{1-x}) in the wide range of 30-55 at.% N. The δ-TiN layer can be thought of as a nitrogen sponge that responds to diffusing nitrogen atoms in the same way as a sponge responds to

water. Essentially, the δ-TiN layer can also be regarded as a "trap" or a "garbage can" for nitrogen atoms at this stage, explaining why the δ-TiN layer growth at the AlN/Ti interface is not evident at 1000°C.

(b) Stage 2: formation of the α_2-Ti_3Al layer

Since the solubility of Al in δ-TiN is rather limited, Al atoms are not dissolved in the δ-TiN layer but diffuse through the δ-TiN layer into Ti, resulting in the formation of α_2-Ti_3Al between δ-TiN and Ti in the second stage, as displayed in Fig. 2.6(b). Excess Al atoms may proceed further beyond the α_2-Ti_3Al layer into Ti, forming an α-Ti(Al) solid solution and probably a two-phase region (α-Ti + β-Ti), according to the Ti-Al-N ternary phase diagram.[25] While Al or N atoms diffuse into β-Ti (A2, bcc) during annealing at 1000°C, the dissolution of up to 5 at.% Al and/or N atoms makes α-Ti (A3, hcp) relatively stable with respect to β-Ti. The α_2-Ti_3Al grows if more than 23 at.% Al is dissolved in α-Ti at 1000°C.

(c) Stage 3: formation of τ_1-Ti_3AlN in the δ-TiN layer

Following the formation of α_2-Ti_3Al, some Al atoms tend to accumulate at the δ-TiN grain boundaries and then react with δ-TiN to form τ_1-Ti_3AlN, as shown in Fig. 2.6(c). The τ_1-Ti_3AlN gradually becomes continuous over a long period. The formation of intergranular τ_1-Ti_3AlN in δ-TiN is given by chemical reaction (1) mentioned above.

The aluminization of the δ-TiN layer gives rise to the formation of intergranular τ_1-Ti_3AlN accompanied with the exsolution of nitrogen. The τ_1-Ti_3AlN is expected to be generated by the nitridization of the α_2-Ti_3Al layer previously formed, but in this stage, the formation obviously proceeds through a different mechanism.

(d) Stage 4: formation of δ-TiN and twinned α_2-$Ti_3Al(N)$ in the α_2-Ti_3Al layer

The excess nitrogen atoms, as described by reaction (1), diffuse into the α_2-Ti_3Al layer and react with α_2-Ti_3Al to become the α_2-$Ti_3Al(N)$ solid solution. As the concentration of N atoms increases, the twinning of α_2-$Ti_3Al(N)$ is triggered, as shown in Fig. 2.3(a). The nitridization of α_2-Ti_3Al also generates δ-TiN in the α_2-Ti_3Al layer, because nitrogen atoms have a high affinity to Ti atoms [Fig. 2.6(d)].

The small interstitial atoms, such as nitrogen and hydrogen, behave very similarly when they are dissolved in α_2-Ti_3Al. Xiao et al.[28] stated that at 373-473 K, deuterium was readily dissolved in α_2-Ti_3Al as a solid solution and that increasing the deuterium concentration to $D/\alpha_2\text{-}Ti_3Al \geq 0.18$ caused the twinning of deuteride with DO_{19}. Additionally, δ-Ti_3AlD_x and twinned deuteride coexisted at $D/\alpha_2\text{-}Ti_3Al \geq 0.59$. It is believed that the phase transformation induced by the dissolution of N atoms in α_2-Ti_3Al corresponds to that induced by the dissolution of deuterium in α_2-Ti_3Al. In this study, the twinned structure was first found in literature at the AlN-Ti interface, and it is comparable to the twinned deuteride in α_2-Ti_3Al as $D/\alpha_2\text{-}Ti_3Al \geq 0.59$.

(e) Stage 5: formation of τ_1-Ti_3AlN in twinned α_2-$Ti_3Al(N)$ during cooling

The high-temperature α_2-$Ti_3Al(N)$ solid solution undergoes an incongruent phase transformation or phase separation during cooling, yielding a high-N phase and a low-N phase. The N atoms in the low-N phase or α_2-$Ti_3Al(N)$ are randomly distributed in an hcp crystal structure, whereas the N atoms in the high-N phase or τ_1-Ti_3AlN occupy one of the octahedral interstitial sites in each unit cell. τ_1-Ti_3AlN and α_2-Ti_3Al have very similar crystal structures, and their crystallographic relationships are as shown in Fig. 2.5(c). However, the

composition of τ_1-Ti_3AlN (60.1 at.% Ti, 19.9 at.% Al, and 20.0 at.% N) differs substantially from that of α_2-$Ti_3Al(N)$ (71.5 at.% Ti, 23.2 at.% Al, and 5.3 at.% N). Notably, the twinning of α_2-Ti_3Al occurs before τ_1-Ti_3AlN is formed, since the twinning will not take place across different phases. Figure 2.6(e) schematically depicts the final microstructure developed at the AlN/Ti interface after cooling.

(3) Diffusion path in the Ti-Al-N ternary phase diagram

The microstructural development at the AlN/Ti interface is related to the diffusion path in the isothermal section of the Al-N-Ti ternary phase diagram.[29] Figure 2.7(a) presents three diffusion paths, represented by the arrowed lines on the isothermal Ti-Al-N phase diagram, in the AlN/Ti diffusion couple upon annealing at 1000°C for various periods. Based on the experimental results, when the diffusion couples of AlN and Ti are isothermally annealed at 1000°C, the diffusion paths associated with the compositions along the longitudinal direction perpendicular to the interface are proposed as follows: (a) A→B→C→H (path 1) for 0.1 h; (b) A→B→C→G→H (path 2) for 0.5 h, and (c) A→B→C→D→E→F→G→H (path 3) for 36 h. It is noted that all diffusion paths do not go through Ti_2N based upon present results. A magnified section of Ti-Al-N ternary phase diagram proposed by Schuster and Bauer[259] are redrawn in the upper right hand corner of Fig. 2.7(a), indicating the coexistence of δ-TiN with τ_1-Ti_3AlN and/or α_2-Ti_3Al in an equilibrium state at 1000ºC. For the case of annealing at 1000°C/36 h, the diffusion path crosses the fields AlN+δ-TiN, δ-TiN, δ-TiN+τ_1-Ti_3AlN, δ-TiN+τ_1-Ti_3AlN+α_2-Ti_3Al, δ-TiN+α_2-Ti_3Al, α_2-Ti_3Al, α_2-Ti_3Al+α-Ti, α-Ti, β-Ti+α-Ti and β-Ti between AlN and Ti. The three-phase region and the tie lines in the two-phase region correspond to the interface between the two reaction layers in the diffusion couple.

Figures 2.7(b) and (c) present the microstructures that developed in the AlN/Ti diffusion couples upon annealing at 1000°C/36 h and subsequent cooling, respectively. The connecting lines delineate the relationship between the microstructure [Fig. 2.7(b)] and the isothermal section of the Ti-Al-N phase diagram [Fig. 2.7(a)]. As displayed in Fig. 2.7(b), the layers of δ-TiN, δ-TiN + τ_1-Ti_3AlN, δ-TiN + twinned α_2-Ti_3Al, α_2-Ti_3Al and Ti (α-Ti, β-Ti + α-Ti, β-Ti, etc.) were formed in sequence from AlN to Ti upon annealing at 1000°C/36 h. Figure 2.7(c) shows the final microstructure, indicating that the twinned α_2-Ti_3Al was transformed to the (α_2-Ti_3Al+τ_1-Ti_3AlN) structure from the two phase region (δ-TiN+α_2-Ti_3Al) during subsequent cooling. β-Ti and β-Ti+α-Ti were absent between α_2-Ti_3Al and α-Ti after cooling, because β-Ti was transformed to α-Ti at the phase transformation temperature (883°C) upon cooling. For other annealing periods, the relationship between microstructural development and diffusion path can be explained in a similar way.

Based upon the foregoing discussion, it was worth mentioning that some new findings were obtained in the present study. For an example, the phase transformation and orientation relations were definitely recognized between δ-TiN and τ_1-Ti_3AlN (or between α_2-Ti_3Al and τ_1-Ti_3AlN) at the AlN/Ti interface on behalf of TEM/EDS works. For the first time, it revealed a twinned α_2-Ti_3Al structure on annealing at 1000°C/10 h, while an ordered cubic τ_1-Ti_3AlN was precipitated from the twinned α_2-Ti_3Al during cooling. This study also illustrated the phase transformation mechanism from α_2-Ti_3Al to τ_1-Ti_3AlN due to the interdiffusion in the AlN/Ti diffusion couple from a crystallographic viewpoint.

2.4 Conclusions

1. The microstructures of various reaction layers in the AlN/Ti diffusion couples after annealing at 1000ºC were thoroughly investigated using analytical SEM and TEM.
2. In the initial stages, one δ-TiN layer was formed between AlN and Ti, and then a α_2-Ti_3Al layer was formed between δ-TiN and Ti.
3. As more Al atoms diffused into the δ-TiN layer, τ_1-Ti_3AlN was formed at the grain boundaries of δ-TiN, together with the exsolution of nitrogen atoms. The orientation relationships of δ-TiN and τ_1-Ti_3AlN were identified as $[111]_{\tau_1-Ti_3AlN} //[111]_{\delta-TiN}$ and $(1\bar{1}0)_{\tau_1-Ti_3AlN} //(1\bar{1}0)_{\delta-TiN}$.
4. The nitridization of the α_2-Ti_3Al layer due to the inward diffusion of the released N gave rise to the formation of δ-TiN and a twinned α_2-$Ti_3Al(N)$ solid solution in the α_2-Ti_3Al layer upon annealing. The α_2-$Ti_3Al(N)$ solid solution was transformed to the chopped fiber-like τ_1-Ti_3AlN structure during subsequent cooling. The orientation relationships of τ_1-Ti_3AlN and α_2-Ti_3Al in the twinned structure were as follows: $[111]_{\tau_1-Ti_3AlN} //[0001]_{\alpha_2-Ti_3Al}$ and $(0\bar{1}1)_{\tau_1-Ti_3AlN} //(\bar{1}\bar{1}20)_{\alpha_2-Ti_3Al}$.
5. Finally, the various stages of the interface reaction between AlN and Ti during annealing and cooling at 1000ºC were proposed. The microstructural development of the AlN/Ti interface was related to the diffusion path in the isothermal section of the Al-N-Ti ternary phase diagram.

Table 2. 1. Summary of some previous studies on the AlN/Ti interfacial reactions

Authors	Type of samples	Annealing conditions	Analyzing instruments	Reaction products	References
He et al.	Ti thick film/AlN thin film or substrate	Annealing at 600º-800ºC for a short time	XRD, XPS, RBS and TEM	$TiAl_3$-TiN-Ti_4N_{3-x}-Ti_2N	13
Imanaka and Notis	Ti thin film/AlN substrate	Annealing at 600º to 950ºC for 2-30 min	RBS, XRD and TEM	Ti_2AlN	12
Pinkas et al.	Ti thin film/AlN thin film	Annealing at 600ºC for 1-10 h in N_2	AES, XRD and TEM	$TiAl_3$-Ti_2N-Ti_3Al-α-$(Ti, Al)_{ss}$	14
Yasumoto et al.	Ti thin film/AlN substrate	Annealing at 700º-950ºC for 60 min	XRD	$TiAl_3$, Ti_2N, TiN	15
Yue et al.	Ti thin film/AlN substrate	Annealing at 200º-850ºC for 1-4 h	SIMS, RBS and XRD	$TiN_{0.3}$, $Ti_3Al_2N_2$, Ti_2AlN, Ti_3Al, TiN and Ti_2N	16
El-Sayed et al.	Ti foil/AlN substrate	Annealing at 1050º to 1200ºC for 2~20 h in vacuum	XRD, SEM and EPMA	TiN-Ti_3AlN-Ti_3Al	17
Han et al.	Ti foil and AlN bulk	Annealing at 1000ºC for 200 h	SEM, XRD and EPMA	TiN-Ti_3AlN	18
Han et al.	Ti powder and AlN powder	Annealing at 1000ºC for 200 h	SEM, XRD and EPMA	TiN-Ti_3AlN-Ti_3Al	18
Paransky et al.	Ti powder and AlN powder	Annealing at 900 and 1100ºC for 1-40 h	SEM/EDS/EBSD, XRD and EPMA	TiN-Ti_3AlN-lamellar (Ti_3AlN+Ti_3Al)-Ti_3Al	19-21
Paransky et al.	Ti bulk and AlN bulk	Annealing at 900 and 1100ºC for 1-40 h	SEM/EDS/EBSD, XRD and EPMA	TiN-Ti_3AlN-lamellar (Ti_3AlN+Ti_3Al)-Ti_3Al	21
Paransky et al.	Ti powder and AlN bulk	Annealing at 900 and 1100ºC for 1-40 h	SEM/EDS/EBSD, XRD and EPMA	TiN-$(Ti)_{Ak}$	21
Chiu and Lin	Ti bulk and AlN bulk	Annealing at 1300º-1500ºC/0.5-36 h	SEM/EDS and TEM/EDS	TiN-Ti_2AlN-Ti_3AlN-Ti_3Al-two phase (Ti_3Al+Ti) at 1300ºC TiN-Ti_2AlN-TiAl-lamellar (TiAl+Ti_3Al)-Ti_3Al-two phase (Ti_3Al+Ti) at 1400ºC TiN-Ti_2AlN- lamellar (TiAl+Ti_3Al) -Ti_3Al-two phase (Ti_3Al+Ti) at 1500ºC	22

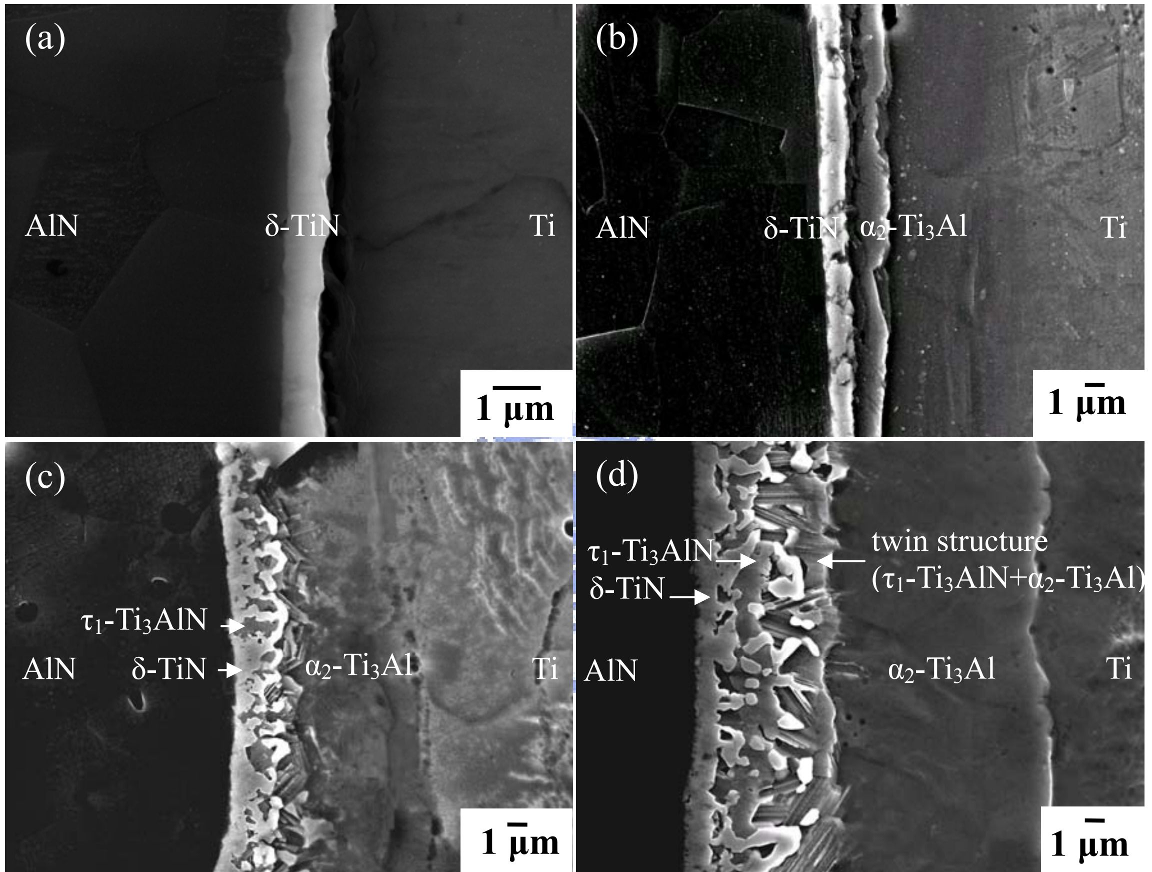

Fig. 2. 1. SEM micrographs showing the AlN/Ti interfaces after annealing at 1000 °C for (a) 0.1 h; (b) 0.5 h; (c) 3 h; (d) 36 h, respectively.

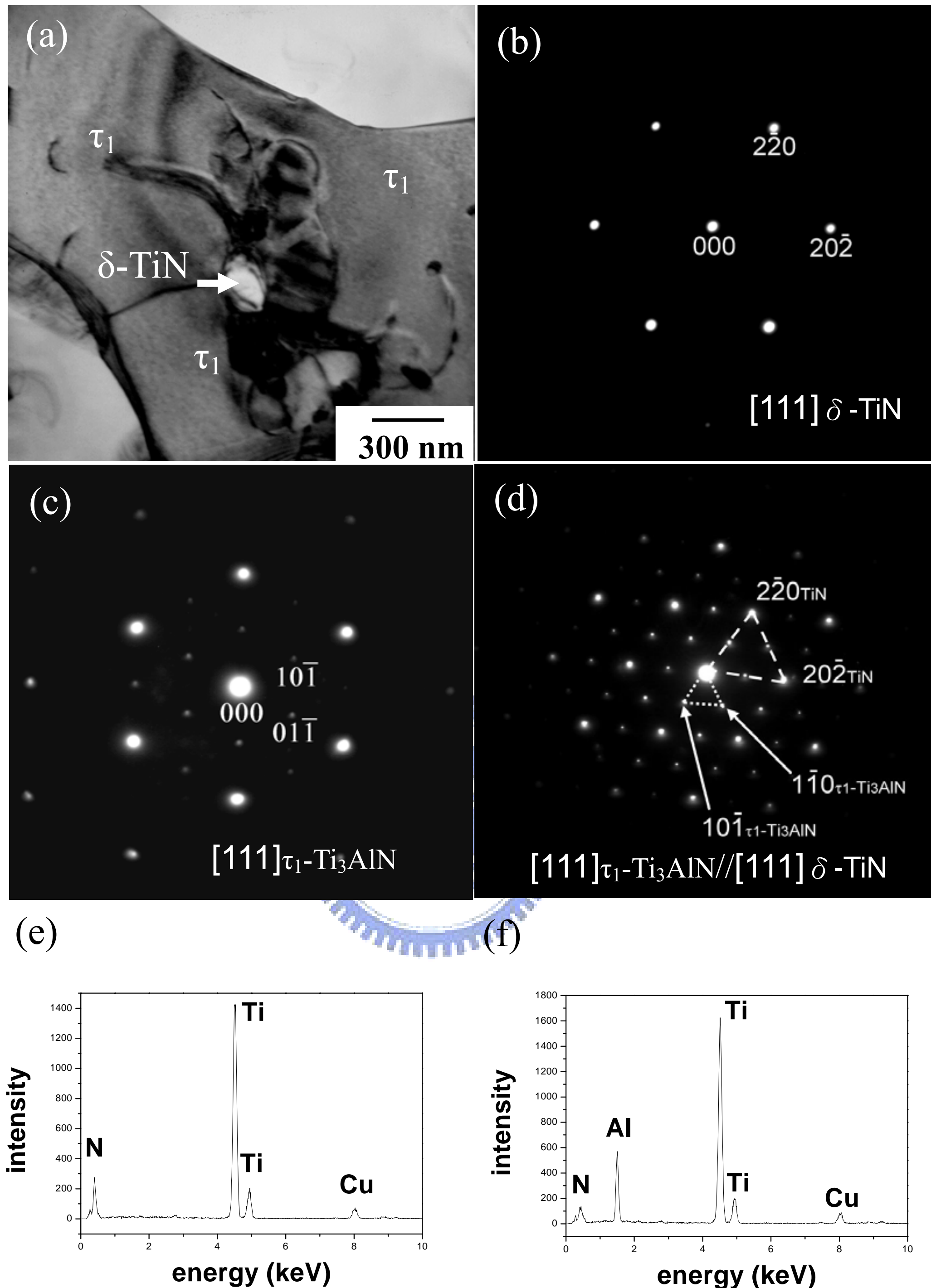

Fig. 2. 2. (a) A bright field image of the residual δ-TiN phase in τ_1-Ti_3AlN after annealing at 1000°C/10 h; (b) an SADP of δ-TiN, z=[111]; (c) an SADP of τ_1-Ti_3AlN, z=[111]; (d) the SADPs of τ_1-Ti_3AlN and δ-TiN, showing the orientation relationships of $[111]_{\tau_1-Ti_3AlN}//[111]_{\delta-TiN}$ and $(1\bar{1}0)_{\tau_1-Ti_3AlN}//(1\bar{1}0)_{\delta-TiN}$; (e) the EDS spectrum of δ-TiN; (f) the EDS spectrum of τ_1-Ti_3AlN.

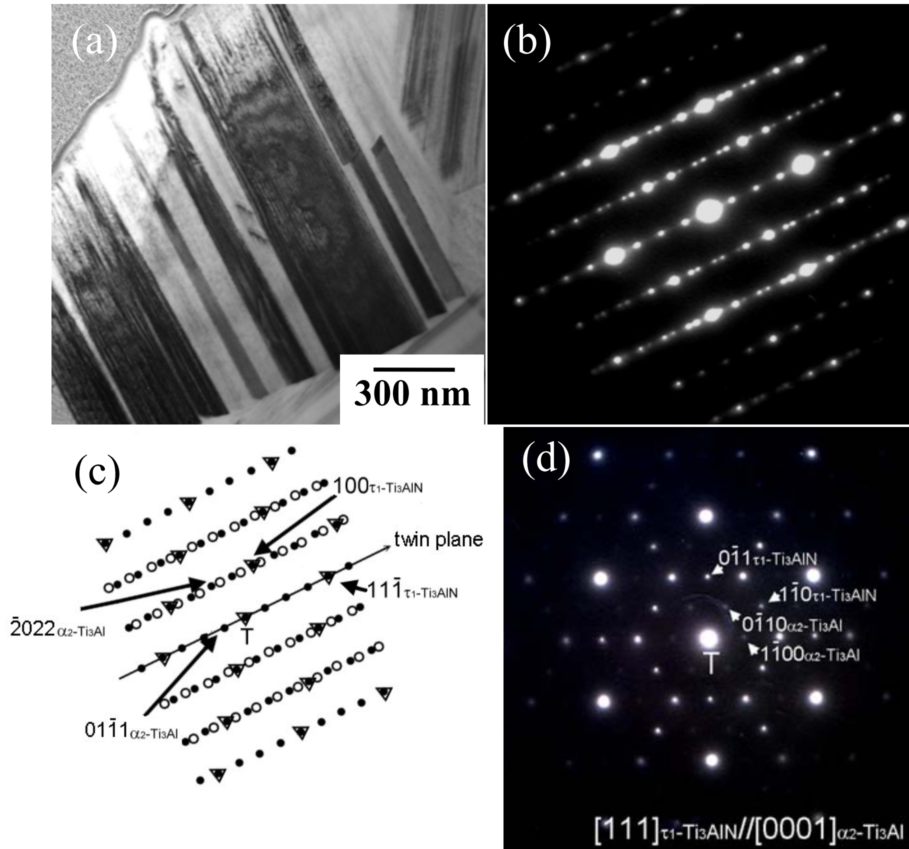

Fig. 2. 3. After annealing at 1000°C/10 h: (a) the bright field image of the (τ_1-Ti_3AlN + α_2-Ti_3Al) twinned structure; (b) the SADPs of τ_1-Ti_3AlN (z=$[1\bar{1}01]$) and α_2-Ti_3Al (z=$[011]$) with the orientation relationships $[011]_{\tau_1-Ti_3AlN}//[1\bar{1}01]_{\alpha_2-Ti_3Al}$ and $(100)_{\tau_1-Ti_3AlN}//(1\bar{1}0\bar{2})_{\alpha_2-Ti_3Al}$; (c) the schematic illustration of the SADPs in (b) (●: α_2-Ti_3Al matrix, ○: α_2-Ti_3Al twin, Δ: τ_1-Ti_3AlN); (d) the SADPs of τ_1-Ti_3AlN (z= $[111]$) and α_2-Ti_3Al (z= $[0001]$) with the orientation relationships $[111]_{\tau_1-Ti_3AlN}//[0001]_{\alpha_2-Ti_3Al}$ and $(0\bar{1}1)_{\tau_1-Ti_3AlN}//(\bar{1}\bar{1}20)_{\alpha_2-Ti_3Al}$.

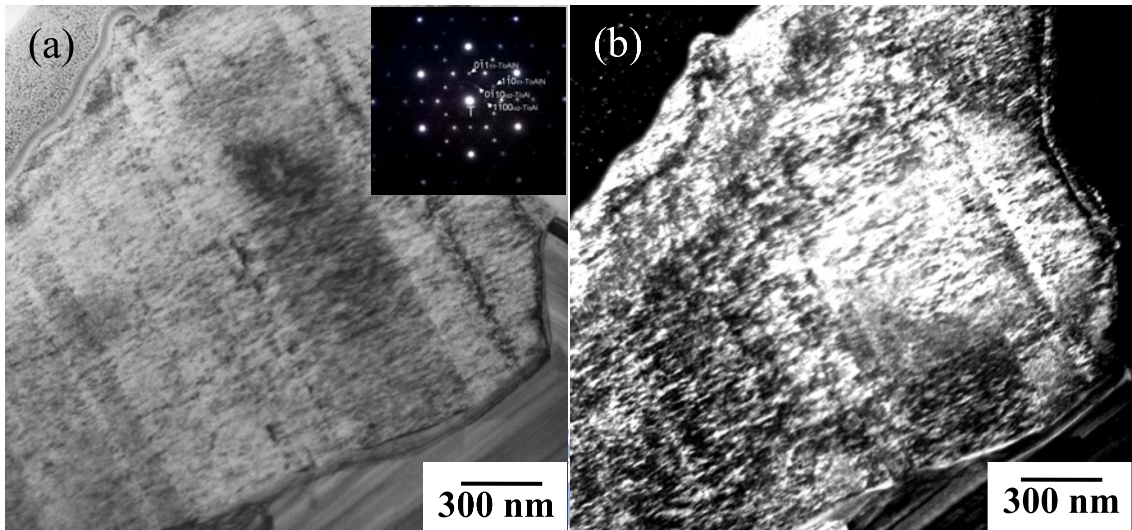

Fig. 2. 4. After annealing at 1000°C/10 h: (a) the bright field image of the (τ_1-Ti_3AlN+α_2-Ti_3Al) twinned structure; (b) the central dark field (CDF) image of the (τ_1-Ti_3AlN+α_2-Ti_3Al) twinned structure formed by the diffraction spot $(0\bar{1}10)$ of α_2-Ti_3Al.

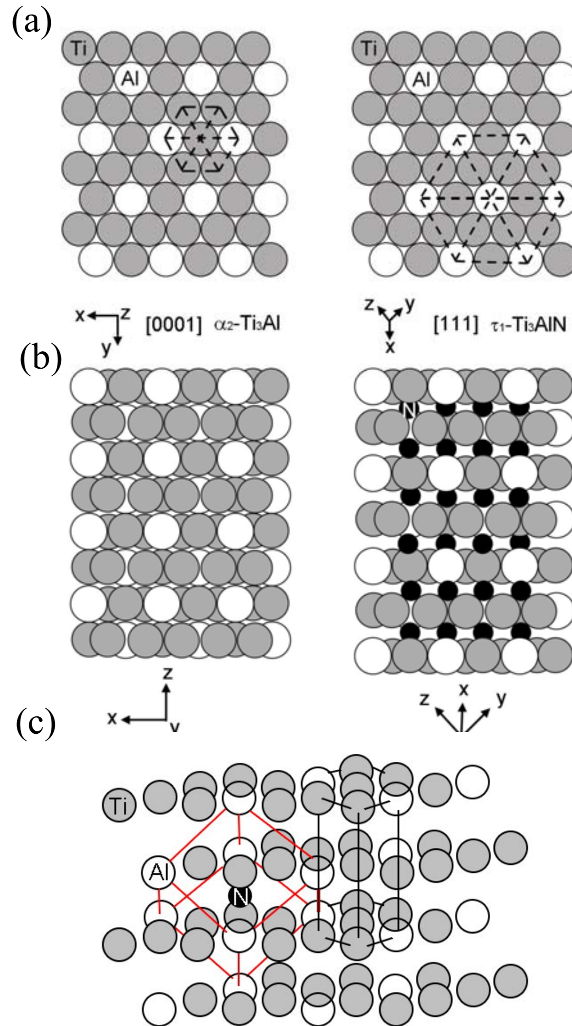

Fig. 2. 5. **(a)** Crystal structures of α_2-Ti_3Al and τ_1-Ti_3AlN projected along the $[0001]_{\alpha-Ti_3Al}$ or $[111]_{\tau_1-Ti_3AlN}$ direction; (b) the stacking sequence of closely packed planes viewed along $[01\bar{1}0]_{\alpha_2-Ti_3Al}$ or $[1\bar{2}1]_{\tau_1-Ti_3AlN}$; (c) the lattice relationship of the cubic τ_1-Ti_3AlN (red line) and the hexagonal α_2-Ti_3Al (black line).

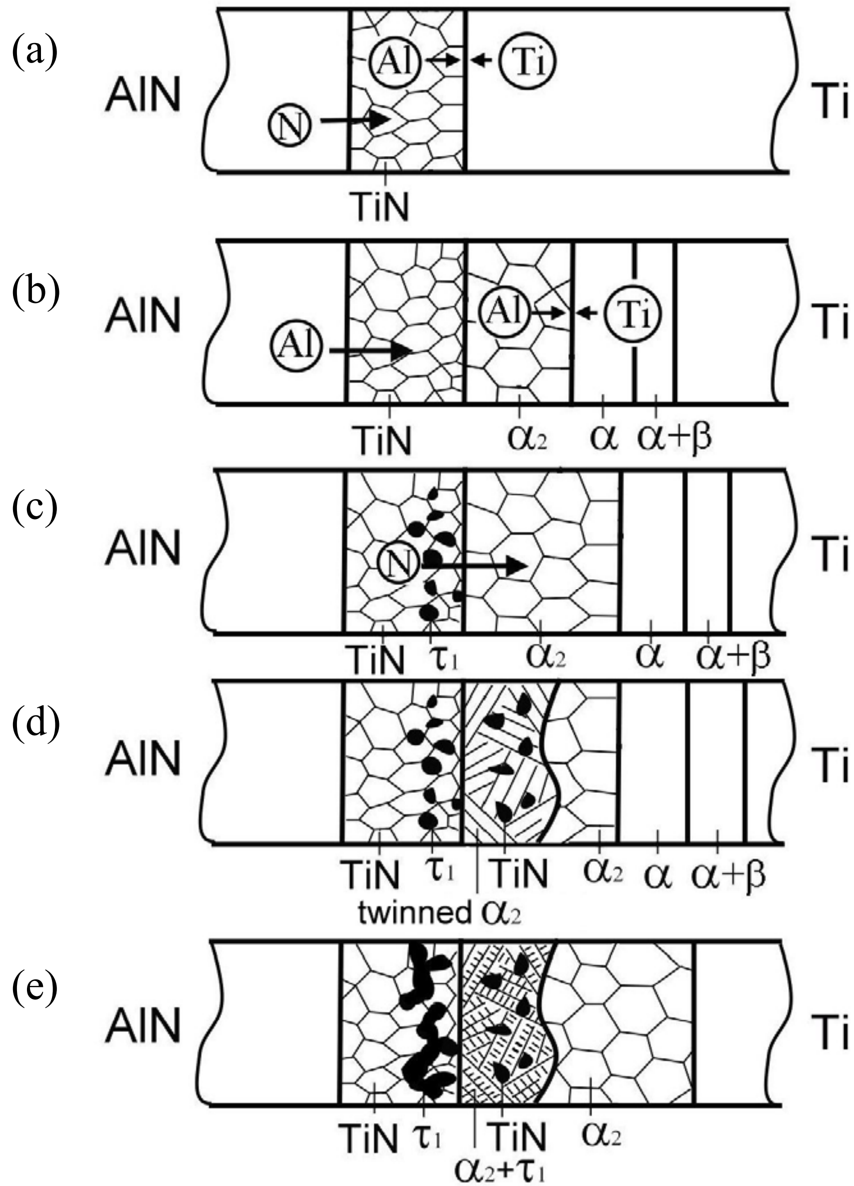

Fig. 2. 6. Microstructural development in the AlN/Ti diffusion couple after annealing at 1000°C for 0.1-36 h; (a) formation of the δ-TiN layer; (b) formation of the α_2-Ti_3Al layer and various titanium aluminides; (c) formation of τ_1-Ti_3AlN in the δ-TiN layer; (d) formation of δ-TiN and twinned α_2-Ti_3Al due to the nitridization of the α_2-Ti_3Al layer; (e) formation of (τ_1-Ti_3AlN+α_2-Ti_3Al) twinned structure during cooling.

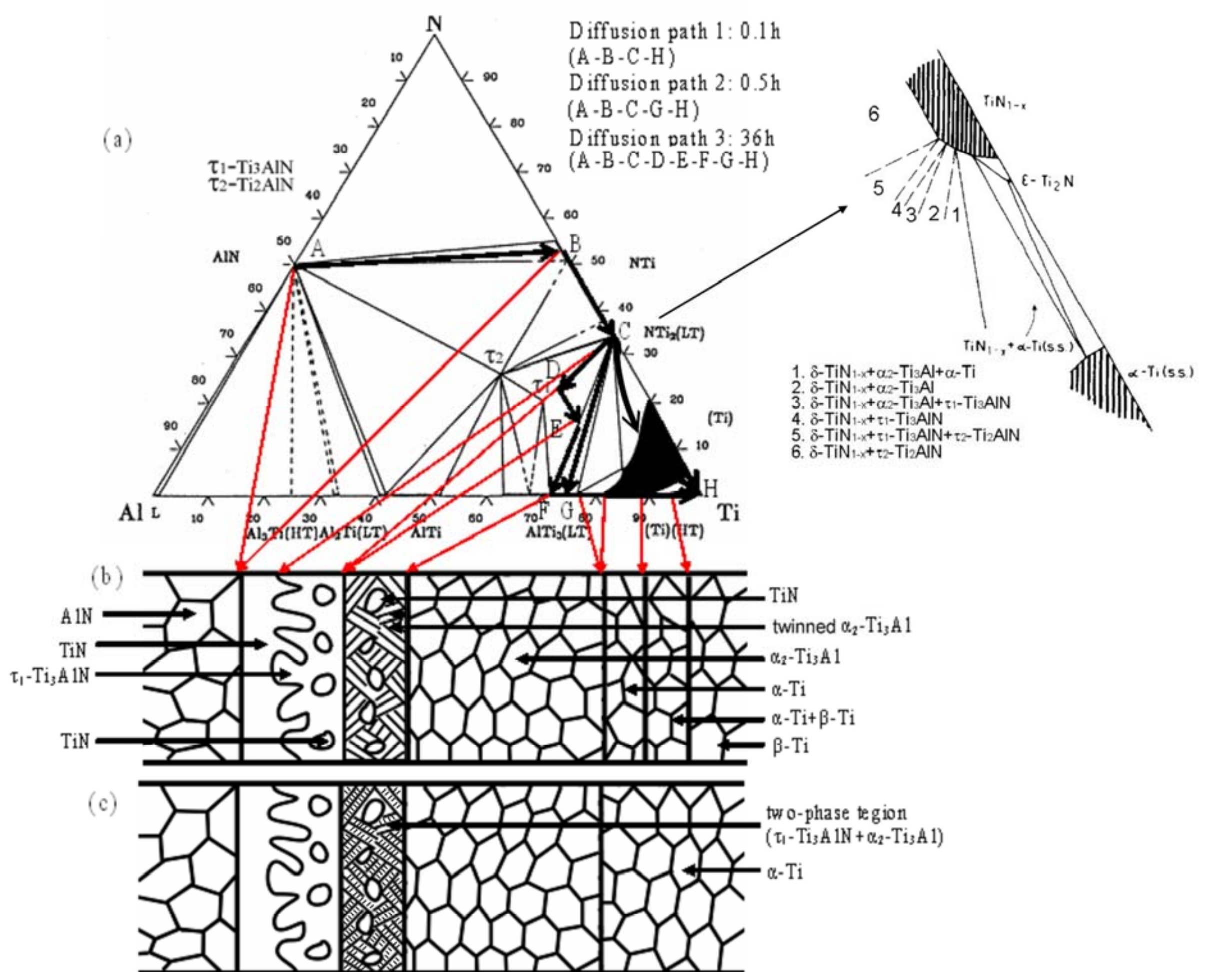

Fig. 2. 7. (a) An isothermal section of the Ti-Al-N system at 1000°C, and the diffusion paths (path 1: A-B-C-H for 0.1h; path 2: A-B-C-G-H for 0.5h; path 3: A-B-C-D-E-F-G-H for 36h); (b) Schematic microstructure at the AlN/Ti interface on annealing at 1000°C/36h; (c) Schematic microstructure of the AlN/Ti interface after cooling.

Chapter 3 Microstructural Characterization and Phase Development at the Interface between Aluminum Nitride and Titanium after Annealing at 1300°–1500°C

3.1 Introduction

Aluminum nitride has been considered one of the most promising substrate materials for use in semiconductor, microwave, optic, electronic and other high performance applications, because of its high thermal conductivity (≈ 320 W/m·k), low dielectric constant (≈ 8.8), high electric resistivity (≦ 10^{12} ~ 10^{14} Ω·cm), and coefficient of thermal expansion similar to that of silicon.[1, 30, 31] Meanwhile, Ti is a highly active metal and easily reacts with almost all ceramics,[16, 32-37] and a high adhesion or bond strength can be achieved by the interface reactions between titanium and the substrate materials. In some applications for microelectronics such as ceramic packaging and metallization,[38-42] where aluminum nitride is placed in direct contact with titanium, the interfacial properties of AlN and Ti are crucial in determining the quality and reliability of electric package and its high temperature applications.

Previous investigations on the interfacial reaction of AlN and Ti are very limited, most of them concerning the reaction of AlN with Ti thin films[7, 12, 15, 43, 44] or Ti-containing brazing foils.[45-47] While available data on the microstructure of the AlN-Ti interfacial reaction zone are often controversial, it is imperative to explore the interdiffusion reactions and mechanisms in the AlN/Ti bonding process in order to make more effective use of AlN and Ti as well.

Some previous studies regarding the thin-film metallization of AlN have been published.[7, 12, 15, 43, 44] As far as the interface reaction between the Ti thin film and the AlN substrate was concerned, Westwood and Notis[43, 44] found the

formation of δ-TiN and $TiAl_3$ at the interface after annealing at 600ºC for 30 min in oxygen-free sample. He et al.[13] investigated the interface reactions of Ti thin films with AlN substrate in the temperature range of 600° to 800°C using x-ray diffractometry (XRD) and Ruthford backscattering spectroscopy (RBS). They indicated that the $TiAl_3$ phase was formed at the interface adjacent to the AlN substrate, while δ-TiN, Ti_4N_{3-x}, and Ti_2N were formed above the $TiAl_3$ layer. Yasurnoto et al.[15] deposited a Ti thin film on AlN with radio frequency (rf) sputtering, revealing that under an argon atmosphere, $TiAl_3$ was formed at 700ºC for 60 min, and $TiAl_3$, Ti_2N, and δ-TiN were detected after annealing at 830ºC for 60 min by using XRD. In the study of the interdiffusion and reaction of Ti (thin film) and AlN (substrate) using RBS and transmission electron microscopy (TEM), Imanaka and Notis[12] found τ_2-Ti_2AlN at the interface after annealing at 800°-950ºC. Recently, Pinkas et al.[14] worked on the early stages of interface reactions between Al and Ti thin films after annealing at 600°C for 1-10 h. They claimed that the AlN decomposed at the AlN/Ti interface and its products, Al and N, reacted with Ti to produce an AlN/Al_3Ti/Ti_2N/Ti_3Al/α-(Ti, Al)$_{ss}$ phase sequence.

As for the brazing of AlN,[45-47] Carim and Loehman[45] reported that continuous δ-TiN and (Ti, Cu, Al)$_6$N at the interface of AlN and Ag-Cu-Ti foil were formed after annealing at 900ºC for 5-30 min. By using TEM and electron probe microanalysis (EPMA), Loehman and Tomsia[46, 47] indicated that $TiN_{0.7}$ was detected at the interface of AlN and Ag-26.7Cu-4.5Ti after reaction at 900ºC for 30 min in an argon atmosphere.

Among other previous studies on the interfacial reaction of AlN and Ti, El-Sayed et al.[17] characterized the reaction zone microstructure of AlN/Ti (20 or 50 μm thick)/AlN joints after annealing at 1050°-1200ºC for 2-20 h in vacuum. The reflection peaks of δ-TiN, τ_2-Ti_2AlN, τ_1-Ti_3AlN, and α_2-Ti_3Al, were

observed in the X-ray diffraction spectra taken from the fracture surfaces of annealed joints. Up to 1200°C for 20 h, both δ-TiN_{1-x} and τ_1-Ti_3AlN did not grow significantly, but the growth kinetics of α_2-Ti_3Al followed the parabolic law. Paransky et al.[20, 21, 23] investigated the interfacial reactions between AlN particles and the Ti matrix, as well as AlN-Ti diffusion couples, after annealing in the temperature range from 900° to 1100°C using energy-dispersive spectroscopy (EDS) and electron back-scattered diffraction (EBSD) attached in an scanning electron microscopy (SEM). A phase sequence of δ-TiN, $Ti_3Al_{0.8}N_{0.8}$, and α_2-Ti_3Al was observed at the interface of Ti and AlN. While the binary nitride δ-TiN and the ternary nitride τ_1-Ti_3AlN exhibited a complex interpenetrating morphology, a lamellar two-phase region was also observed between τ_1-Ti_3AlN and α_2-Ti_3Al layers after annealing at 1000° and 1100°C.

Many applications of the industrial AlN/Ti joints, such as metallization, brazing, and composites mentioned above, are determined by the characteristics of the interface between AlN and Ti. In the last few decades, extensive studies have been carried out on the interface reaction between aluminum nitride and titanium. However, the microstructure evolution at the interface has not been elucidated to date, even though fundamental understanding of reaction and diffusion mechanisms is of great importance for industrial applications and scientific meaning.

The present study is devoted to the microstructural characterization of the interfacial reaction zone in AlN and Ti diffusion couples after annealing at temperatures ranging from 1300° to 1500ºC by SEM/EDS and TEM/EDS. We will try to explain the microstructural development at the Ti/AlN interface on the basis of the ternary Al-Ti-N phase diagram and the diffusion paths that connect the phases formed by the reaction between AlN and Ti. The present study is to expect to contribute to the understanding of the ternary Ti-Al-N system at high

temperatures and to aid in the processing of ceramic-metal joints.

3.2 Experimental Procedure

Highly pure AlN plates (SH-15, Tokuyama Soda Corp., Japan) and Cp-Ti plates (99.7% purity, Alfa Aesar, Ward Hill, MA) were used in this study. All the plates (about 15 x 10 x 4 mm in dimension) were ground with a diamond (15 μm) matted disk and then polished with the diamond paste (3 μm) and an alumina suspension (1μm) using a precision polishing machine (Model Minimet 1000, Buehler Ltd, Lake Bluff, IL). The specimens were then rinsed in acetone (ultrasonic bath) and distilled water, and then air-dried.

In order to characterize the microstructure of the Ti/AlN interface, samples were prepared as a sandwich mode with the Ti metal placed in between two pieces of AlN. Then, the samples were annealed in an argon atmosphere (with $O_2 < 1$ ppm, $H_2O < -76$ ppm, THC < 0.5 ppm and $N_2 < 3$ ppm) under a pressure of 2 MPa at temperatures ranging from 1300° to 1500°C with holding time from 0.5 to 36 h, and then the specimen was continuously cooled down to room temperature at a rate of 10°C/min.

The cross-sectional TEM and SEM samples were prepared as follows: each annealed sample was cut into two halves in a direction perpendicular to the interface of AlN/Ti, and then ground and polished by the standard procedures as mentioned above. The samples were etched with the Kroll reagent (10 mL HF + 30 mL HNO_3 + 60 mL H_2O) in order to emphasize the features of different phases and to remove the deformed surface layer. Thereafter the samples were rinsed in acetone (ultrasonic bath) and distilled water, and then air-dried. To avoid charging, all the SEM samples were coated with a thin layer of platinum (finished preparation of SEM samples). The cross-sectional slab was ground down to an 80~100 μm thickness using a precision polishing machine, then the

sample was thinned to 20~30 μm by dimpling, and finally argon ion milled at 5 kV and 20 μA (finished preparation of TEM samples).

Microstructural characterization of the cross-sections of AlN/Ti was carried out using a high-resolution scanning electron microscope (Model JSM-6500, JEOL, Tokyo, Japan) and an analytical TEM (Model 2000Fx, JEOL, Tokyo, Japan). The Cliff–Lorimer standardless technique was used to analyze the compositions of the various phases. The technique was performed on the TEM, equipped with an ultra-thin window EDS detector (Model 9900, EDAX International, Prairie View, IL). A conventional ZAF correction procedure included in the LINK ISIS software was used for the quantitative analyses.

3.3 Results and Discussion

The products formed in the AlN/Ti interfacial reaction zone are listed in Table 3.1, after annealing at 1300°-1500°C for various periods. The reaction zone consisted of δ-TiN, τ_2-Ti_2AlN, τ_1-Ti_3AlN, α_2-Ti_3Al, and a two-phase (α_2-Ti_3Al + α-Ti) region in sequence after annealing at 1300°C. The γ-TiAl and a lamellar two-phase (γ-TiAl + α_2-Ti_3Al) structure were found instead of τ_1-Ti_3AlN in between τ_2-Ti_2AlN and α_2-Ti_3Al after annealing at 1400°C. In comparison with the results after annealing at 1400°C, γ-TiAl was not formed at the interface after annealing at 1500°C. It was noted that there were some exceptions for the initial transition stage. For instance, no τ_2-Ti_2AlN had been found after annealing at 1350°C for 0.5 h, while γ-TiAl and the lamellar two-phase (γ-TiAl + α_2-Ti_3Al) layer did not existed after annealing at 1400°C for 0.5 h, whereas a layer of γ-TiAl was found after annealing at 1500°C for 0.5 h. In contrast to the reaction of AlN and α-Ti thin films annealed at lower temperatures (e.g., 600°-800°C),[13, 14] no $TiAl_3$ was found in the present study.

(1) SEM/EDS analyses

Figure 3.1 shows the secondary electron images (SEI) of the cross-sectional microstructures of the AlN/Ti diffusion couples after annealing at various temperatures for 36 h. Fig. 3.1(a) displays that the reaction zone between AlN and Ti consists of δ-TiN, τ_2-Ti_2AlN, τ_1-Ti_3AlN, α_2-Ti_3Al and a two-phase (α_2-Ti_3Al + α-Ti) region in sequence after annealing at 1300°C for 36 h. The microstructure of AlN/Ti after annealing at 1400°C for 36 h is demonstrated in Fig. 3.1(b), which displayed the reaction phase sequence of δ-TiN/τ_2-Ti_2AlN/γ-TiAl/(γ-TiAl + α_2-Ti_3Al)/α_2-Ti_3Al/(α_2-Ti_3Al + α-Ti). The γ-TiAl layer and lamellar structure (γ-TiAl + α_2-Ti_3Al), instead of τ_1-Ti_3AlN, were formed between the τ_2-Ti_2AlN and α_2-Ti_3Al,. Fig. 3.1(c) displays the reaction phase sequence of δ-TiN/τ_2-Ti_2AlN/(γ-TiAl + α_2-Ti_3Al)/ α_2-Ti_3Al/(α_2-Ti_3Al + α-Ti). The TiAl layer was not found at the interface after annealing at 1500°C for 36 h as mentioned above.

El-Sayed et al.[17] found that the sequence of reaction layer was AlN/δ-TiN/τ_1-Ti_3AlN/α_2-Ti_3Al/α-Ti. However, they did not observe the lamellar two-phase (γ-TiAl + α_2-Ti_3Al) and (α_2-Ti_3Al + α-Ti) layers. Paransky et al.[20, 21, 23] showed that the sequence of δ-TiN, τ_1-Ti_3AlN and α_2-Ti_3Al was formed at the interface of Ti (matrix) and AlN (particle) and that the δ-TiN and τ_1-Ti_3AlN exhibited a complex interpenetrating morphology. Furthermore, a lamellar two-phase region was also observed between τ_1-Ti_3AlN and α_2-Ti_3Al layers after annealing at 1000° and 1100°C. However, in the present study, τ_2-Ti_2AlN and a two-phase (α_2-Ti_3Al + α-Ti) region existed at the interface after annealing at 1300°C, while γ-TiAl and a lamellar structure (γ-TiAl + α_2-Ti_3Al) were found in the interface at 1400°C. In the temperature range used in this study, two lamellar layers were found: one layer (α-Ti + α_2-Ti_3Al) was developed because of the precipitation of α_2-Ti_3Al from α-Ti; the other layer (α_2-Ti_3Al + γ-TiAl) was formed because of the eutectoid reaction

($\alpha - Ti \rightarrow \alpha_2 - Ti_3Al + \gamma - TiAl$) during cooling.

In Fig. 3.1, the nitride layers, e.g., δ-TiN, τ_2-Ti_2AlN, and τ_1-Ti_3AlN, were so brittle that there were cracks in these layers. The crack formation was attributed to the mismatch of thermal expansion coefficients (CTE) between aluminium nitride and titanium, resulting in a significant residual thermal stress.

It was also noted that there existed some pores in aluminide layers (i.e., γ-TiAl, α_2-Ti_3Al, etc.) of the reaction zone. These pores were caused because of the formation of nitrogen bubbles during cooling. A significant amount of nitrogen was dissolved in aluminide layers on heating. However, the solubilities of nitrogen in aluminide layers sharply decreased with decreasing temperature, so that nitrogen was supersaturated. The nitrogen bubbles were thus precipitated through a nucleation and growth mechanism like the gas bubble formation commonly encountered in the casting of alloys. It is worth noting that the decrease in the solubility of nitrogen, not the solubility itself, gave rise to the precipitation of nitrogen bubbles or pores during cooling. That is the reason why nitrogen bubbles primarily existed in α_2-Ti_3Al, although the solubility of nitrogen in α_2-Ti_3Al is much larger than that in γ-TiAl. Like the existence of spherical oxygen bubbes in Ti because of the Ti/ZrO_2 interfacial reaction,[48] nitrogen bubbles were formed in α-Ti even though the α-Ti is capable of dissolving a large amount of oxygen. On comparisoning Fig. 3.1(a)-(c), it was concluded that the amount of bubbles increased with annealing temperature.

(2) TEM/EDS analyses

Figure 3.2(a) shows the bright-field (BF) image of the AlN/Ti interface after annealing at 1300°C for 3 h, showing the phases of δ-TiN, τ_2-Ti_2AlN, τ_1-Ti_3AlN, and α_2-Ti_3Al. Note that the two-phase (α_2-Ti_3Al + α-Ti) region has not been shown in Fig. 3.2(a). As shown in Fig. 3.2(b), the selection area diffraction

pattern (SADP) of δ-TiN was indexed as a cubic unit cell with lattice parameters of a = 0.426nm. The TEM/EDS analyses revealed that the layers of τ_2-Ti_2AlN and τ_1-Ti_3AlN were ternary compounds with the approximate composition Ti:Al:N = 2:1:1 and Ti:Al:N = 3:1:1, respectively. The first extensive study of phase equilibria in the Ti-Al-N system was conducted by Schuster and Bauer,[25] with two isothermal sections at 1000° and 1300°C being published. Recently, Pietzka and Schuster[49] showed that three ternary nitride phases $Ti_3Al_2N_2$, τ_2-Ti_2AlN_{1-x} and τ_1-Ti_3AlN_{1-x}.are present in a much more detailed section at 1300°C. The SADPs of τ_2-Ti_2AlN and τ_1-Ti_3AlN are shown in Figs. 3.2(c) and (d), respectively. On indexing these SADPs, it was found that τ_2-Ti_2AlN had a hexagonal crystal structure with the lattice parameters a = 0.299 nm, c = 1.361 nm, while the τ_1-Ti_3AlN was indexed to be a cubic unit cell with lattice parameters of a = 0.4284nm.

The α_2-Ti_3Al layer, as shown in Figs. 3.1(a) and 3.2(a), displayed two distinct features, whose BF images are displayed in Figs. 3.3(a) and (b), respectively. The α_2-Ti_3Al layer had two different morphologies, i.e. equiaxed α_2-Ti_3Al and elongated α_2-Ti_3Al. Both equiaxed α_2-Ti_3Al and elongated α_2-Ti_3Al had the same crystal structure but with different compositions (the Al concentration ranging from 22 to 39 at%). The equiaxed structure marked "A" in Fig. 3.3(a) was corresponding to the regions also marked as "A" in Figs. 3.1(a) and 3.2(a), respectively. In the same way, the elongated texture structure marked "B" in Fig. 3.3(b) was corresponding to the regions both marked as "B" in Figs. 3.1(a) and 3.2(a). The EDS quantitative analyses indicated the equiaxed α_2-Ti_3Al in Fig. 3.3(a) and elongated α_2-Ti_3Al in Fig. 3.3(b) were 66.90 at% Ti, 25.07 at% Al, 8.03at% N and 62.21 at% Ti, 23.42 at% Al, 14.37at% N, respectively. The elongated α_2-Ti_3Al grains in Fig. 3.3(b) were well aligned nearly perpendicular to the interface of AlN/Ti. As Al and N diffuse much faster than Ti, the Ti region will be subjected to a state of compression because of the interdiffusion.

However, the fact that the equiaxed α_2-Ti_3Al became elongated along the direction perpendicular to the interface is attributed to the mismatch in the thermal expansion coefficient between AlN and Ti.

Based upon our TEM investigation, the equiaxed α_2-Ti_3Al was not randomly oriented, because it displayed the same contrast when the specimen was tilted. The equiaxed α_2-Ti_3Al in Fig. 3.3(a) was likely to be formed by recrystallization. Previous studies have reported that the α_2-Ti_3Al alloys could exhibit admirable superplasticity of elongation greater than 1200% at temperatures between 960-1000°C and strain rates between 10^{-4}-10^{-5} s^{-1}.[50, 51] It is believed that the large deformation of textured α_2-Ti_3Al is likely to trigger the recrystallization. Figure 3.3(c) displays the variation in the grain sizes of α_2-Ti_3Al along the direction from the AlN side (bottom) to the Ti side (top). The grain size varies from 150 nm to 450 nm, implying the different degrees of grain growth after recrystallization. When the α_2-Ti_3Al, with a deformation texture, was recrystallized, the new equiaxed grains usually had a preferred orientation.[52] However, the orienatation of the equiaxed α_2-Ti_3Al was different from that of the textured α_2-Ti_3Al. The SADP, as shown in Fig. 3.3(d), revealed that the orientation relationship of the equiaxed and the elongated α_2-Ti_3Al should be as follows: $[0001]_{equiaxed} // [\bar{1}100]_{elongated}$ and $(\bar{1}010)_{equiaxed} // (\bar{1}\bar{1}22)_{elongated}$. The fact that the exquiaxed α_2-Ti_3Al had a recrystallization texture was because of the influence that the texture of the α_2-Ti_3Al had on the nucleation and/or growth of the new grains.

Figure 3.4(a) and (b) show the bright and dark field images of the two-phase (α_2-Ti_3Al + α-Ti) layer near the Ti-side, respectively. In Fig. 3.4(b), it can be seen that α-Ti is distributed along the grain boundaries of α_2-Ti_3Al. The lattice parameters of α-Ti, calculated from the SADPs in Fig. 3.4(c), were a = 0.310 nm and c = 0.441 nm, while those of α_2-Ti_3Al were a = 0.605 nm and c = 0.487 nm.

The a value of α_2-Ti_3Al was approximately twice that of α-Ti. It was inferred that the α_2-Ti_3Al was precipitated in the matrix of α-Ti. From the SADPs, where the superlattice diffraction spots of α_2-Ti_3Al were clearly observed, the α_2-Ti_3Al precipitates were found to satisfy the following orientation relationship with respect to α-Ti: $[0001]_{\alpha-Ti} // [0001]_{Ti_3Al}$ and $(1\bar{1}00)_{\alpha\text{-Ti}} // (1\bar{1}00)_{Ti_3Al}$. The orientation relations are schematically demonstrated in Fig. 3.4(d).

According to the Ti-Al binary phase diagram,[4] α_2-Ti_3Al was stable up to 1210°C, being a nonstoichiometric compound with a relatively wide range extending from 23 to 35 at.%. It seemed that α_2-Ti_3Al could only be formed during isothermal annealing below 1210°C. However, the α_2-Ti_3Al phase was formed after isothermal annealing at temperatures higher than 1300°C, as mentioned previously. It implied that the α_2-Ti_3Al precipitated from α-Ti during cooling. The existence of (α-Ti + α_2-Ti_3Al), α_2-Ti_3Al, or (α_2-Ti_3Al + γ-TiAl) various aluminide layers in the reaction zone of the AlN-Ti diffusion couple, which was isothermally annealed above 1300°C, can be explained by a modified Ti-Al binary phase diagram, and will be described afterwards.

Figure 3.5(a) shows the BF image of the AlN/Ti interfacial reaction zone after annealing at the 1500°C for 0.5 h, showing τ_2-Ti_2AlN, γ-TiAl and the two-phase (γ-TiAl + α_2-Ti_3Al) layer. The inset on the upper right corner shows the SADP of γ-TiAl with the zone axis of [110]. The (γ-TiAl + α_2-Ti_3Al) lamellar structure is displayed at a higher magnification in Fig. 3.5(b). The two-phase (γ-TiAl + α_2-Ti_3Al) region usually forms a lamellar morphology consisting of colonies of thin parallel α_2-Ti_3Al and γ-TiAl platelets. Based upon the Ti-Al phase diagram, the lamellar structure resulted from the eutectoid reaction of $\alpha \rightarrow \alpha_2 + \gamma$. From the SADPs of the lamellar structure (Fig. 3.5(c)) and its corresponding schematic diagram (Fig. 3.5(d)), the orientation relationship of

γ-TiAl and α_2-Ti_3Al was identified: $[011]_{TiAl} // [2\bar{1}\bar{1}0]_{Ti_3Al}$ and $(1\bar{1}\bar{1})_{TiAl} // (01\bar{1}0)_{Ti_3Al}$. In addition, the schematic SADP patterns in Fig. 3.5(d) show some extra spots caused by the structure of twinning in tetragonal crystals of γ-TiAl. The matrix of γ-TiAl was oriented with its [011] zone axis parallel to the electron beam, while the twinning plane $(1\bar{1}1)$,was in the edge-on direction along the electron beam. The diffraction patterns of the matrix and the twin were related by a mirror reflection across the $(1\bar{1}1)$ twinning plane or by a rotation of 180° around the normal to the twinning plane.

(3) Microstructural development and diffusion path at 1300°C

When Ti comes into contact with AlN, the system becomes unstable. It is generally acknowledged that the interfacial reactions between Ti and AlN include the following steps. AlN is reduced under the effect of Ti at the annealing temperature. The decomposed Al and N atoms then diffuse into the Ti; and they react with each other to produce binary or ternary nitrides and aluminides. While the nitrides are stable during the subsequent cooling, the aluminides will be subjected to phase transformation based on the Ti-Al binary phase diagram.

Figure 3.6 illustrates the relationship between the Ti-Al-N phase diagram[25] and the microstructure developed in the Ti/AlN diffusion couple, which was isothermally annealed at 1300°C. Figure 3.6(a) illustrates the isothermal section of the Ti-Al-N ternary phase diagram at 1300°C. Based on experiment results, it is proposed that the diffusion path, indicative of the compositions along the longitudinal direction perpendicular to the interface, was A-B-C-D-E-F-G-H when the diffusion couple was annealed at 1300°C.

It is worth noting that the diffusion path is deviated from the ideal direct path between the compositions of the end points, i.e., Ti and AlN, as the diffusion velocities of the Ti, Al, and N atoms are significantly different in the Ti-AlN diffusion couple. The radii of N, Ti, and Al atoms are 0.07, 0.1448, and 0.1431 nm, respectively, so that N atoms, diffusing interstitially in the Ti, should have a higher diffusion velocity that that of Al atoms which diffuse mainly by substitution. In the literature, the diffusion coefficient of Al and N atoms in Ti are reported to be 7.4×10^{-7} cm^2/s at 600-850°C and 1.2×10^{-2} cm^2/s at 900-1570°C, respectively.[53, 54] Thus the δ-TiN layer will firstly be formed at the interface, leading to the deviation of the diffusion path toward the δ-TiN end (edge BC in Fig. 3.6(a)). As δ-TiN has a wide range of nitrogen solubility and hardly dissolves Al atoms, much more Al atoms than N atoms will diffuse into the titanium side beyond the δ-TiN layer, resulting in the formation of τ_2-Ti_2AlN and τ_1-Ti_3AlN, and various aluminide layers.

The diffusion path crosses the fields of AlN + δ-TiN, δ-TiN, δ-TiN + τ_2-Ti_2AlN, τ_2-Ti_2AlN + τ_1-Ti_3AlN, τ_1-Ti_3AlN + α-Ti, α-Ti, α-Ti + β-Ti, and β-Ti. The tie lines of the ternary phase diagram correspond to the interface of two reaction layers in the diffusion couple, similar to the case for the interface between carbon and titanium aluminides presented by Viala et al.[55] As shown in Fig. 3.6(b), the layers of δ-TiN, τ_2-Ti_2AlN, τ_1-Ti_3AlN, α-Ti(Al, N), α-Ti(Al, N) + β-Ti(Al, N), β-Ti(Al, N) will be formed in sequence from AlN to Ti at the annealing temperature (1300°C).

Figure 3.6(c) shows the microstructure formed during cooling stage. It is believed that the nitride layers, including δ-TiN, τ_2-Ti_2AlN, and τ_1-Ti_3AlN, remained during cooling. However, the aluminide layers (i.e., α-Ti(Al, N), α-Ti(Al, N) + β-Ti(Al, N), and β-Ti(Al, N)) were subjected to phase

transformation during the subsequent cooling, causing the formation of the α_2-Ti_3Al layer and the lamellar two-phase (α_2-Ti_3Al + α-Ti) layer.

The phase transformation of aluminides, mentioned above, can be shown schematically in Ti-Al binary phase diagram as shown in Fig. 3.7. Because nitrogen is an α-Ti stabilizer, the β/(α + β) and (α + β)/α boundaries of the Ti-Al binary phase diagram are shifted upwards by dissolving N atoms. The β-Ti layer abutting the reaction-unaffected Ti, with a small amount of Al and N in solid solution, was transformed into α-Ti on cooling, as indicated by the line 1 in Fig. 3.7. The α-Ti + β-Ti layer at 1300°C was transformed into the α-Ti + α_2-Ti_3Al layer after cooling (line 2 in Fig. 3.7), while the α-Ti layer was transformed into α_2-Ti_3Al (line 3 in Fig. 3.7).

For comparison, a α-Ti layer and/or a γ-TiAl layer with a higher Al content were likely formed when the diffusion couple was isothermally annealed at temperatures higher than 1300°C. Thus, more aluminide layers, including the two-phase (γ-TiAl + α_2-Ti_3Al) layer and/or γ-TiAl layer, could exist in the Ti/AlN diffusion couple because of the more extensive Al diffusion after annealing at 1400° or 1500°C. After isothermal annealing at 1400°C, the α-Ti layer with a high Al content underwent the following reaction: α-Ti → γ-TiAl + α_2-Ti_3Al as indicated by the line 4 in Fig. 3.7, while the γ-TiAl layer still remained as it was on cooling (line 5 in Fig. 3.7). It is worth noting that no γ-TiAl existed in the diffusion couple after annealing at 1500°C. After δ-TiN_{1-x} was saturated in N at such a high temperature, the excess nitrogen would diffuse from the δ-TiN_{1-x} layer, resulting in the nitidization of γ-TiAl.

(4) Reaction zone growth mechanisms at 1300°C

Based upon the results and the discussion mentioned above, an attempt was made to propose an interfacial reaction model between AlN and Ti. The

formation mechanisms for several different stages at 1300°C, as an example, are schematically shown in Fig. 3.8.

(a) First stage: formation of δ-TiN

In the first stage, AlN decomposes at the original AlN/Ti interface into Al and N under the effect of Ti. As Ti has a strong affinity with N, the fast diffusion species N atoms will go into Ti, leading to the formation of δ-TiN with Al in solid solution. The formation of δ-TiN in the intatial stage can be expressed by the following reaction, as shown in Fig. 3.8(a):

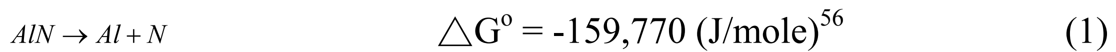

$$AlN \rightarrow Al + N \qquad \triangle G^{o} = -159{,}770\ (J/mole) \quad (1)$$

[56]

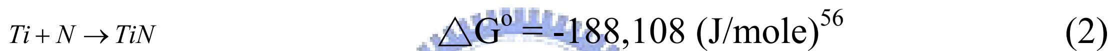

$$Ti + N \rightarrow TiN \qquad \triangle G^{o} = -188{,}108\ (J/mole) \quad (2)$$

[56]

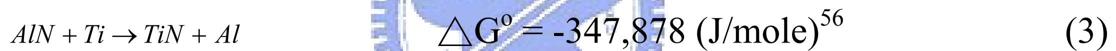

$$AlN + Ti \rightarrow TiN + Al \qquad \triangle G^{o} = -347{,}878\ (J/mole) \quad (3)$$

[56]

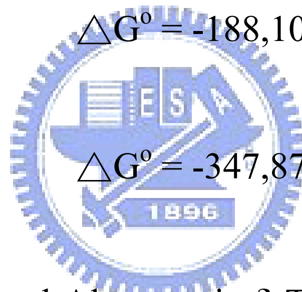

The diffusion of N atoms and Al atoms in δ-TiN is much faster than that of Ti atoms in AlN (diffusivities of N and Al in δ-TiN are 5.4×10^{-3} cm^2/s at 1000°-1500°C and 3×10^{-14} cm^2/s at 300°-550°C, the diffusivity of Ti in AlN is 4×10^{-17} at 1280°-1400°C).[24] Thus Al and N continuously diffuse through the δ-TiN layer and the reaction (2) takes place at the interface of δ-TiN and Ti. The highly negative Gibbs free energy change of the reaction (3) indicates that the reaction between aluminum nitride and titanium is thermodynamically favorable.

(b) Second stage: formation of τ_1-Ti_3AlN and various titanium aluminides

When the concentrations of Al and N increase to a certain amount, τ_1-Ti_3AlN is formed, as shown in Fig. 3.8(b), at the interface of δ-TiN/Ti according to the

following reaction:

$$3Ti + Al + N \rightarrow \tau_1 - Ti_3AlN \quad (4)$$

The formation of τ_1-Ti_3AlN instead of τ_2-Ti_2AlN at this stage is consistent with the fact that τ_1-Ti_3AlN was found after annealing at 1300°C/0.5 h, which was at a relatively early stage. Meanwhile, excess Al and N atoms further go into Ti as a solid solution, leading to the formation of various titanium aluminonitrides, for example, α-Ti(Al, N) and the α-Ti(Al, N) + β-Ti(Al, N) two-phase region.

(c) Third stage: formation of τ_2-Ti_2AlN

As shown in Fig. 3.8(c), τ_2-Ti_2AlN is formed at this stage. The growth of the τ_2-Ti_2AlN was controlled by the diffusion of Al and N through δ-TiN, accumulating at the δ-TiN/τ_1-Ti_3AlN interface, leading to the disappearance of τ_1-Ti_3AlN based upon the following reaction:

$$\tau_1 - Ti_3AlN + \frac{1}{2}Al + \frac{1}{2}N \rightarrow \frac{3}{2}\tau_2 - Ti_2AlN \quad (5)$$

(d) Fourth stage: formation of α_2-Ti_3Al and/or the two-phase layer (α_2-Ti_3Al + α-Ti) during cooling

Figure 3.8(d) shows that the α-Ti(Al, N) + β-Ti(Al, N) two-phase region was transformed into the (α_2-Ti_3Al + α-Ti) two-phase layer, while the α-Ti(Al, N) layer was transformed into the α_2-Ti_3Al layer during cooling, depending upon the local composition. Not shown in Fig. 8(d) is that the β-Ti(Al, N) was transformed into the α-Ti(Al, N). The phase transformations mentioned above can be expressed by the following reactions,

$$\beta - Ti(Al, N) \xrightarrow{cooling} \alpha - Ti(Al, N) \quad (6)$$

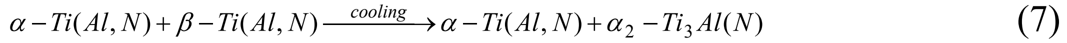

$$\alpha - Ti(Al,N) + \beta - Ti(Al,N) \xrightarrow{cooling} \alpha - Ti(Al,N) + \alpha_2 - Ti_3Al(N) \qquad (7)$$

$$\alpha - Ti(Al,N) \xrightarrow{cooling} \alpha_2 - Ti_3Al(N) \qquad (8)$$

3.4 Conclusions

1. An interfacial reaction zone, consisting of δ-TiN, τ_2-Ti_2AlN, τ_1-Ti_3AlN, α_2-Ti_3Al, and a two-phase (α_2-Ti_3Al + α-Ti) region in sequence, was observed in between AlN and Ti after annealing at 1300°C.
2. After annealing at 1300°C, a textured structure existed in the α_2-Ti_3Al layer probably because of the internal stresses resulting from the mismatch in the thermal expansion coefficient between AlN and Ti. The fine equaixed α_2-Ti_3Al grains implied the occurrence of recrystallization. The orientation relationship between the equiaxed and elongated α_2-Ti_3Al was as follows: $[0001]_{equiaxed} // [\bar{1}100]_{elongated}$ and $(\bar{1}010)_{equiaxed} // (\bar{1}\bar{1}22)_{elongated}$.
3. In the two-phase (τ_1-Ti_3AlN + α-Ti) region after annealing at 1300°C, α_2-Ti_3Al and α-Ti were found to satisfy the following orientation relationship: $[0001]_{\alpha-Ti} // [0001]_{Ti_3Al}$ and $(1\bar{1}00)_{\alpha\text{-Ti}} // (1\bar{1}00)_{Ti_3Al}$. The a value of α_2-Ti_3Al was approximately twice that of α-Ti.
4. The γ-TiAl and a lamellar two-phase (γ-TiAl + α_2-Ti_3Al) structure were found in between τ_2-Ti_2AlN and α_2-Ti_3Al after annealing at 1400°C. The orientation relationship of γ-TiAl and α_2-Ti_3Al in the lamellar structure was identified to be as follows: $[\bar{2}4\bar{2}3]_{T_3Al} // [012]_{TiAl}$ and $(10\bar{1}0)_{Ti_3Al} // (100)_{TiAl}$. Compared with the results after the reaction at 1400°C, γ-TiAl was not formed at the interface after the reaction at 1500°C.
5. The diffusion path, connecting the phases formed by the reaction between AlN and Ti, was drawn on the Ti-Zr-O ternary phase diagram. Futhermore, the relationships among the Ti-Al-N ternary phase diagram, a modified

binary phase diagram, and the microstructural development between AlN and Ti at 1300°C and subsequent cooling have been proposed.

Table 3. 1. New phases formed in the interfacial reaction zone of AlN/Ti diffusion couples

Annealing conditions	Phases						
	TiN	Ti_2AlN	Ti_3AlN	TiAl	Lamellar structure ($TiAl+Ti_3Al$)	Ti_3Al	two phase region (Ti_3Al+Ti)
1300°C/0.5hrs	●	x	●	x	x	●	●
1300°C/3hrs	●	●	●	x	x	●	●
1300°C/10hrs	●	●	●	x	x	●	●
1300°C/36hrs	●	●	●	x	x	●	●
1400°C/0.5hrs	●	●	x	x	x	●	●
1400°C/3hrs	●	●	x	●	●	●	●
1400°C/10hrs	●	●	x	●	●	●	●
1400°C/36hrs	●	●	x	●	●	●	●
1500°C/0.5hrs	●	●	x	●	●	●	●
1500°C/3hrs	●	●	x	x	●	●	●
1500°C/10hrs	●	●	x	x	●	●	●
1500°C/36hrs	●	●	x	x	●	●	●

●: observed, x: none

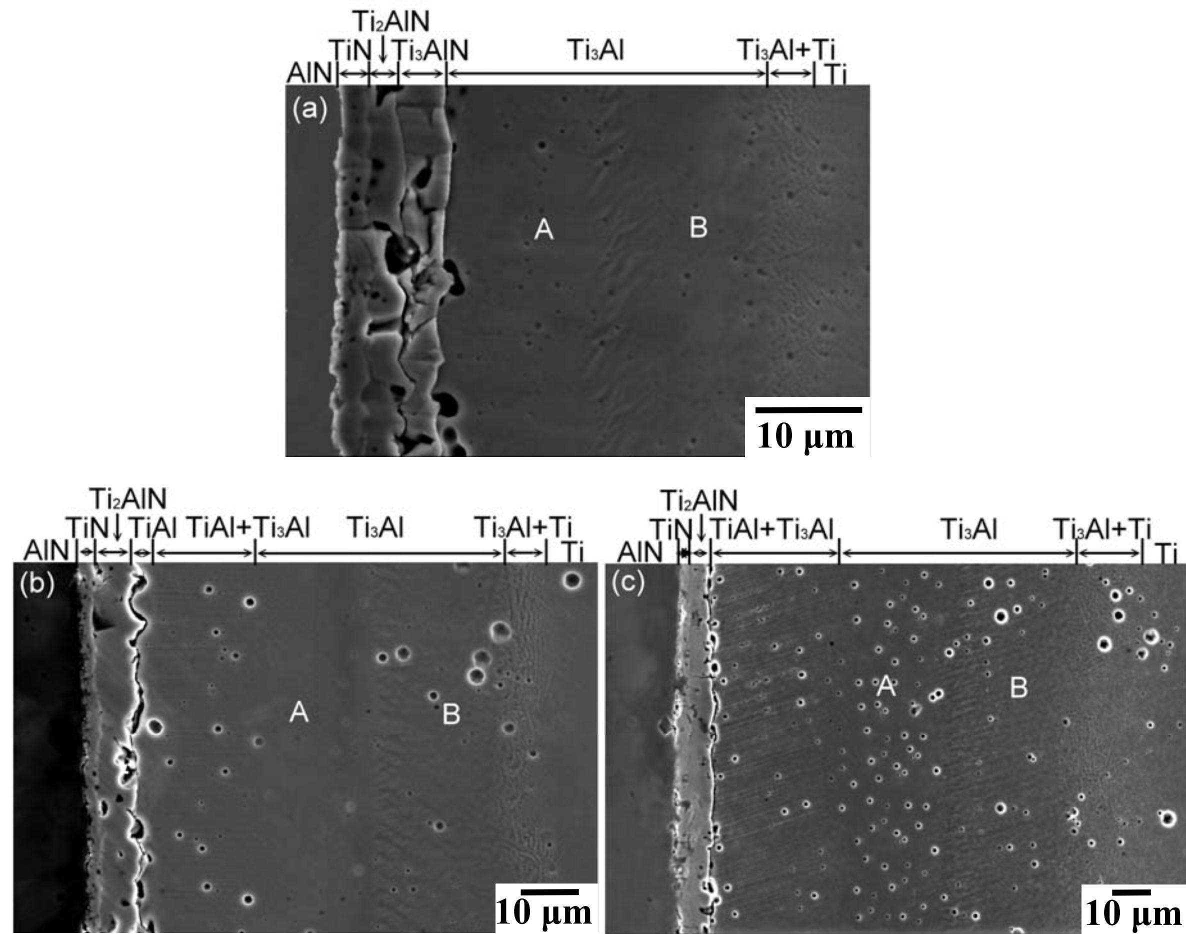

Fig. 3. 1. SEM micrographs of the interface between AlN and Ti after annealing at: (a) 1300°C/36 h; (b) 1400°C/36 h; (c) 1500°C/36 h.

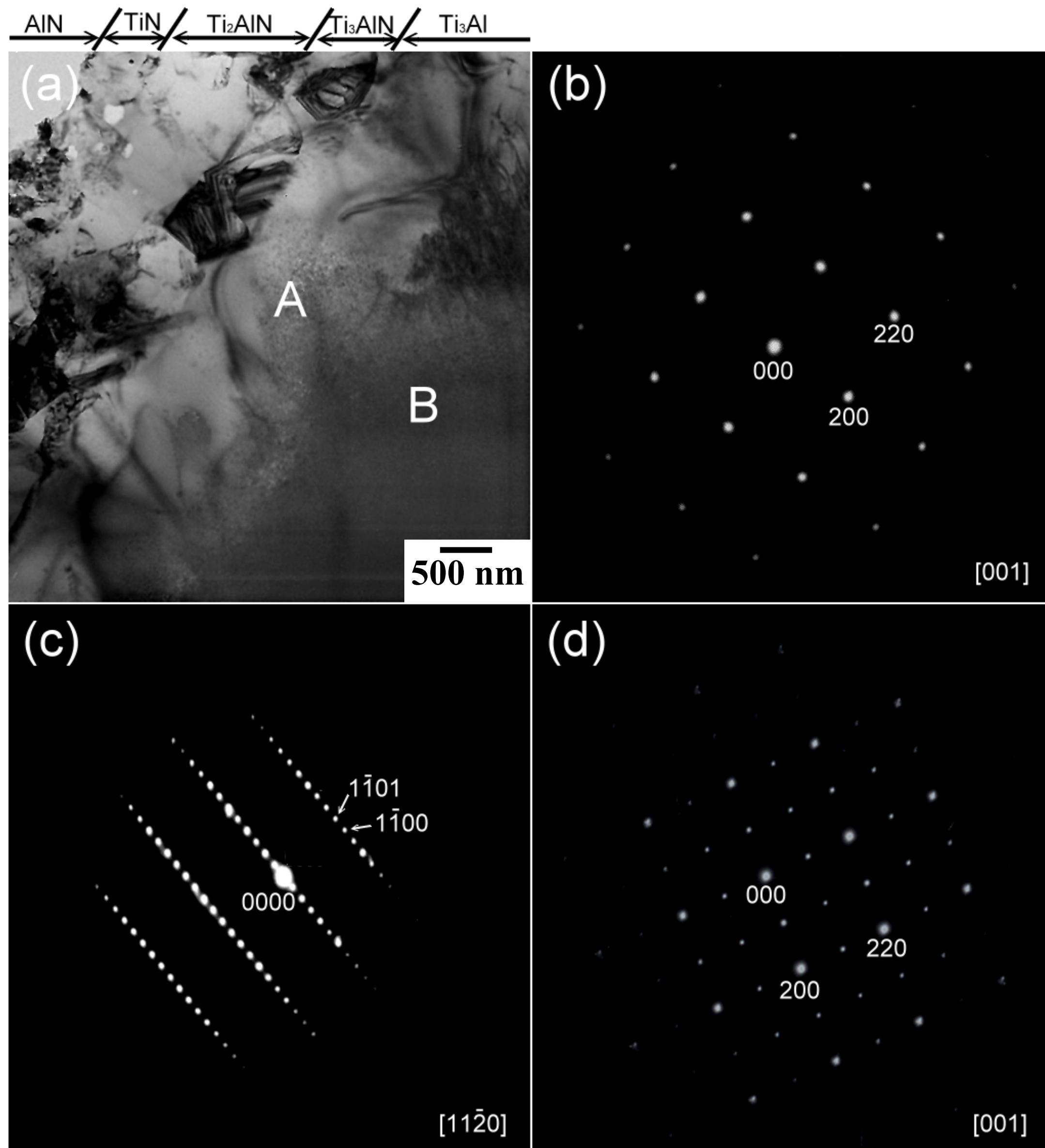

Fig. 3. 2. (a) BF image of the AlN/Ti interface after annealing at 1300°C for 3 h; (b) SADP of δ-TiN, Z=[001]; (c) SADP of τ_2-Ti_2AlN, Z=[$11\bar{2}0$]; and (d) SADP of τ_1-Ti_3AlN, Z=[001].

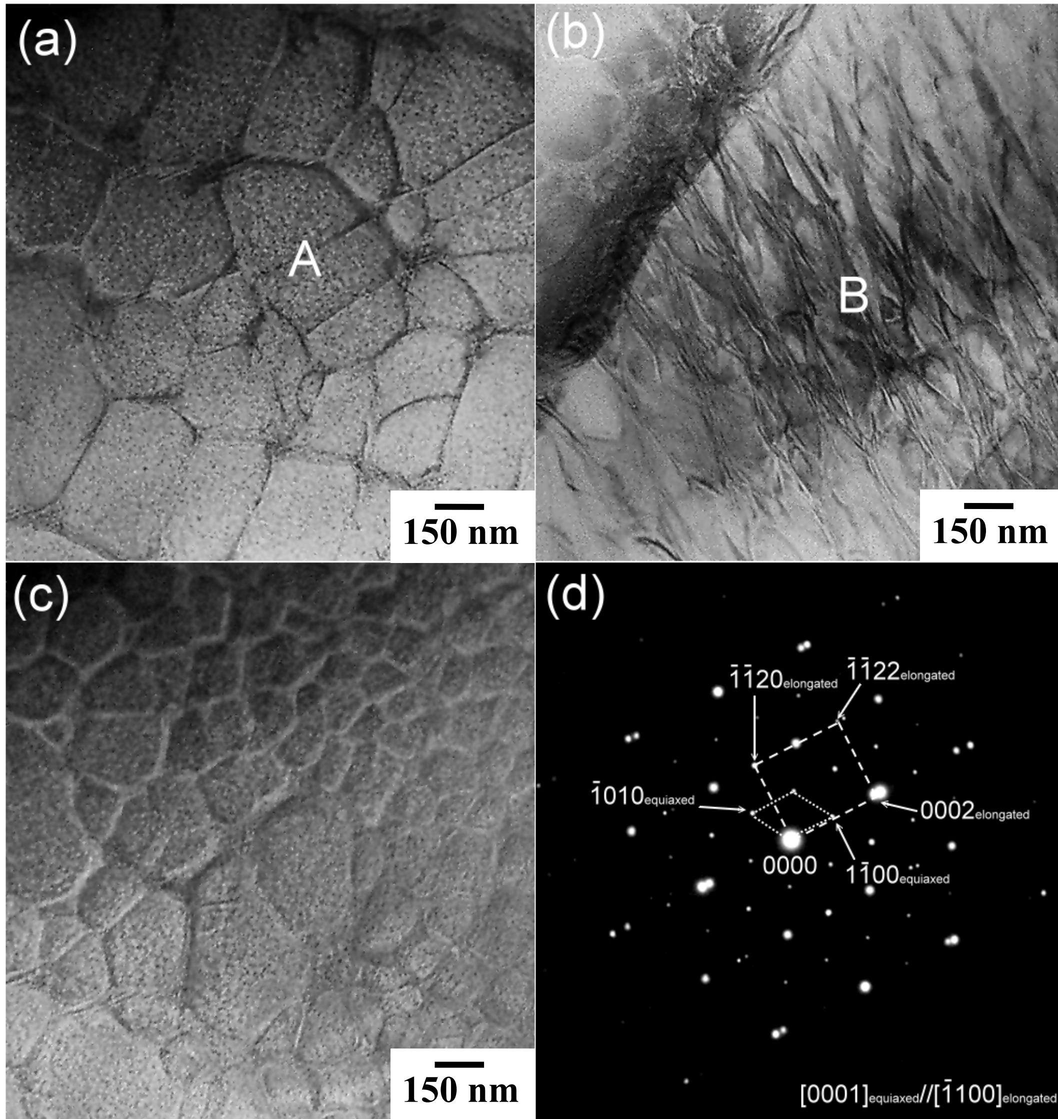

Fig. 3. 3. After annealing at 1300°C for 3 h: (a) BF image of the equiaxed α_2-Ti_3Al (abutting the τ_1-Ti_3AlN layer in Fig. 3.1(a)); (b) BF image of the elongated α_2-Ti_3Al (abutting the two-phase (α_2-Ti_3Al + α-Ti) layer in Fig. 3.1(a)); (c) Variation in the grain size of the equiaxed α_2-Ti_3Al along the direction from the AlN side (bottom) to the Ti side (top); (d) SADP of both elongated and equiaxed α_2-Ti_3Al, showing the orientation relationship of $[0001]_{equiaxed} // [\bar{1}100]_{elongated}$ and $(\bar{1}010)_{equiaxed} // (\bar{1}\bar{1}22)_{elongated}$.

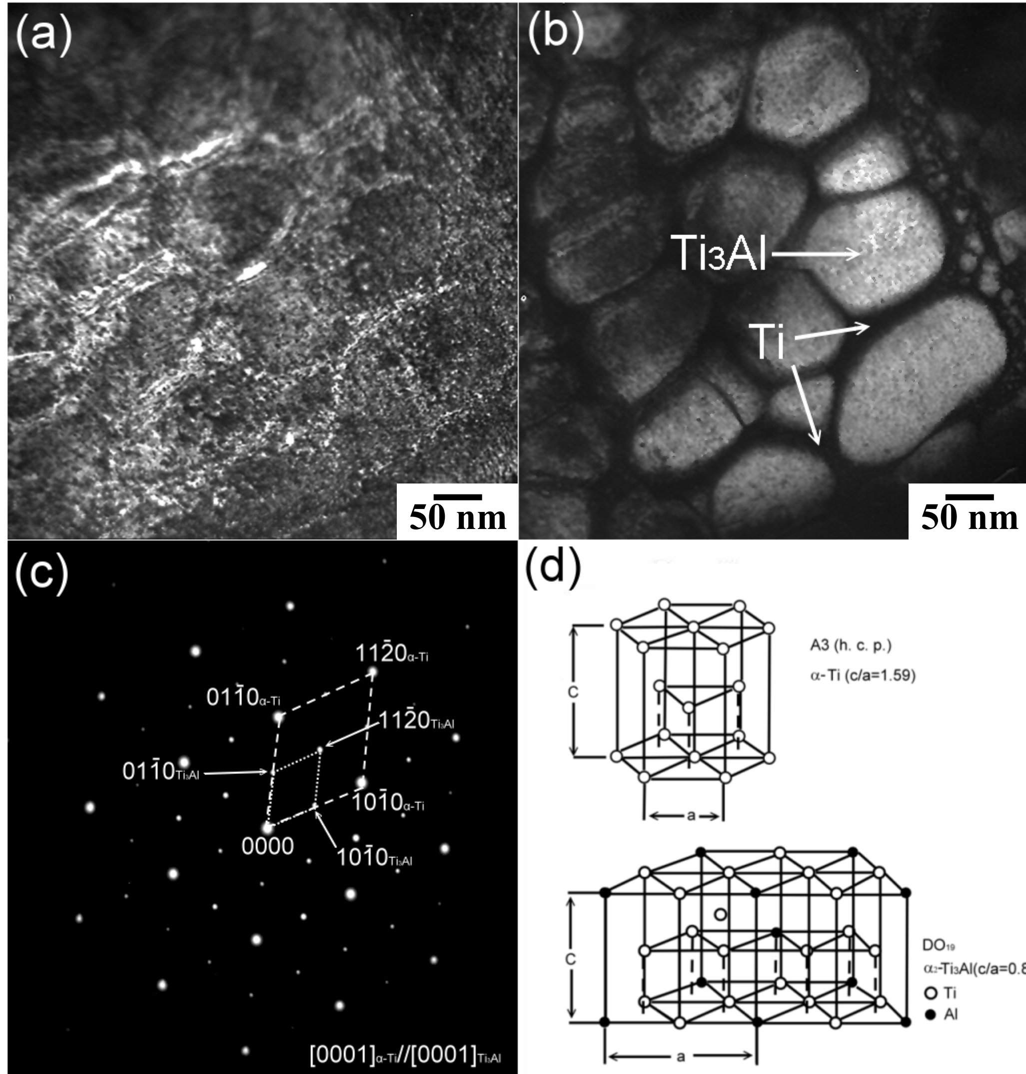

Fig. 3. 4. After annealing at 1300°C for 3 h: (a) BF image of the two-phase (α_2-Ti_3Al + α-Ti) region in Fig. 3.1(a); (b) DF image of α_2-Ti_3Al from the $\left(11\bar{2}0\right)_{Ti_3Al}$ diffraction spot; (c) Superimposed SADPs obtained from the two-phase (α_2-Ti_3Al + α-Ti) region, showing the orientation relationship of $[0001]_{\alpha-Ti} // [0001]_{Ti_3Al}$ and $(1\bar{1}00)_{\alpha\text{-Ti}} // (1\bar{1}00)_{Ti_3Al}$; (d) Schematic illustration of α-Ti and α_2-Ti_3Al crystals structure.

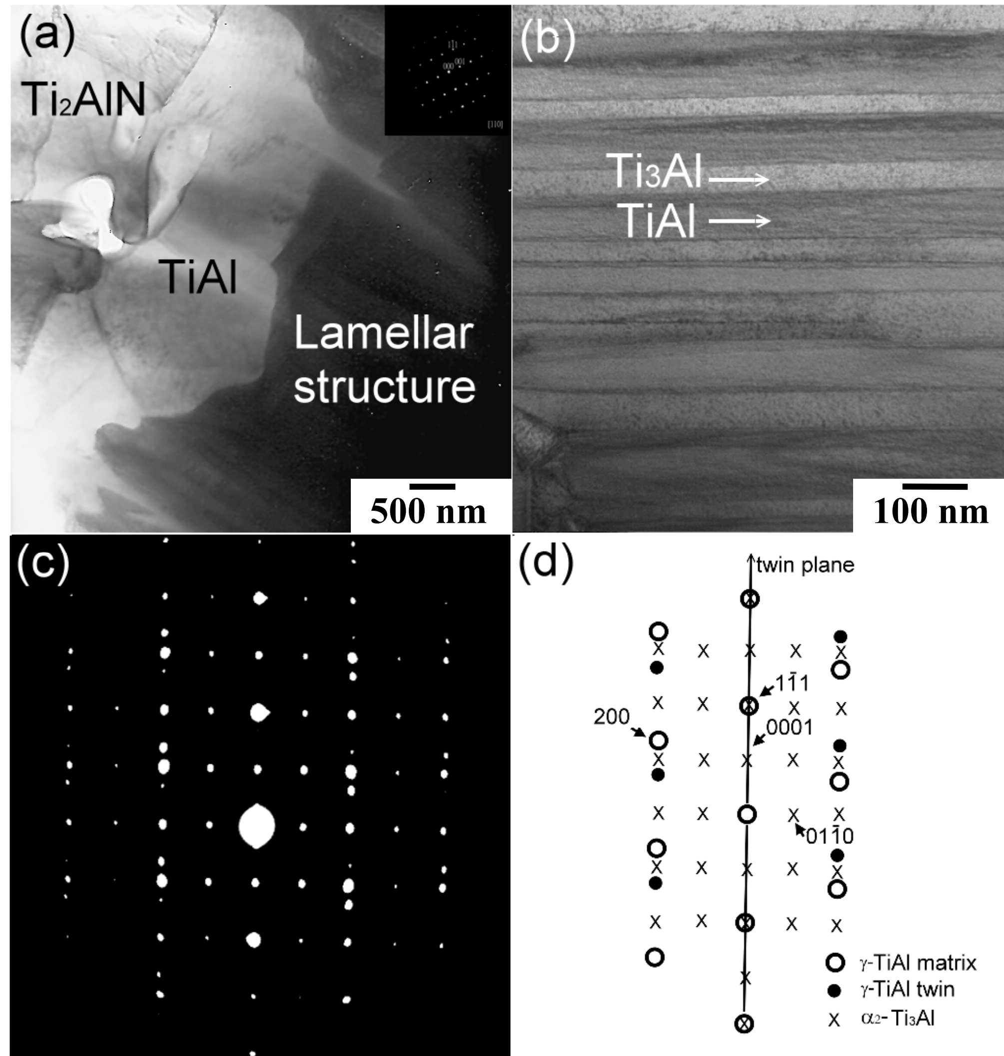

Fig. 3. 5. (a) BF image of γ-TiAl between the τ_2-Ti_2AlN and the lamellar structure after annealing at 1500°C/0.5 h; (b) BF image of the lamellar two-phase (γ-TiAl + α_2-Ti_3Al) structure; (c) Superimposed SADP's of γ-TiAl (Z = [011]) and α_2-Ti_3Al (Z = $[2\bar{1}\bar{1}0]$) from the lamellar structure region, and the orientation relationship of γ-TiAl and α_2-Ti_3Al was identified to be as follows: $[011]_{TiAl}//[2\bar{1}\bar{1}0]_{Ti_3Al}$ and $(1\bar{1}\bar{1})_{TiAl}//(01\bar{1}0)_{Ti_3Al}$; (d) Schematic illustration corresponding to the SADP's in (c).

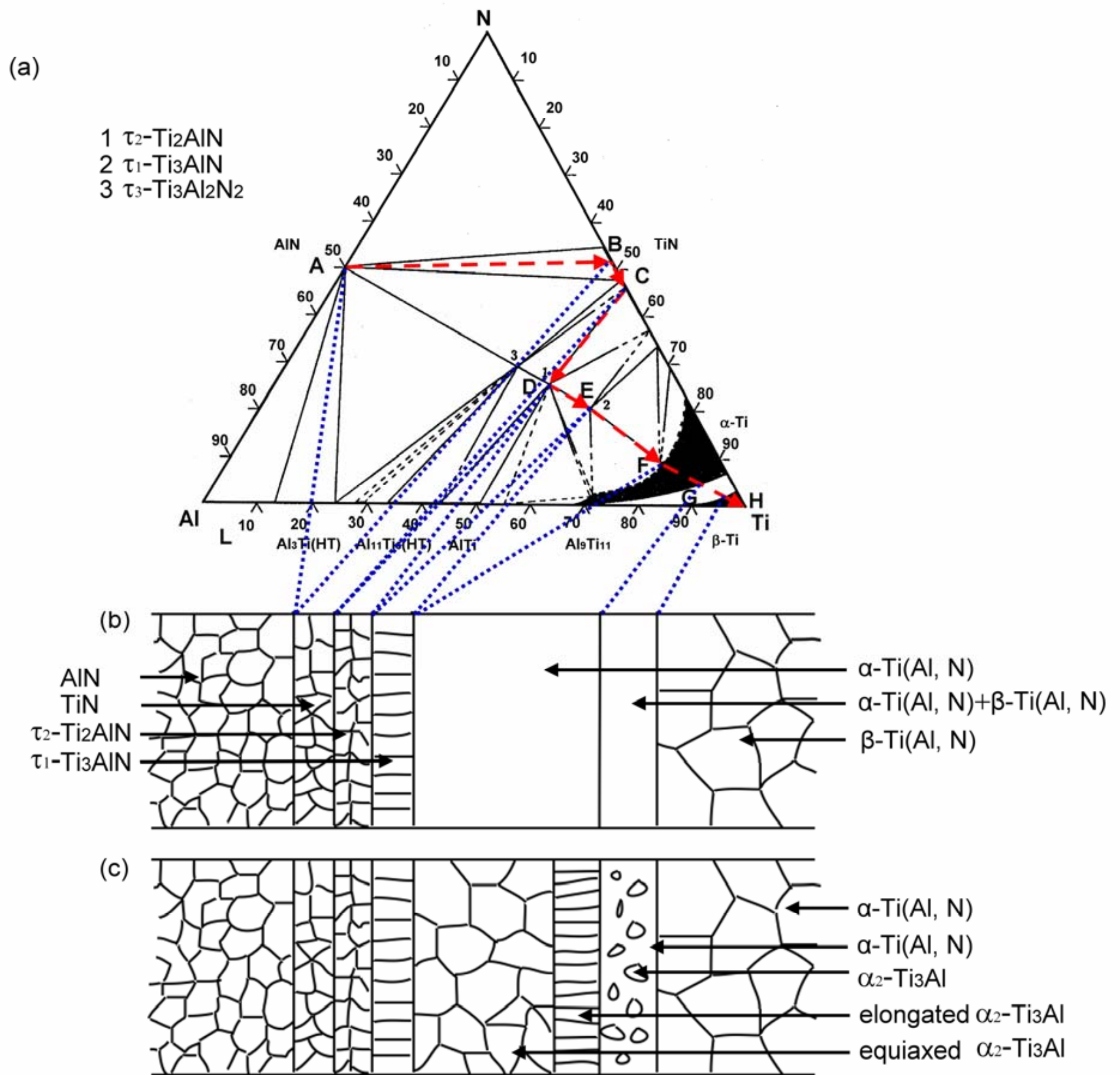

Fig. 3. 6. (a) Isothermal section of the Ti-Al-N phase diagram at 1300°C.[3] The diffuse path was drawn as arrows; (b) the microstructure of an AlN/Ti diffusion couple at 1300°C; (c) the microstructure of an AlN/Ti diffusion couple after cooling.

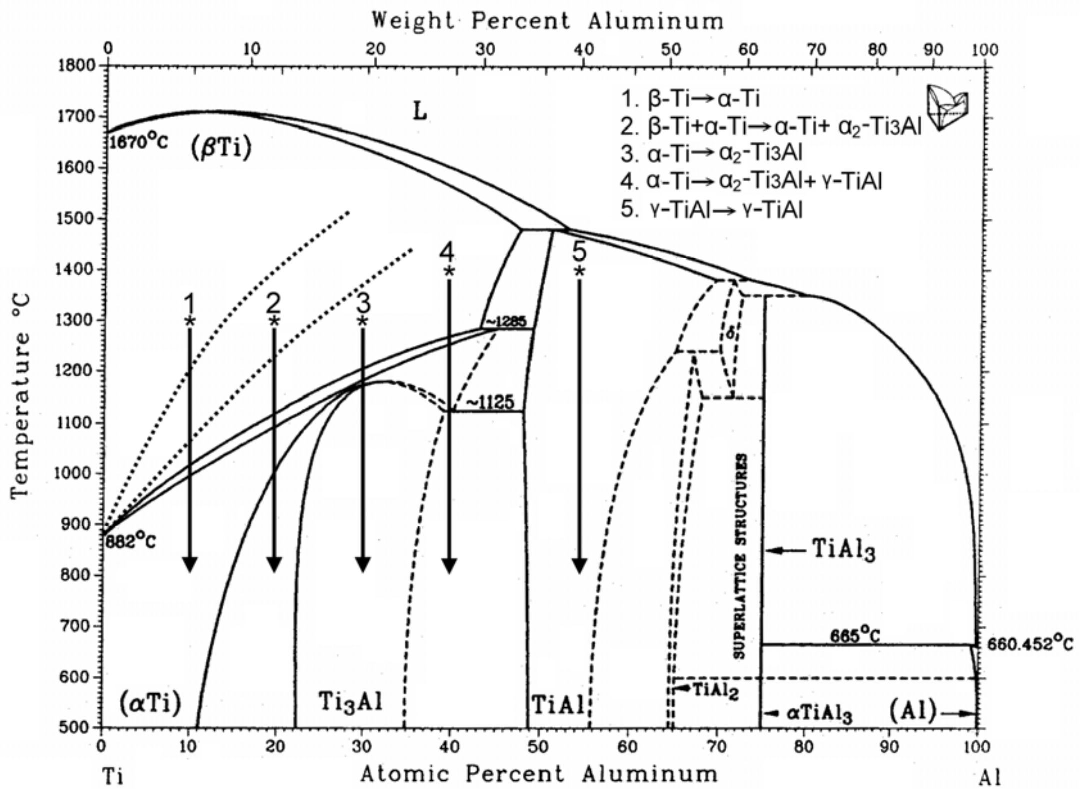

Fig. 3. 7. A modified Ti-Al phase diagram because of the stabilization of α-Ti by dissolving N (see the dashed line), showing the cooling processes of the various aluminides after annealing at 1300°C (lines 1-3) and at 1400°C (lines 4 and 5). The increase in the α → β transformation temperature has been exaggerated for clarification.[4]

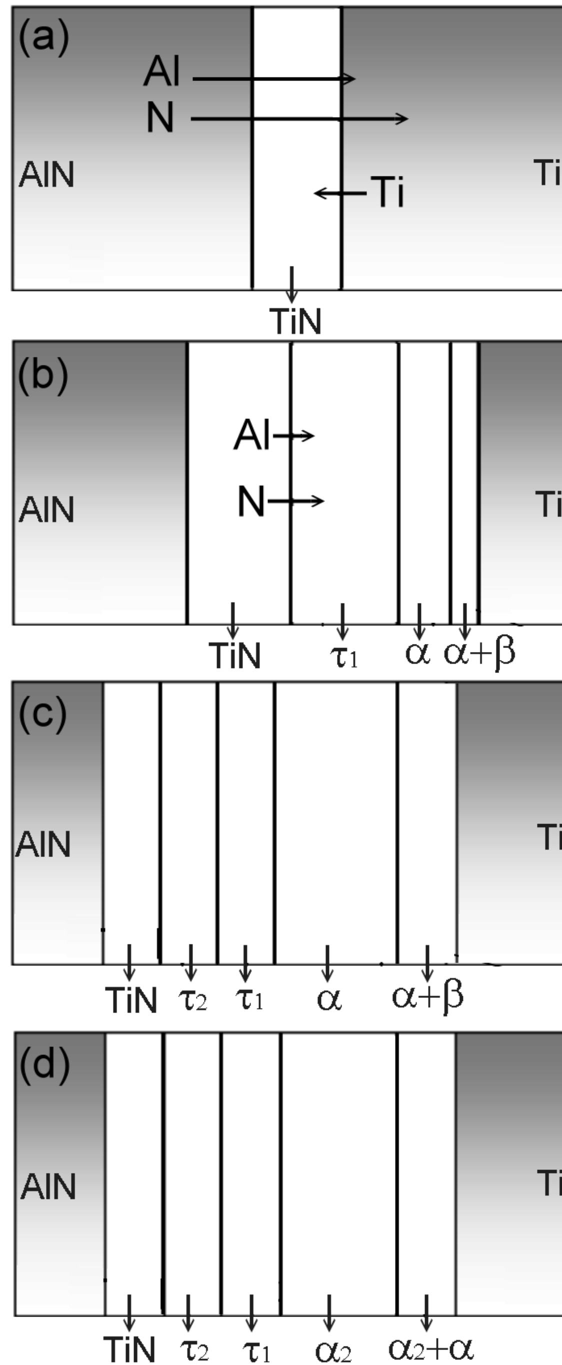

Fig. 3. 8. Proposed reaction mechanisms of the AlN and Ti diffusion couple annealed at 1300°C: (a) first stage: formation of δ-TiN; (b) Second stage: formation of τ_1-Ti_3AlN, α-Ti(Al, N)+β-Ti(Al, N), and α-Ti(Al, N); (c) third stage: formation of τ_2-Ti_2AlN; (d) fourth stage: formation of α_2-Ti_3Al and/or the two-phase layer (α_2-Ti_3Al + α-Ti) during cooling. (τ_1: Ti_3AlN; τ_2: Ti_2AlN; α_2:Ti_3Al; α: hexagonal Ti(Al, N); β: cubic Ti(Al, N)).

Chapter 4 Formation Mechanisms and Atomic Configurations of Nitride Phases at the Interface of Aluminum Nitride and Titanium

4.1 Introduction

The interfacial reactions of the AlN/Ti system have attracted a substantial amount of attention in the last few years since the AlN/Ti joints are used for microelectronic packaging and some high temperature applications[14, 19-21, 41, 57]. Interfacial reactions between Ti and AlN are of a great interest due to the high affinity of Ti to Al and N, leading to the formation of various nitrides and titanium aluminides. In order to obtain reliable mechanical properties of AlN and Ti joints, understanding the interfacial reactions between AlN and Ti is highly desirable for the design and processing of AlN/Ti bonding or joints.

Previous studies on the AlN/Ti interface shed light on the microstructural development of the reaction zone for various forms of starting materials, such as powders,[19-21] thin films,[12, 14, 15, 17] and bulk materials.[22] Pinkas et al.[14] investigated the early stages of interfacial reactions between AlN(film) and Ti(film) after annealing at 600°C for 1 to 10 h, showing that the AlN film reacted with Ti to form a phase sequence of AlN/$TiAl_3$/Ti_2N/α_2-Ti_3Al/α-Ti(Al, N) solid solution. El-Sayed et al.[17] indicated that the diffusion path followed the route of δ-TiN/τ_1-Ti_3AlN/α_2-Ti_3Al between 20 or 50 μm thick Ti foils and AlN plates after annealing at 1050° to 1200°C for 1 to 20 h, while τ_2-Ti_2AlN was formed following the complete consumption of Ti. Paransky et al.[19-21] found that δ-TiN and τ_1-Ti_3AlN exhibited a complex interpenetrating morphology at the AlN(powder)/Ti(powder) interface, as well as in the AlN/Ti diffusion couple after annealing at 900° to 1100°C. In addition, a two-phase (τ_1-Ti_3AlN + α_2-Ti_3Al) layer was observed between τ_1-Ti_3AlN and α_2-Ti_3Al layers after annealing at 1000° to 1100°C. Microstructural characterization of the AlN/Ti

interfaces has often been conducted using scanning electron microscopy (SEM) and x-ray diffraction (XRD), in spite of the overwhelming advantages of analytical transmission electron microcopy (TEM) including simultaneous image observation, compositional, and crystal structural analyses.

Recently, based on TEM microanalyses, Chiu and Lin[22] revealed that δ-TiN, some ternary compounds (i.e., τ_2-Ti_2AlN and/or τ_1-Ti_3AlN), and distinctive Ti-Al layers (i.e., γ-TiAl and/or α_2-Ti_3Al) were formed in the AlN/Ti diffusion couple after annealing at 1300º to 1500ºC. It was reported that τ_2-Ti_2AlN was formed between AlN and Ti after annealing at temperatures above 1300ºC. Imanaka and Notis[12] found that the formation activation energy of τ_2-Ti_2AlN between AlN and Ti thin films was 224 kJ/mol at temperatures ranging from 800º to 850ºC, which approximated that of the diffusion of N atoms in α-Ti(Al). This implied that the formation of τ_2-Ti_2AlN was controlled by the diffusion of N atoms in α-Ti(Al). Even though the nitridization of various Ti-Al layers is likely to play a critical role, its effect on the microstructural development at the AlN/Ti interface has not been investigated to date.

In another respect, nitridization experiments have been conducted on some Ti-Al intermetallic compounds such as γ-TiAl and/or α_2-Ti_3Al, leading to the formation of various nitrides on their surfaces with subsequent improvements of their mechanical properties.[58-61] Saito and Matsushima[62] showed that implanted nitrogen atoms could react with γ-TiAl, resulting in the formation of Ti_2N and AlN. Zhao et al.[58] observed δ-TiN, τ_2-Ti_2AlN, some new nitrides (such as η-Ti_3N_{2-x} and Ti_2N), and Al-rich intermetallic phases (such as Ti_2Al_5, $TiAl_3$, and $TiAl_2$) when γ-TiAl based alloys were nitridized in ammonia atmosphere after annealing at temperatures ranging from 800º to 940ºC. Tian and Nemoto[59] observed needle-like τ_1-Ti_3AlN precipitated after the $L1_o$-ordered γ-TiAl was nitridized at 800ºC. The needle-like τ_1-Ti_3AlN phase was further

replaced by plate-like τ_2-Ti_2AlN after aging at higher temperatures or for longer periods.

The interfacial reaction layers are thoroughly investigated using analytical TEM as well as SEM in this study. Two AlN plates are bonded with a thin Ti foil, so that a relatively large amount of N atoms are able to diffuse into the thin metal foil, wherein various Ti-Al reaction layers are formed at an early stage. The main purpose of this investigation is to shed light on the role of N atom inward diffusion into Ti-Al reaction layers in the microstructural evolution at the AlN/Ti interface. The phase transformation mechanisms at the AlN/Ti interface are explained in terms of atomic configurations from the viewpoint of the nitridization of Ti-Al intermetallic compounds mentioned in previous studies.

4.2 Experimental Procedures

The starting materials were AlN plates (nominal composition of 62.8 wt% Al, 32.1 wt% N, 3.4 wt% Y, 1.7 wt% O; SH-15, Tokuyama Soda Corp., Tokyo, Japan) and Ti foils (99.7 wt% in purity, 200 μm in thickness; Alfa Aesar, Ward Hill, MA). AlN plates and Ti foils were cut into pieces with dimensions of 15 mm × 10 mm × 4 mm and 15 mm × 10 mm × 200 μm, respectively. Specimen surfaces were ground with a diamond matted disc, and polished with diamond pastes of 6, 3, and 1 μm in sequence using a precision polishing machine (Model Minimet 1000, Buehler Ltd, Lake Bluff, IL). The specimens were then rinsed ultrasonically first in an acetone bath and then in distilled water prior to diffusion bonding. One Ti foil was inserted in between two AlN plates. The sandwiched specimens were then diffusion-bonded in a hot press furnace (Model HP50-MTG-7010, Thermal Techno. Inc., Santa Rosa, CA). The working chamber was pre-evacuated to 1×10^{-4} Pa and purged with Ar to 1 atm three times. The bonding conditions were 1400°C for up to 1 h using a 2 MPa bonding pressure in an Ar atmosphere. The specimens were cooled down to

room temperature at a rate of 10°/min.

The cross-sectional SEM specimens were cut perpendicular to the AlN/Ti interface. They were ground with a diamond matted disc and polished with diamond pastes using the aforementioned procedure for further microanalyses by standard metallographic procedures. The cross-sectional TEM specimens of the AlN/Ti interface were prepared by two methods. First, they were cut perpendicular to the interface and then polished, dimpled, and subsequently ion-beam thinned using a precision ion polishing system (PIPS, Model 691, Gatan, San Francisco, CA). The details of this traditional technique for preparing cross-sectional TEM specimens were described in a previous study.[22] Second, the samples were acquired by an innovative technique, whereby a specific location on a metallographic sample was ion bombarded using a focused ion beam (FIB, Model Nova 200, FEI Co., Hillsboro, OR). The FIB operating parameters were as follows: the electron beam was 5 keV at 98 to 1.6 Pa, and the ion beam was 30 keV at 7 to 10 Pa. A thin TEM specimen was acquired along the direction perpendicular to the surface of a cross-sectional SEM specimen. The TEM specimen must be thinner than 100 nm in order to be electron transparent. The final TEM specimen was approximately 20 μm × 10 μm × 0.1 μm in size.

Microstructural characterization was carried out using a scanning electron microscope (SEM, Model JSM-6500, JEOL, Tokyo, Japan) and a transmission electron microscope (TEM, Model 2000Fx, JEOL, Tokyo, Japan), both attached with a characteristic x-ray energy dispersive spectrometer (EDS, Model 9900, EDAX International, Prairie View, IL). Quantitative analyses of the chemical compositions for various phases were conducted by the Cliff–Lorimer standardless technique.[63] Relative errors were estimated 1% for concentrated elements and more than 10% for diluted elements. The analyses of atomic

configurations for various phases were performed using computer simulation software for crystallography (CaRIne Crystallography3.1, Cyrille Boudias & Daniel Monceau, Senlis, France).

4.3 Results and Discussion

Figure 4.1(a) displays an SEM micrograph of the cross-section of the AlN/Ti/AlN specimen after annealing at 1400°C for 0.1 h, indicating that the interfacial reaction zone in the AlN/Ti/AlN specimen consists of δ-TiN, τ_2-Ti_2AlN, γ-TiAl, α_2-Ti_3Al, a two-phase region (α_2-Ti_3Al+α-Ti), and α-Ti (Al, N) in sequence after annealing at 1400°C for 0.1 h. The phase sequence in Fig. 4.1(a) was the same as that found in the AlN/Ti diffusion couple after annealing at 1400ºC for 3 h as mentioned previously,[22] where the microstructures were characterized using analytical TEM and SEM. It was attributed to the fact that that the thickness of Ti in the AlN/Ti/AlN specimen was much larger than $(4Dt)^{1/2}$ for a very short annealing time. As shown in Fig. 4.1(b), the original Ti was replaced by a reaction zone consisting of several distinct layers, which were symmetrical with respect to the central line and designated as a reaction layer sequence of A-B-C-D-E-D-C-B-A, after annealing at 1400°C for 1 h. Reaction layers A, B, and E represent the δ-TiN, τ_2-Ti_2AlN and α-Ti (Al, N) solid solutions, respectively, and correspond to the results obtained in the AlN/Ti diffusion couple after annealing at 1400°C.[22] Reaction layers C and D are very different in appearance from those aluminide and/or nitride layers found in the AlN/Ti diffusion couple after annealing at the same conditions. Figure 4.1(c) and (d) illustrates the microstructures of reaction layers C and D, as shown in Fig. 4.1(b), at a higher magnification after annealing at 1400ºC for 1 h. Figure 4.1(c) reveals that a chopped fiber-like phase exists in reaction layer C. The chopped fiber-like phase and the matrix were further identified as τ_2-Ti_2AlN and (Ti_3Al_5+γ-TiAl), respectively using TEM/EDS analyses. Figure 4.1 (d) displays a lamellar structure with different variations in reaction layer D. The

lamellar structure was characterized to be composed of δ-TiN and α-Ti using TEM/EDS analyses. The chopped fiber-like τ_2-Ti_2AlN and the Al-rich Ti_3Al_5 in reaction layer C and the lamellar (δ-TiN+α-Ti) structure in reaction layer D have not been reported in previous studies and are the most notable findings in the present study.

It was believed that α_2-Ti_3Al and the two-phase region (α_2-Ti_3Al+α-Ti), as shown in Fig. 4.1(a), did not exist during annealing at 1400°C, but were instead formed during cooling. The isothermal section of the Ti-Al-N system [Fig. 4.2(a)][64] shows that the α_2-Ti_3Al is not a stable phase at 1400°C, while the Ti-Al binary phase diagram [Fig. 4.2(b)][4] displays that α_2-Ti_3Al is a stable phase below 1210°C. This implies that the α_2-Ti_3Al was precipitated from α-Ti(Al) solid solution during cooling.

Figure 4.3(a) displays a residual γ-TiAl grain embedded in the growing τ_2-Ti_2AlN in reaction layer B, as shown in Fig. 4.1(b), after annealing at 1400ºC for 1 h. Note that Ti reacted with AlN to produce Al and δ-TiN at the initial stage. Subsequently, Al atoms diffused into Ti to form γ-TiAl. The inward diffusion of N atoms into the γ-TiAl resulted in the precipitation of τ_2-Ti_2AlN between the δ-TiN and γ-TiAl layers, while the γ-TiAl layer gradually diminished. In contrast, Tian and Nemoto[59] indicated that the needle-like τ_1-Ti_3AlN and the plate-like τ_2-Ti_2AlN precipitated because γ-TiAl was nitridized at temperatures above 800ºC. The tendency of the phase transformation of γ-TiAl into τ_2-Ti_2AlN, resulting from the inward diffusion of N atoms, can be explained by the similarity in their crystal structures. The precipitation of τ_2-Ti_2AlN was predominantly governed by the substitution of N atoms for Al atoms (not Ti atoms) in γ-TiAl because of the strong attractive ionicity between Ti atoms and N atoms.[65] Figure 4.3(b) shows the alternating (001) layers of Ti and Al as viewed along the [110] direction of γ-TiAl. Once

each alternate Al atomic layer of γ-TiAl was replaced with an N atomic layer, the γ-TiAl was transformed into τ_2-Ti_2AlN with a stacking sequence AB'ABAB'AB…, where A and B represent the atomic planes of Ti and Al, respectively, and B' represents the substitution of an N atomic layer for each alternate Al atomic layer. Figure 4.3(c) shows that the layer A, B, and B' are parallel to (0001) planes of τ_2-Ti_2AlN while being viewed along the direction $[11\bar{2}0]$. From the atomic configurations in Figs. 4.3(b) and (c), it can be inferred that $[110]_{\gamma-TiAl} // [11\bar{2}0]_{\tau_2-Ti_2AlN}$ and $(001)_{\gamma-TiAl} // (0001)_{\tau_2-Ti_2AlN}$.

When N atoms are dissolved in γ-TiAl, two corresponding conditions are likely to arise: (1) in case that N atoms occupy the Al planes, one N atom is surrounded by eight Ti atoms, and (2) in case that N atoms occupy the Ti planes, one N atom is surrounded by eight Al atoms. Since a strong coulomb attractive interaction exists between Ti and N atoms, the substitution of N atoms for a half Al atoms in γ-TiAl is predominant from the viewpoint of the atomic configuration. As a consequence, N atoms were located more favorably in Al planes than in Ti planes.

It was unlikely that τ_2-Ti_2AlN precipitated due to the reduced solubility during cooling. Conversely, the τ_2-Ti_2AlN was most likely to precipitate as N atoms diffused into γ-TiAl upon annealing. The isothermal section of the Ti-Al-N phase diagram at 1400°C [Fig. 4.2(a)] shows that the τ_2-Ti_2AlN is in equilibrium with the Ti-Al compounds such as γ-TiAl and the β-Ti(Al) solid solution and that the solubility of nitrogen in γ-TiAl is very limited. It is thus inferred that τ_2-Ti_2AlN is precipitated in γ-TiAl when more than 2 at.% N diffuses inwards to the γ-TiAl layer upon annealing at 1400°C.

Figure 4.4(a) displays the precipitation of τ_2-Ti_2AlN in reaction layer C, as shown in Figs. 4.1(b) and 1(c), after annealing at 1400ºC for 1 h. Using

TEM/EDS analyses, the composition of this precipitate was measured as 46.9 at% Ti, 23.5 at% Al, and 29.6 at% N in correspondence to the composition of τ_2-Ti_2AlN. The superimposed selected area diffraction patterns (SADPs), as shown in Fig. 4.4(b), were taken from the region encompassing τ_2-Ti_2AlN and its matrix. The lattice parameters of τ_2-Ti_2AlN with a hexagonal crystal structure were calculated as a = 0.30 nm and c = 1.36 nm. These calculated lattice parameters of τ_2-Ti_2AlN were consistent with those reported in literature (a= 0.2989 nm and c= 1.3615 nm).[66] The matrix was identified to be composed of Ti_3Al_5 and γ-TiAl as discussed below. The incident electron beam was parallel to the $[011]$ zone axis of γ-TiAl (or Ti_3Al_5) and the $[11\bar{2}0]$ zone axis of τ_2-Ti_2AlN. The orientation relationships between γ-TiAl (or Ti_3Al_5) and τ_2-Ti_2AlN can be expressed as follows: $[110]_{\gamma-TiAl} // [11\bar{2}0]_{\tau_2-Ti_2AlN}$ and $(1\bar{1}\bar{1})_{\gamma-TiAl} // (1\bar{1}0\bar{3})_{\tau_2-Ti_2AlN}$. They are consistent with the atomic configurations as shown in Figs. 4.3(b) and (c). The precipitation of τ_2-Ti_2AlN in reaction layer C was accompanied with the release of Al atoms, since N atoms diffused into the γ-TiAl and went to the regular sites of the Al sublattice.

Figure 4.5(a) displays a bright field image of the matrix in reaction layer C, as shown in Figs. 4.1(b) and 1(c), after annealing at 1400ºC for 1 h. When the electron beam was incident along some specific directions, the γ-TiAl and Ti_3Al_5 were discernible as illustrated in Fig. 4.5(a). It was evident that the matrix was composed of two phases, identified as γ-TiAl and Ti_3Al_5, respectively. The selected area diffraction pattern, as shown in Fig. 4.5(b), illustrates the corresponding superstructures of Al-rich γ-TiAl or Ti_3Al_5. The 1/2{002} superlattice diffractions resulted from the ordered $L1_0$ superstructure of γ-TiAl, while the 1/4{100} superlattice diffractions resulted from the ordering of substitutional Al atoms in the Ti sublattice of Ti_3Al_5. The 1/4(100) superlattice diffractions in Fig. 4.5(b) indicate that the ordering repeats once every four unit

cells of the underlying $L1_0$ structure along the a- and b-axes. When τ_2-Ti_2AlN was formed by the replacement of Al atoms with N atoms, the released Al atoms diffused into the γ-TiAl, resulting in an Al-rich γ-TiAl. After Al became enriched in γ-TiAl to a certain degree, a new intermetallic compound or Ti_3Al_5 precipitated during cooling. This finding is consistent with previous studies[67-69] for the ordering process of rapidly solidified Al-rich γ-TiAl alloys with fcc-based, long-period superstructures, and point defects in γ-TiAl. Doi et al.[67] indicated that Al-rich γ-TiAl sometimes decomposed into a two-phase structure (Ti_3Al_5 + γ-TiAl) with undulating surfaces. The dark field image [Fig. 4.5(c)] was formed by the (001) superlattice diffraction of Ti_3Al_5, marked by the circle in Fig. 4.5(b), so that the bright phase represented Ti_3Al_5.

The stoichiometric γ-TiAl compound has an $L1_0$-type ordered structure with an axial ratio c/a of 1.01, and is thus considered essentially an fcc structure. This structure consists of alternate layers of Ti and Al atoms along the direction perpendicular to [001]. Fu and Yoo[70] revealed that the effect of lattice distortion due to the ordering is generally small in γ-TiAl. For Ti-rich γ-TiAl, the lattice relaxation decreases the inter-atiomic distance of substitutional defects (Ti) with the first neighboring shell of Ti atoms in correspondence to a decrease in the lattice constant ratio c/a to 1.00. On the other hand, for Al-rich γ-TiAl, the lattice relaxation of the neighboring Al shell increases the c/a ratio to 1.02. Using X-ray diffraction, Swaminathan et al.[71] concluded that Ti atoms could be replaced in an ordering manner with excess Al atoms in Al-rich γ-TiAl. In addition, Vujic et al.[72] reported that the c/a ratio of Al-rich γ-TiAl increased with the Al content up to 60 at% Al. In Al-rich γ-TiAl, excess Al atoms can occupy Ti regular sites and the resultant stress field is accommodated by the lattice distortion from the stoichiometric γ-TiAl. If the Al content becomes sufficiently large, an ordering of the Al atoms on the Ti sublattice takes place and eventually leads to an ordering transformation of γ-TiAl into Ti_3Al_5 by the

introduction of a periodic array of defects in Ti_3Al_5.

Based upon the above discussion, the precipitation of τ_2-Ti_2AlN and the formation of Ti_3Al_5 can be expressed by the following reactions.

$$2\ \gamma\text{-TiAl} + \text{N} \rightarrow \tau_2\text{-Ti}_2\text{AlN} + \text{Al} \qquad (1)$$

$$3\ \gamma\text{-TiAl} + 2\ \text{Al} \rightarrow \text{Ti}_3\text{Al}_5 \qquad (2)$$

Reaction (1) indicates that the N inward diffusion into γ-TiAl results in τ_2-Ti_2AlN with the release of Al atoms. As a consequence, the released Al atoms go into the matrix γ-TiAl, leading to the formation of Ti_3Al_5 as expressed by reaction (2).

Figure 4.6(a) displays the bright field image of the lamellar structure (δ-TiN_{1-x} + α-Ti(Al, N) in reaction layer D, as shown in Figs. 4.1(b) and 1(d), after annealing at 1400ºC for 1 h. It was obvious that the δ-TiN_{1-x} was twinned. The TEM specimen for this observation was acquired from a cross-sectional SEM specimen perpendicular to the longitudinal direction of the precipitates using FIB. It thus excludes the possibility that the δ-TiN_{1-x}, as shown in Fig. 4.1(d), is a needle-like phase, since it would otherwise show a circular image in Fig. 4.6(a). As mentioned previously,[4] δ-TiN is a non-stoichiometric compound, stable in the compositional range from 30 to 55 at% N, and is usually designated as δ-TiN_{1-x}. The α-Ti can dissolve Al and N in solid solution and, is expressed as α-Ti(Al, N). Figure 4.6(b) reveals the SADPs of δ-TiN_{1-x} and α-Ti(Al, N) along the zone axes $[110]_{\delta-TiN_{1-x}}$ or $[1\bar{1}20]_{\alpha-Ti(Al,N)}$ with their closely packed planes in the edge-on direction. The orientation relationships between δ-TiN_{1-x} and α-Ti(Al, N) were identified as

$[110]_{\delta-TiN_{1-x}} // [11\bar{2}0]_{\alpha-Ti(Al,N)}$ and $(111)_{\delta-TiN_{1-x}} // (0001)_{\alpha-Ti(Al,N)}$. The SADPs are redrawn and diffracting spots are indexed in Fig. 4.6(c) for clarity. The extra spots were caused by the twinning of δ-TiN_{1-x}. The twinning and/or plate-like shape leads to the streaking of the diffraction spots as shown in Fig. 4.6(b). Figure 4.6(d) shows the atomic configurations at the δ-TiN_{1-x}/α-Ti(Al, N) interface as viewed along the $[110]_{\delta-TiN_{1-x}}$ and $[11\bar{2}0]_{\alpha-Ti(N)}$. It should be noted that the stoichiometric δ-TiN and the pure α-Ti were taken as examples, respectively, in Fig. 4.6(d) for simplicity. The crystal structures of δ-TiN and α-Ti are distinguished from each other based on the stacking sequences of their closely packed Ti atoms, which are ABCABC… and ABAB…, respectively. Furthermore, small N atoms were inserted in the octahedral interstitial sites of the NaCl crystal structure like δ-TiN. Different stacking sequences of the Ti, Al, and N layers along the direction perpendicular to the closely packed planes were also found in some Ti-Al-C or Ti-Al-N systems such as TiAl/Ti_2AlC, TiC/Ti_2AlC, TiAl/Ti_2AlN, TiN/Ti_2AlN, and Ti/TiC.[59, 73-75] According to the Ti-N binary phase diagram,[4] the maximum concentration of solute interstitially dissolved in α-Ti is about 23 at% N, while α-Ti(Al, N) solid solution and δ-TiN_{1-x} can coexist over the temperature range from 1050° to 2350°C. While a significant percentage of N atoms were dissolved into the Ti sublattice to form α-Ti(Al, N) solid solution, the remaining N atoms reacted with α-Ti to form δ-TiN_{1-x} during annealing at 1400ºC.

4.4 Conclusions

1. After AlN was bonded with a Ti foil at 1400ºC for up to 1 h in an Ar protective atmosphere, the AlN/Ti interfaces were investigated using analytical transmission microscopy as well as analytical scanning electron microscopy.
2. Two nitride layers (δ-TiN and τ_2-Ti_2AlN), one aluminide layer (γ-TiAl), and

α-Ti solid solution were initially formed due to the interfacial reactions between AlN and Ti on annealing at 1400°C for 0.1 h. Further diffusion of N atoms into the reaction zone played an important role of phase development at the AlN/Ti interface.

3. The chopped fiber-like τ_2-Ti_2AlN was precipitated in the γ-TiAl matrix due to nitridization of γ-TiAl or the replacement of one half Al atoms in γ-TiAl with N atoms after annealing at 1400°C for 1 h. The orientation relationships between γ-TiAl and τ_2-Ti_2AlN were $[110]_{\gamma-TiAl} // [11\bar{2}0]_{\tau_2-Ti_2AlN}$ and $(1\bar{1}\bar{1})_{\gamma-TiAl} // (1\bar{1}0\bar{3})_{\tau_2-Ti_2AlN}$.
4. After the precipitation of τ_2-Ti_2AlN in the γ-TiAl matrix, the diffusion of the released Al atoms into the γ-TiAl matrix resulted in an ordered aluminum-rich γ-TiAl or Ti_3Al_5 after annealing at 1400°C for 1 h.
5. A lamellar structure consisting of α-Ti(Al, N) and heavily twinned δ-TiN_{1-x} was formed due to the nitridization of α-Ti after annealing at 1400°C for 1 h. The orientation relationships between δ-TiN_{1-x} and α-Ti were identified to be $[110]_{\delta-TiN} // [11\bar{2}0]_{\alpha-Ti(Al,N)}$ and $(111)_{\delta-TiN} // (0001)_{\alpha-Ti(Al,N)}$.

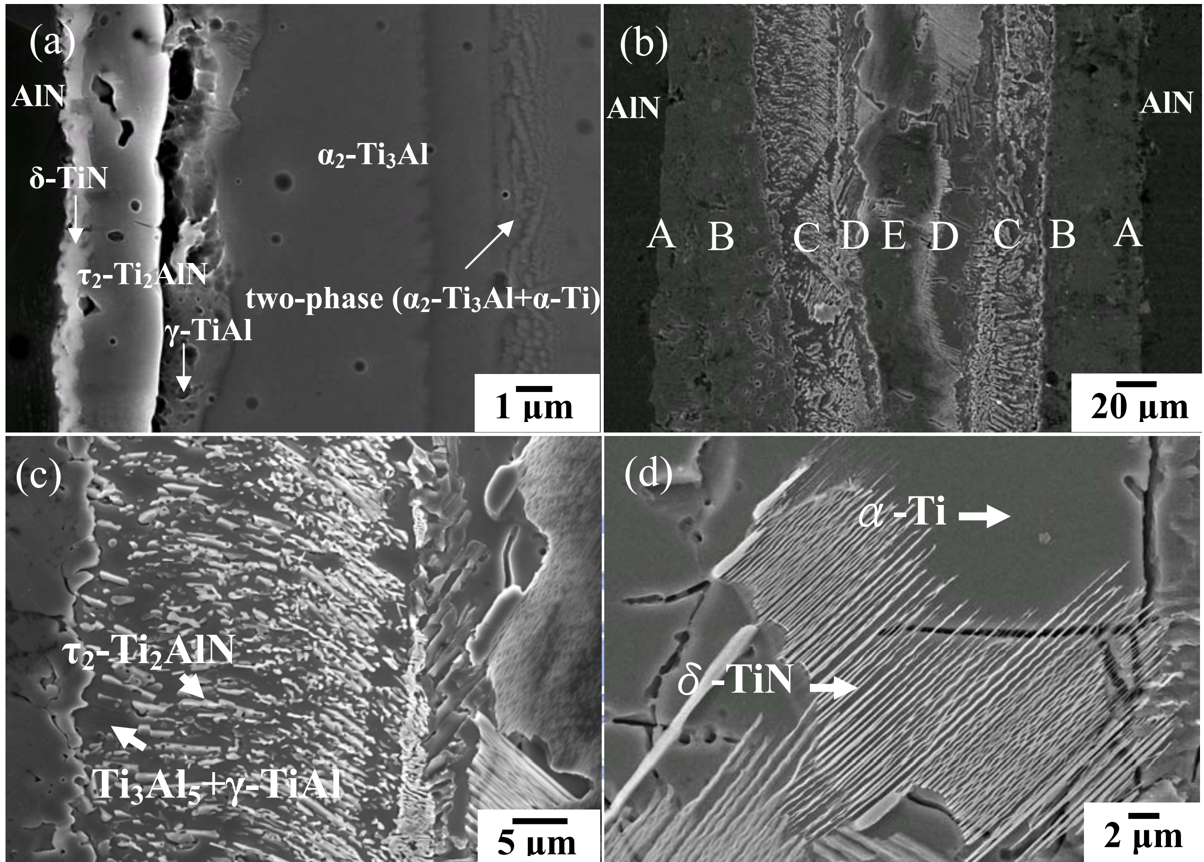

Fig. 4. 1. Secondary electron images showing the interfacial microstructures of the AlN/Ti/AlN specimens: (a) after annealing at 1400°C/0.1 h; (b) after annealing at 1400°C/1 h [A: δ-TiN, B: τ_2-Ti_2AlN, C: τ_2-Ti_2AlN+γ-TiAl+Ti_3Al_5, D: a lamellar structure (δ-TiN+α-Ti), E: α-Ti]. (c) A magnified secondary electron image of reaction layer C in Fig. 1(b) showing a chopped fiber like τ_2-Ti_2AlN in the (Ti_3Al_5+γ-TiAl) matrix; (d) a magnified secondary electron image of reaction layer D showing a lamellar structure of (δ-TiN+α-Ti). All specimens were etched by the Kroll reagent.

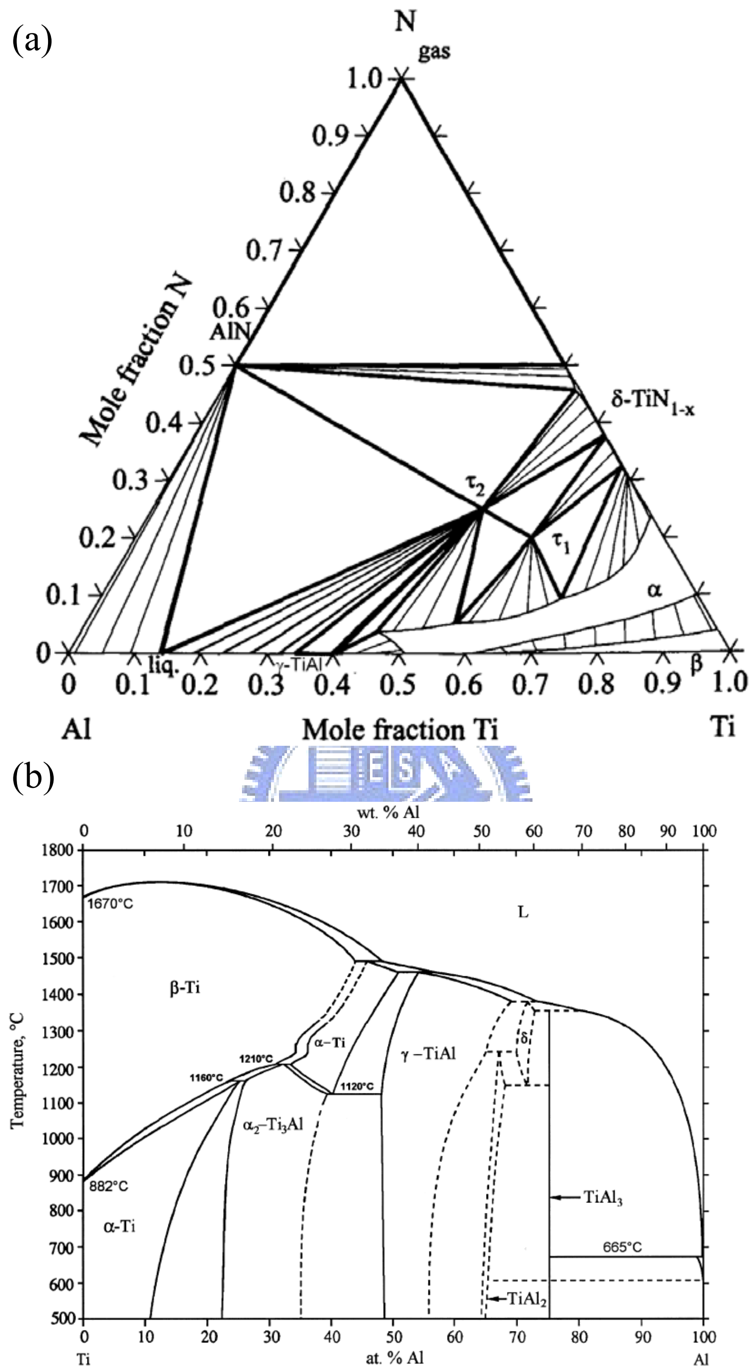

Fig. 4. 2. (a) The isothermal section of the Ti-Al-N phase diagram at 1400°C and (b) the Ti-Al binary phase diagram.[4, 64]

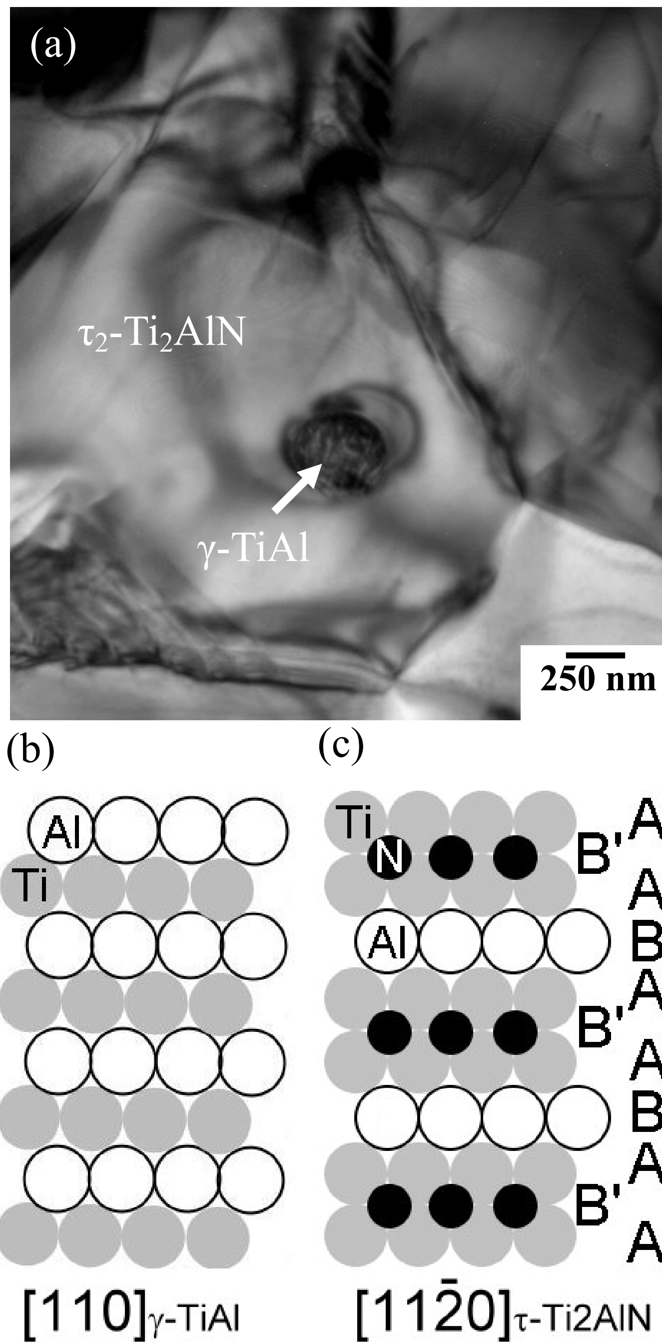

Fig. 4. 3. (a) A bright field image showing a residual γ-TiAl grain embedded in τ_2-Ti_2AlN after annealing at 1400°C/1 h; (b) the alternating (001) layers of Ti and Al viewed along the direction [110] in γ-TiAl; (c) the stacking sequence AB'ABAB'AB… of the (0001) layers viewed along the direction $[11\bar{2}0]$ in τ_2-Ti_2AlN.

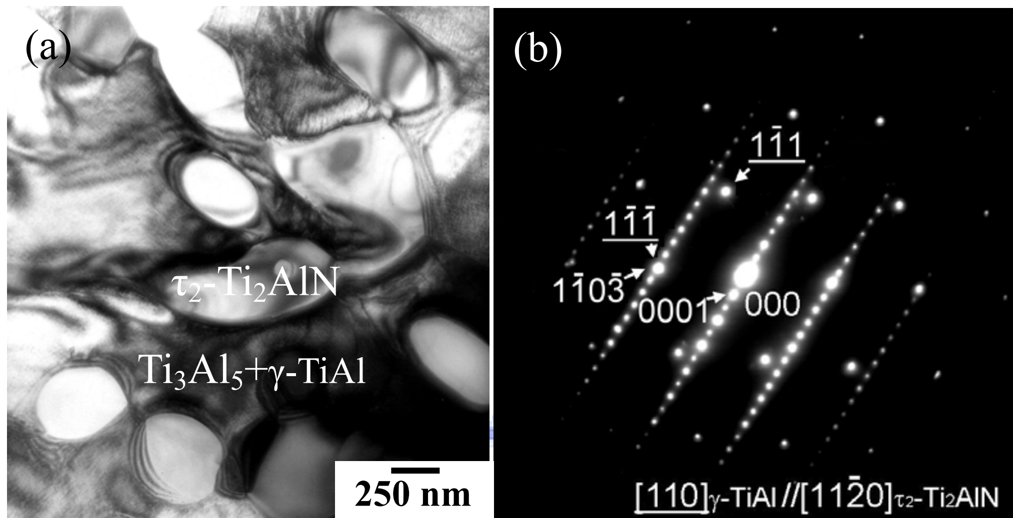

Fig. 4. 4. (a) A bright field image showing the precipitation of τ_2-Ti_2AlN in the matrix of Ti_3Al_5+γ-TiAl, taking place in reaction layer C in Fig. 4.1(b) after annealing at 1400°C/1 h; (b) the superimposed selected area diffraction patterns (SADPs) of τ_2-Ti_2AlN and a two-phase (Ti_3Al_5+γ-TiAl), showing the orientation relationships $[110]_{\gamma-TiAl}//[11\bar{2}0]_{\tau_2-Ti_2AlN}$ and $(1\bar{1}\bar{1})_{\gamma-TiAl}//(1\bar{1}0\bar{3})_{\tau_2-Ti_2AlN}$.

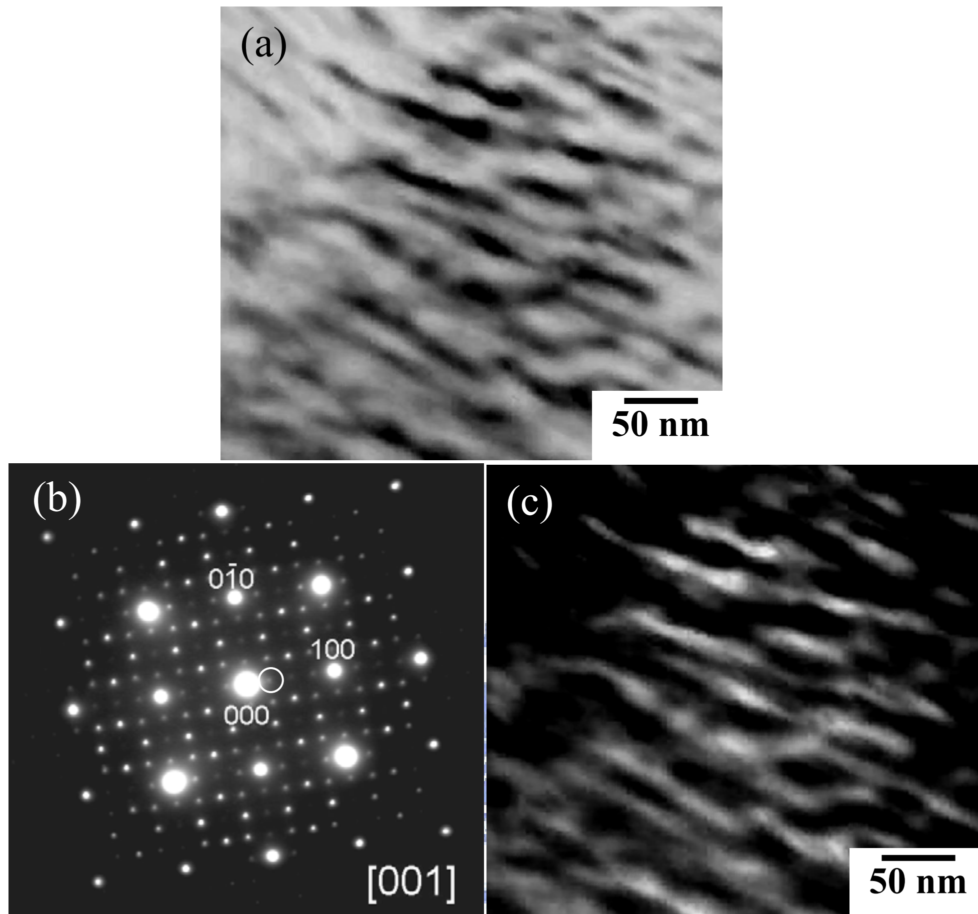

Fig. 4. 5. After annealing at 1400°C/1 h: (a) a bright field image of the modulated structure of Ti_3Al_5+γ-TiAl; (b) the superimposed SADPs of Ti_3Al_5 and γ-TiAl, with the superlattice deflections resulting from the ordering of substitutional Al atoms on the Ti sublattice; (c) a central dark field image of Ti_3Al_5+γ-TiAl formed by the 1/4(100) superlattice diffraction of Ti_3Al_5, as marked by a circle in Fig. 4.5 (b).

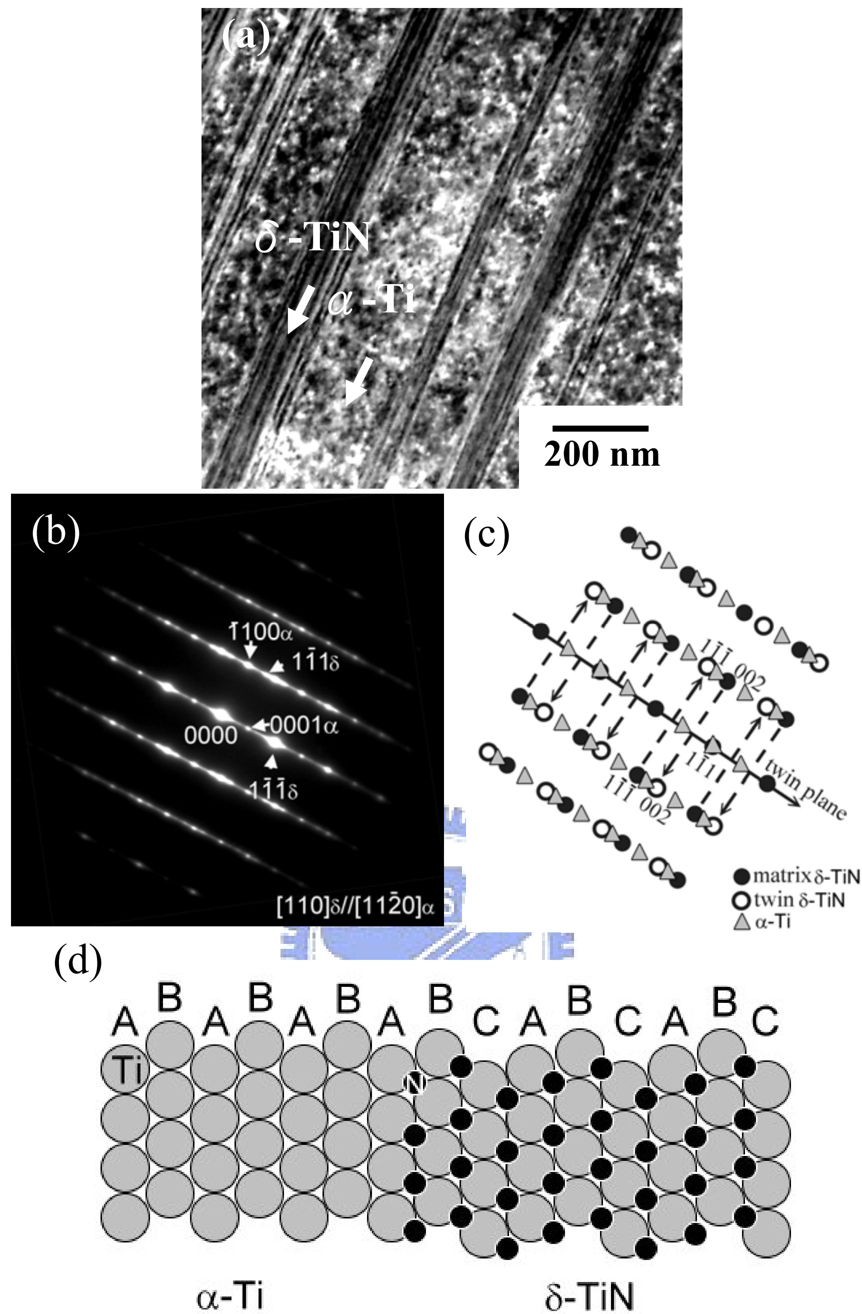

Fig. 4. 6. (a) A bright field image of the lamellar structure (δ-TiN+α-Ti) after annealing at 1400°C/1 h; (b) the SADPs of δ-TiN (Z=$[110]_{\delta-TiN}$) and α-Ti (Z=$[11\bar{2}0]_{\alpha-Ti}$); (c) the schematic illustration of the SADPs in (b); (d) the atomic configuration at the δ-TiN/α-Ti interface viewed along the $[110]_{\delta-TiN}$ or $[11\bar{2}0]_{\alpha-Ti}$ direction. The TEM specimen was acquired from a cross-sectional SEM specimen along the direction perpendicular to the precipitate using FIB.

Chapter 5 Summary

The interfacial reactions between AlN and Ti have been examined by using SEM/EDS and TEM/EDS after annealing at 1000°-1500°C. As a result, the following conclusions have been obtained:

1. After annealing at 1000°C, a δ-TiN layer was initially formed in the reaction zone between AlN and Ti, and the α_2-Ti_3Al layer subsequently developed between δ-TiN and Ti. A twinned α_2-Ti_3Al structure was observed on annealing on 1000°C, while an ordered cubic τ_1-Ti_3AlN was precipitated from the twinned α_2-Ti_3Al during cooling. The orientation relationships between τ_1-Ti_3AlN and α_2-$Ti_3Al(N)$ were $[111]_{\tau_1-Ti_3AlN}//[0001]_{\alpha_2-Ti_3Al(N)}$ and $(0\bar{1}1)_{\tau_1-Ti_3AlN}//(\bar{1}\bar{1}20)_{\alpha_2-Ti_3Al(N)}$.

2. A sequence of phases was observed at the interface consisted of δ-TiN, τ_2-Ti_2AlN, τ_1-Ti_3AlN, α_2-Ti_3Al, and a two-phase (α_2-Ti_3Al + α-Ti) region After annealing at 1300°C. The α_2-Ti_3Al region revealed equiaxed and elongated morphologies with $[0001]_{equiaxed}//[\bar{1}100]_{elongated}$ and $(\bar{1}010)_{equiaxed}//(\bar{1}\bar{1}22)_{elongated}$. In the two-phase ($\alpha_2$-$Ti_3Al$ + α-Ti) region, α_2-Ti_3Al and α-Ti were found to satisfy the following orientation relationship: $[0001]_{\alpha-Ti}//[0001]_{\alpha_2-Ti_3Al}$ and $(1\bar{1}00)_{\alpha\text{-Ti}}//(1\bar{1}00)_{\alpha_2\text{-Ti}_3\text{Al}}$.

3. After annealing at 1400°C, the γ-TiAl and a lamellar two-phase (γ-TiAl+α_2-Ti_3Al) structure, instead of τ_1-Ti_3AlN, were found in between τ_2-Ti_2AlN and α_2-Ti_3Al. The orientation relationship of γ-TiAl and α_2-Ti_3Al in the lamellar structure was identified to be as follows: $[011]_{\gamma-TiAl}//[2\bar{1}\bar{1}0]_{\alpha_2-Ti_3Al}$ and

$(1\bar{1}\bar{1})_{\gamma-TiAl}//(01\bar{1}0)_{\alpha_2-Ti_3Al}$. Compared with the reaction zone after annealing at 1400ºC, the γ-TiAl was not found at the interface after annealing at 1500°C.

5. After AlN was bonded with a Ti foil at 1400ºC for up to 1 h, a chopped fiber-like τ_2-Ti_2AlN precipitated in the matrix of γ-TiAl, with $[110]_{\gamma-TiAl}//[11\bar{2}0]_{\tau_2-Ti_2AlN}$ and $(1\bar{1}\bar{1})_{\gamma-TiAl}//(1\bar{1}0\bar{3})_{\tau_2-Ti_2AlN}$, by substituting N atoms for one-half Al atoms after annealing at 1400°C for 1 h. The released Al atoms, due to the precipitation of τ_2-Ti_2AlN, resulted in an ordered Al-rich γ-TiAl or Ti_3Al_5. Furthermore, the α-Ti (Al, N) was nitridized into a lamellar layer (δ-TiN + α-Ti) with $[110]_{\delta-TiN}//[11\bar{2}0]_{\alpha-Ti}$ and $(111)_{\delta-TiN}//(0001)_{\alpha-Ti}$.

References

1. L. M. Sheppard, "Aluminum Nitride: A Versatile but Challenging Material," *Am. Ceram. Soc. Bull.*, **69** [11] 1801-12 (1990).

2. N. Iwase, A. Tsuge, and Y. Sugirua, "Development of A High Thermal Conductive AlN Ceramic Substrate Technology," *Int. J. Hybrid Microelectronics*, **7** [4] 49-53 (1984).

3. P. Villars, A. Prince, and H. Okamoto, *Handbook of Ternary Alloy Phase Diagrams*, ASM International, Materials Part, OH, 1994.

4. J. L. Murray, *Phase Diagrams of Binary Titanium Alloys*, ASM International, Metals park, Ohio, 1987.

5. J. Braun and M. Ellner, "Phase Equilibria Investigations on the Aluminum-Rich Part of the Binary System Ti-Al," *Met. Trans. A*, **32A** 1037-47 (2001).

6. V. Raghavan, "Al-Ti(Aluminum-Titanium)," *J. Phase Equilibria and Diffusion*, **26** [2] 171-72 (2005).

7. X. He, K. Tao, and Y. Fan, "Solid-State Reaction of Ti and Ni Thin Film with Aluminum Nitride," *J. Vac. Sci. Technol.*, **14** [4] 2564-69 (1996).

8. C. Tsai, J. Tseng, and C. His, "Interfacial Adhesion and Microstructure of Thick Film Metallized Aluminum Nitride Substrates," *Ceram. Inter.*, **28** 23-28 (2002).

9. M. Borowski and J. P. Dallas, "Structural Characterization of Ti Implanted AlN," *J. Mater. Res.*, **12** [10] 3136-42 (1995).

10. K. Komeya, "Development of Nitrogen Ceramics," *Am. Ceram. Soc. Bull.*, **63** [9] 1158-59 (1984).

11. N. Kuramoto, H. Taniguchi, and I. Aso, "Translucent AlN Ceramic Substrate," *IEEE Trans. Compon., Hybrids, Manuf. Technol*, **CHMT-9** [4] 386-90 (1986).

12. Y. Imanaka and M. R. Notis, "Interfacial Reaction between Titanium Thin

Films and Aluminum Nitride Substrates," *J. Am. Ceram. Soc.*, **82** [6] 1547-52 (1999).

13. X. He, Si-Ze Yang, K. Tao, and Y. Fan, "Investigation of the Interface Reactions of Ti Thin Films with AlN Substrate," *J. Mater. Res.*, **12** [3] 846-51 (1997).

14. M. Pinkas, N. Frage, N. Froumin, J. Pelleg, and M. P. Dariel, "Early Stages of Interface Reactions between AlN and Ti Thin Films," *J. Vac. Sci. Technol.*, **20** [3] 887-96 (2002).

15. T. Yasumoto, K. Amakawa, N. Iwase, and N. Shinsawa, "Reaction between AlN and Metal Thin Films during High Temperature Annealing," *J. Ceram. Soc. Jpn.*, **101** [9] 969-73 (1993).

16. R. Yue, Y. wang, C. Chen, and C. Xu, "Interface Reaction of Ti and Mullite Ceramic Substrate," *Appl. Surf. Sci.*, **126** 255-64 (1998).

17. M. H. El-Sayed, M. Naka, and J. C. Schuster, "Interfacial Structure and Reaction Mechanism of AlN/Ti Joints," *J. Mater. Sci.*, **32** 2715-21 (1997).

18. Y. S. Han, K. B. Kalmykov, S. F. Dunaev, and A. I. Zaitsev, "Phase Equilibria in the Ti-Al-N System at 1273K," *Dok. Phy. Chem.*, **396** [2] 134-37 (2004).

19. Y. Paransky, A. Berner, and I. Gotman, "Microstructure of Reaction Zone at the Ti-AlN Interface," *Mater. Let.*, **40** 180-86 (1999).

20. Y. Paransky, A. Berner, I. Gotman, and E. Gutmanas, "Phase Recognition in AlN-Ti System by Energy Dispersive Spectroscopy and Electron Backscatter Diffraction," *Mikrochim. Acta*, **134** 171-77 (2000).

21. Y. Paransky, I. Gotman, and E. Y. Gutmanas, "Reactive Phase Formation at AlN-Ti and AlN-TiAl Interfaces," *Mater. Sci. Eng.*, **A277** 83-94 (2000).

22. C. H. Chiu and C. C. Lin, "Microstructural Characterization and Phase Development at the Interface Between Aluminum Nitride and Titanium After Annealing at 1300°-1500°C," *J. Am. Ceram. Soc.*, **89** [4] 1409-18 (2006).

23. Y. Paransky, A. Berner, and I. Gotman, "Microstructure of Reaction Zone at

the Ti-AlN Interface," *Mater. Let.*, **40** 180-86 (1990).
24. L. Hultman, "Thermal Stability of Nitride Thin Films," *Vacuum*, **57** 1-30 (2000).
25. J. C. Schuster and J. Bauer, "The Ternary System Titanium-Aluminum-Nitrogen," *J. Solid State Chem.*, **53** [2] 260-65 (1984).
26. R. Yue, Y. Wang, Y. Wang, and C. Chen, "Study on Interfacial Reaction of Ti/AlN by SIMS, RBS and XRD," *Surf. Interface Anal.*, **27** 98-102 (1999).
27. J. Magnan, G. C. Weatherly, and M. C. Cheynet, "The Nitriding Behavior of Ti-Al Alloys at 1000°C," *Metall. Mater. Trans. A*, **30A** 19-29 (1999).
28. H. Xiao, I. M. Robertson, and H. K. Birnbaum, "Deuterium Driven Phase Transitions in the Ti_3Al Intermetallic," *Acta Mater.*, **50** 3671-82 (2002).
29. P. Villars, A. Prince, and H. Okamoto, *Handbook of Ternary Alloy Phase Diagrams*, ASM International, Materials Part, OH, 1995.
30. C. A. Slack, "Nonmetallic Crystals with High Thermal Conductivity," *J. Phys. Chem. Solids*, **34** 321-35 (1973).
31. N. Iwase, K. Anzai, and K. Shinozaki, "Aluminum Nitride Substrates Having High Thermal Conductivity," *Toshiba Review*, **153** 49-53 (1985).
32. P. Martineau, R. Pailler, M. Lahaye, and R. Naslain, "SiC Filament/Titanium Matrix Composites Regarded as Model Composites. II.--Fiber/Matrix Chemical Interactions at High Temperatures," *J. Mater. Sci.*, **19** 2749-70 (1984).
33. J. C. Feng, M. Naka, and J. C. Schuster, "Reaction Mechanism between SiC Ceramic and Titanium Foil in Solid State Bonding," *J. Japan Inst. Metals*, **59** 978-83 (1995).
34. W. J. Whatley and F. E. Wawner, "Kinetics of the Reaction between SiC(SCS-6) Filaments and Titanium(6Al-4V) Matrix," *J. Mater. Sci. Let.*, **4** [2] 173-75 (1985).
35. D. Travessa and M. Ferrante, "The Al_2O_3-Titanium Adhesion in the View of the Diffusion Bonding Process," *J. Mater. Sci.*, **37** 4385-90 (2002).
36. E. Faran, I. Gotman, and E. Y. Gutmanas, "Experimental Study of the

Reaction Zone at Boron Nitride Ceramic-Ti Metal Interface," *Mater. Sci. Eng.*, **A288** 66-74 (2000).
37. K. L. Lin and C. C. Lin, "Ti_2ZrO Phases Formed in the Titanium and Zirconia Interface After Reaction at 1550°C," *J. Am. Ceram. Soc.*, **88** [5] 1268-72 (2005).
38. P. A. Janeway, "Making the Grade in Demanding Electronic Application," *Ceram. INd.*, **137** 28-32 (1991).
39. J. A. Chediak, "Ceramic Engineers in the 21st Century," *Am. Ceram. Soc. Bull.*, **75** [1] 52-55 (1996).
40. T. B. Jackson, A. V. Virkar, K. L. More, R. B. Dinwiddie, and R. A. Cutler, "High-Thermal-Conductivity Aluminum Nitride Ceramics: the Effect of Thermodynamic, Kinetic and Microstructural Factors," *J. Am. Ceram. Soc.*, **80** [6] 1421-35 (1997).
41. S. Nakahata, K. Sogabe, T. Matsuura, and A. Yamakawa, "One Role of Titanium Compound Particles in Aluminum Nitride Sintered Body," *J. Mater. Sci.*, **32** 1873-76 (1997).
42. H. D. Lee, *Phase Chemistry, Thermodynamic and Kinetic Characterization of Interfacial Reaction Between Aluminum Nitride and Titanium*, ; Ph.D. Dissertation, Arizona State University, Tempe, AZ, 1993.
43. A. D. Westwood and M. R. Notis, "Analytical Electron Microscopy Study of AlN Substrates and Metallization Interfaces," *Adv. Ceram*, **26** 171-87 (1989).
44. A. D. Westwood and M. R. Notis, "An Issue in Thermal Management: Metallizing High Thermal Conductivity Ceramic Substrates in Microelectronics," *J. Miner. Met. Mater. Soc.*, **43** [6] 10-15 (1991).
45. A. H. Carim and R. E. Loehman, "Microstructure at the Interface between AlN and A Ag-Cu-Ti Braze Alloy," *J. Mater. Res.*, **5** [7] 1520-29 (1990).
46. R. E. Loehman, "Interfacial Reactions in Ceramic-Metal Systems," *Ceram. Bull.*, **68** [4] 891-96 (1989).
47. R. E. Loehman and A. P. Tomsia, "Reactions of Ti and Zr with AlN and

Al_2O_3," *Acta Metall. Mater.*, **40** [suppl.] S75-S83 (1992).

48. K. L. Lin and C. C. Lin, "Zirconia-Related Phases in the Zirconia/Titanium Diffusion Couple After Annealing at 1000°-1550°C," *J. Am. Ceram. Soc.*, **88** [10] 2928-34 (2005).

49. M. A. Pietzka and J. C. Schuster, "Phase Equilibria in the Quaternary System Ti-Al-C-N," *J. Am. Ceram. Soc.*, **79** [9] 2321-30 (1996).

50. A. Dutta and D. Banerjee, "Superplastic Behaviour in A Ti_3Al-Nb Alloy," *Scripta Metall. Mater.*, **24** [7] 1319-22 (1990).

51. J. M. Kim, C. G. Park, T. K. Ha, and Y. W. Chang, "Microscopic Observation of Superplastic Deformation in A 2-Phase Ti_3Al-Nb Alloy," *Mater. Sci. Eng.*, **A269** 197-204 (1999).

52. B. D. Cullity, *Elements of X-Ray Diffraction*, Addison-Wesley Publishing Company, Inc., California, 1978.

53. J. Raisanen, A. Anttila, and J. Keinonen, "Diffusion of Aluminum in Ion-Implanted a-Ti," *J. Appl. Phys.*, **57** [2] 613-14 (1985).

54. A. Anttila, J. Raisanen, and J. Keinonen, "Diffusion of Nitrogen in a-Ti," *Appl. Phys. Lett.*, **42** [6] 498-500 (1983).

55. J. C. Viala, N. Peillon, L. Clochefert, and J. Bouix, "Diffusion Paths and Reaction Mechanisms in the High-Temperature Chemical Interaction between Carbon and Titanium Aluminides," *Mater. Sci. Eng.*, **A203** 222-37 (1995).

56. I. Barin, *Thermochemical Data of Pure Substances,*, VCH, Weinheim, Germany, 1989.

57. Y. Paransky, L. Klinger, and I. Gotman, "Kinetics of Two-Phase Layer Growth during Reactive Diffusion," *Mater. Sci. Eng.*, **A270** 231-36 (1999).

58. B. Zhao, J. Sun, J. S. Wu, and Z. X. Yuan, "Gas Nitriding Behavior of TiAl Based Alloys in an Ammonia Atmosphere," *Scripta Mater.*, **46** 581-86 (2002).

59. W. H. Tian and M. Nemoto, "Precipitation Behavior of Nitrides in $L1_o$-ordered TiAl," *Intermetallics*, **13** 1030-37 (2005).

60. J. C. Pivin, P. Zheng, and M. O. Ruault, "Transmission Electron Microscopy

Investigation of the Structural Transformations in Titanium or TiAl Implanted with Nitrogen, Carbon, Oxygen and Boron," *Mater. Sci. Eng.*, **A115** 83-88 (1989).

61. A. B. Kloosterman and J. Th. M. De Hosson, "Microstructural Characterization of Laser Nitrided Titanium," *Scripta Metal. Mater.*, **33** [4] 567-73 (1995).

62. K. Saito and T. Matsushima, "Nitrogen Ion Implantation into the Intermetallic Compound TiAl," *Mater. Sci. Eng.*, **A115** 355-59 (1989).

63. G. Cliff and G. W. Lorimer, "The Quantitative analysis of thin specimens," *Journal for Microscopy*, [103] 203-07 (1975).

64. Q. Chen and B. Sundman, "Thermodynamic Assessment of the Ti-Al-N System," *J. Phase Equilibria*, **19** [2] 146-60 (1998).

65. M. Inoue, M. Nunogaki, and K. Suganuma, "Chemical Reaction of TiAl Intermetallics wiht a Nitrogen Plasma," *J. Solid State Chem.*, **157** 339-46 (2001).

66. P. Villars and L. D. Calvert, *Pearson's Handbook of Crystallographic Data for Intermetallic Phases*, ASM International, Materials Park, OH, 1991.

67. M. Doi, T. Koyama, T. Taniguchi, and S. Naito, "Morphological Changes of the Ti_3Al_5 Phase Formed by Phase-decomposition of TiAl Intermetallics," *Mater. Sci. Eng.*, **A329-331** 891-97 (2002).

68. G. Sattonnay and O. Dimitrov, "Long-Range Order Relaxation and Phase Transformation in g-TiAl Alloys," *Acta Mater.*, **47** [7] 2077-88 (1999).

69. T. Nakano, A. Negishi, K. Hayashi, and Y. Umakoshi, "Ordering Process of Al_5Ti_3, h-Al_2Ti and r-Al_2Ti with F.C.C.-Based Long-Period Superstructures in Rapidly Solidified Al-Rich TiAl Alloys," *Acta Mater.*, **47** [4] 1091-104 (1999).

70. C. L. Fu and M. H. Yoo, "Bonding Mechanisms and Point Defects in TiAl," *Intermetallics*, **1** 59-63 (1993).

71. S. Swaminathan, I. P. Jones, A. W. S. Johnson, and H. L. Fraser, "Debye-Waller Factors in off-stoichiometric TiAl: Effect of Ording of Excess Al Atoms on Ti Sites," *Philo. Maga. Let.*, **73** [6] 319-30 (1996).

72. D. Vujic, Z. Li, and S. H. Whang, "Effect of Rapid Solidification and Alloying Addition on Lattice distortion and Atomic Ordering in $L1_0$ TiAl Alloys and Their Ternary Alloys," *Metall. Trans. A*, **19A** [10] 2445-55 (1988).
73. W. Lu, C. L. Chen, F. H. Wang, J. P. Lin, G. L. Chen, and L. L. He, "Phase Transformation in the Nitride Layer during the Oxidation of TiAl-based Alloys," *Scripta Mater.*, **56** 773-76 (2007).
74. R. Yu, S. Zhang, L. L. He, W. T. Wu, and H. Q. Ye, "Metal/Ceramic Interface in An in Situ Synthesized Ti/TiC_P Compostie Coating by Laser Processing," *J. Mater. Res.*, **16** [1] 9-12 (2001).
75. Z. J. Lin, M. J. Zhuo, Y. C. Zhou, M. S. Li, and J. Y. Wang, "Microstructural Characterization of Layered Ternary Ti_2AlC," *Acta Mater.*, **54** 1009-15 (2006).

List of Publications

1. Chia-Hsiang Chiu and Chien-Cheng Lin, “Microstructural Characterization and Phase Development at the Interface Between Aluminum Nitride and Titanium After Annealing at 1300°-1500°C,” J. Am. Ceram. Soc., 89 [4] 1409-1418(2006).

2. Chia-Hsiang Chiu and Chien-Cheng Lin, “Microstructural Development of the AlN/Ti Diffusion Couple Annealed at 1000°C,” J. Am. Ceram. Soc., 91 [4] 1273-1280(2008).

3. Chia-Hsiang Chiu and Chien-Cheng Lin, “Formation mechanisms and atomic configurations of nitride phases at the interface of aluminum nitride and titanium,” J. Mater. Res., in press.